6-1-2015

Innovative polymer nanocomposite membranes for industrial applications

Irene Fahim

The American University in Cairo

School of Sciences and Engineering

Innovative Polymer Nanocomposite membranes for Industrial Applications

By

Irene Samy Fahim

Dissertation submitted in partial fulfillment of the requirements of the degree of Doctor of Philosophy in Engineering with a concentration Mechanical Engineering

Under Supervision of

Dr. Hanadi Salem

Professor, Mechanical Engineering Department

&

Dr. Wael Mamdouh

Assistant Professor, Chemistry Department

Spring 2015

Acknowledgments

First of all, I am grateful to the Almighty God for blessing my life with so many gifts and opportunities that are much more than I deserve, and for carefully and timely planning my life and for being there by my side every step of the way.

I would first like to thank Mr. Yousef Jameel for his generous contribution to the PhD program in Applied Sciences and Engineering and for the Fellowship Award I was granted for the four academic years. His generosity has made it possible to initiate a PhD program at the American University in Cairo which came to the benefit of Egyptian students especially qualified females who were not able to travel outside Egypt to pursue their studies and dreams. I am also grateful to the Office of the Dean for Graduate Studies for approving research and conference grants that covered most of the expenses of my research, conferences and publications.

It gives me great pleasure to express my sincere gratitude to my supervisors, Professor Hanadi Salem and Dr Wael Mamdouh, for their supervision through the course of this research work. I have benefited immensely from their considerable help, encouragement and inspiration throughout this time.

I was fortunate to receive the help of Dr. Khalil Elkodary in Finite element analysis. I deeply appreciate all that they have done for me.

I would like also to thank Dr Hatem Elayat for his help in statistical analysis.

I would like to thank the Academy of Scientific Research and Technology (ASRT) for its financial support, which has made this research possible.

I am also very grateful to the Yousef Jameel Science and Technology Research Center (YJ-STRC) for providing the equipment and training for performing all the experimental work.

I would also like to express my appreciation to all the staff and research students in the Mechanical Engineering department and the chemistry department for their help and support. Last, but not least, I wish to thank my sons, Farid and wahid , for their support during my study.

ABSTRACT

The present study aimed at developing novel polymer nanocomposites (PNC) membranes by investigating the different preparation factors (e.g. cross-linking of the membranes, filler type and wt% of the fillers added to the polymers) on the PNC membranes' properties such as: pore size, permeability, tensile strength, melt flow index, and thermal stability, recorded at different temperatures (ranging from 23 – 60 ºC). The main goal is to have PNC membranes with enhanced tensile properties as well as improved barrier properties which would make PNCS potential candidates for possible industrial application such as packaging, wrapping materials and filtration membranes. Mainly, two polymers were used in this study: Low density polyethylene LDPE as an example of a synthetic polymer, and chitosan (CS) as another example of a natural polymer. In the current research, emphasis was made on the natural polymer due to its biodegradable nature and for proving better performance in concerning its permeability as membrane matrices. PNCS were prepared by mixing each polymer with two nanofillers (graphene and fullerene) with different concentration (0.1, 0.5 and 1wt.%) for studying their influence on the PNCs membrane properties.

LDPE ,CS nanocomposite membranes were fabricated by mixing the polymer with graphene (G) and Fullerene (F) nanofillers. Physical cross-linking of CS by sodium tripolyphosphate (TPP) was carried out in order to enhance the binding between the internal CS chains. F and G with different weight percentages (0.1, 0.5 and 1wt.%) were added on physically cross-linked chitosan (CLCS) as well as the non cross-linked chitosan (NCLCS) membranes by wet mixing technique.

In the current research, permeability and the pore morphology of the LDPE, CLCS and NCLCS with and without fillers were assessed at room temperature and as a function of increasing the ambient temperature under constant strain. Scanning electron microscopy (SEM) was employed for the evaluation of the fabricated plain and composite membranes structures and pore size, shape and pore size and nanofiller distribution. The average pore sizes were determined using a porosimeter. Validation of the experimental results was conducted using Abaqus/Standard software provided a simulation modelling of steady-state diffusion of the fabricated membranes. The tensile strength and % elongation were also assessed at 25, 30 and 60^{o}C. Response surface methodology (RSM), a statistical analysis tool, was used to determine the

optimized mixture for the various factors (temperature, cross-linking of CS, filler type and wt% of the fillers).

The results revealed that cross-linking, filler type and filler wt.% play a crucial role in controlling the pore size and accordingly the rest of the physicochemical and mechanical properties of all fabricated LDPE, CS nanocomposite membranes. The pore size of the fabricated LDPE were found to be microporous(0.1-0.2μm) while, CS nanocomposite membranes were found to be in the mesoporous range (i.e. 2-30nm). Moreover, the addition of G and F nanofillers to LDPE, CLCS and NCLCS solutions aided in controlling the CS nanocomposite membranes' pore size. It enhanced the barrier effect of the membranes by decreasing the pore size. The theoretical modelling results validated the experimental findings, The simulation showed the mass diffusion along the membrane thickness, which could not be calculated experimentally. Increasing the ambient temperature resulted in the decrease in tensile strength due to coarsening of pores upon heating.

The optimum membrane conditions were selected according to the membrane's filtration application The RSM results were found to be in agreement with the experimental results, whereby cross-linking of CS, filler type and filler wt.% were significant factors. The factors had a direct influence on the pore size, diffusion time and tensile strength of the PNC membranes.

The current research shows that fabricated CS nanocomposite membranes were effective candidates in membrane filtration systems. They could be used for blocking particles such as atmospheric dust, fumes, paint pigments, viruses and bacteria. NCLCS/1wt. % could be used to filter gases. CLCS/1 wt. %F could be used for combustion smoke filtration. LDPE/1 wt. %G could be used for filtration of bromine and lead smoke particles.

Table of Contents

Nomenclature

ASAP	Accelerated surface area and porosimeter
CA	Cellulose acetate
CDS	Concentration dependent system
CIS	Concentration independent system
CLCS	Cross-linked chitosan
CS	Chitosan
DA	Deacetylation
DL	Digital logic
DOE	Design of experiments
EPA	Environmental protection agency
F	Fullerene
FEA	Finite element analysis
G	Graphene
HMWC	High molecular weight chitosan
LDPE	Low density polyethylene (LDPE)
LMWC	Low molecular weight chitosan
MF	Microfiltration
MFI	Melt flow index
MMWC	Medium molecular weight chitosan
NCLCS	Non cross-linked chitosan
NF	Nanofiltration
PAN	Polyacrylonitrile
PNCs	Polymer nanocomposites
PSU	Polysulfone
PVC	Polyvinyl chloride
PVDF	Poly vinylidenefluoride
RO	Reverse Osmosis
RSM	Response surface methodology
SEM	Scanning electron microscopy
SEM	Scanning electron microscopy
TEM	Transmission electron microscopy
TFC	Thin film composite
TGA	Thermo gravimetric analysis
TPP	Sodium tripolyphosphate
UF	Ultrafiltration

List of Figures

List of Tables

Chapter 1

INTRODUCTION

1. Introduction

1.1. Introduction

Air and water pollution are considered among the most crucial problems facing the community with negative impact on human health as well as on the environment. Pollution has two main sources of occurrence; either from natural or manmade resources. The natural resources include gases released from the processes of living beings; carbon dioxide from humans and plants during respiration, methane from cattle during digestion, smoke from the combustion of various inflammable objects and volcanic eruptions [1].

On the other hand, the man made resources include burning of fossil fuels, and gases emitted from vehicles such as carbon monoxide that is also caused by improper or incomplete combustion. The non-balance caused by any increase or decrease in the percentage of these gases in the atmosphere hinders the survival of plants, animals and humans.

Moreover, agricultural man made activities are another prominent reasons for air pollution, where ammonia is a very common byproduct released from such agriculture related activities and is one of the most hazardous gases present in the atmosphere. In addition, the use of insecticides, pesticides and fertilizers emits harmful chemicals into the air such as nitrogen and nitrate ions which turn into acid rain later on with negative impact on the soil, oceans and other living systems.

Moreover, petroleum refineries release hydrocarbons and various other chemicals that pollute the atmosphere. Mining is another process wherein minerals below the earth are extracted using large equipments. During this process, dust and chemicals are released into the atmosphere causing massive air pollution. This is one of the reasons responsible for the deteriorating health conditions of workers and nearby residents.

In addition, indoor air pollution is a crucial source of pollution including household cleaning products, painting supplies which emit toxic chemicals into the air [1].

Water pollution is another dreadful problem, and is powerful enough to result in a negative impact on the environment. Water pollution affects humans and amphibians where several people die each day due to consumption of polluted and infected water.

The industrial wastes that are being dumped into rivers and other water bodies cause an imbalance in the water purity leading to its severe contamination and mostly death of aquatic species. For example, water-borne diseases like cholera, diarrhea increased recently due to severe water pollution [2].

After mentioning the several sources of pollution, one can conclude that the effects of air pollution are alarming. They are known to create several respiratory and heart conditions along with Cancer among other threats to the body. Another direct negative impact of air pollution is the immediate alterations that the world is witnessing due to Global warming. The later is considered one of the factors behind increasing the atmospheric temperature worldwide, thus an increase in sea levels and melting of ice from colder regions and icebergs. Another severe consequence is the formation of acid rain, which causes great damage to human, animals and crops and on wildlife. Toxic chemicals present in the air force wildlife species to move to new places and change their habitat. The toxic pollutants deposit over the surface of the water can also affect aquatic life [3].

Environmental protection agency (EPA) scientists and a number of other health organizations are concerned about pollution caused by these very fine particles (dust, soot, smoke particles) to get deeper into the lungs. These fine dusts cause an enormous increase in respiratory illnesses, aggravate asthma, acute respiratory symptoms such as coughing, reduced lung function resulting in shortness of breath and chronic bronchitis as shown in Figure 1.1, also these fine particles are the main reason for reducing visibility in places like national parks and wilderness areas that are known for their scenic vistas. In many parts of the United States for example, pollution has reduced the distance and clarity of what we see by 70 %. Fine particles can remain suspended in the air and travel long distances with the wind. For example, over 20 percent of the particles that form haze in the Rocky mountains national park have been estimated to come from hundreds of miles away [4].

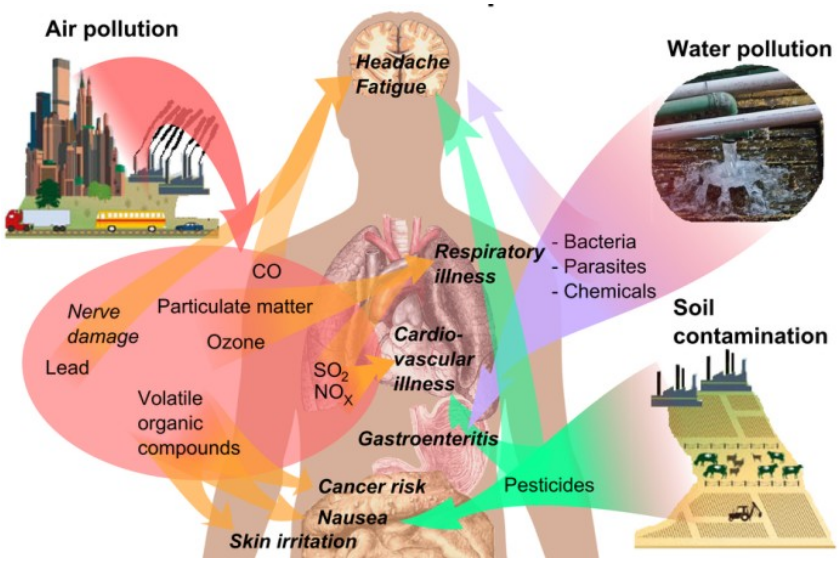

Figure 1.1 Effects of Air pollution on humans[4]

The most important steps that are necessary to keep the level of air pollution to an acceptable limit is by changing the life style and not interfering with nature. A number of environmentalist organization and laws have been formed and implemented in order to find possible solutions for this problem. On the other hand, filtration processes have emerged into the scene in order to help the industry to limit their polluting factors from getting into the air. The first record of experimentation in filtering came from Sir Francis Bacon in 1627. Hearing rumors that seawater could be purified and cleansed for drinking purposes, he began experimenting in the desalination of seawater. Sadly, his sand filtration technique did not prove to work for desalination, but later scientists have followed his lead and continued to experiment with this technique, by implementing the technology in early treatment plants.

Woven materials have been used to strain out unwanted particles as long as man has manufactured cloth materials for clothing. Non-woven material has been used since before recorded history when early man used animal skins for body protection from the elements, long before Henri Darcy described the flow of liquids through saturated porous material. These proven methods of liquid/solid separation are still the most widely used today. Newer technologies include centrifugation and selective porous membranes have been proposed. [5]

Membrane technology is one of the most promising solutions to air and water pollution. There are different categories of synthesized membranes (also referred to as thin films) manufactured by either synthetic or natural polymers. The preparation of synthetic membranes and their utilization on a large industrial scale is a recent development that gained substantial importance due to the large number of their practical applications including water treatment, filtration, food and drug packaging, gas and vapor separation.

The membranes used in various applications differ in their structure and their function and the way they are operated. They are classified according to their pore size. Microporous thin films have pore diameters of less than 2nm while macroporous have pore diameters greater than 50nm and the mesoporous category lies between 2-50nm. However, all membranes have several features in common that make them particularly attractive tools for separation of molecular mixtures. Most importantly is that the separation is performed by physical means without chemically altering the constituents of a mixture. Furthermore, the separation and purification of molecular structures are major problems in several industries. Efficient separation processes are also needed to obtain high grade products in food and pharmaceutical industries to supply communities and industries with high quality water, to remove or recover toxic or valuable components from industrial effluents, and to separate gases and vapors in petrochemical processes [6-7].

1.2. Thesis Scope and Objectives

The main focus in this work is developing novel polymer nanocomposite (PNC) membranes with enhanced tensile strength and improved barrier properties. An important aspect in fabricating the novel PNC membranes is studying the effect of nanofiller type and weight % on the overall properties of the PNC membranes and how to retain their properties (permeability - tensile strength) at temperatures up to 60 ºC. The PNC membrane fabrication is based on the concept of controlled porosity. It entails the complex process of tailoring the membrane according to the filtration application needed and determining the suitable range of pore size (microporous or mesoporous).

In this study, the main objectives are divided into the following activities

- Preparation of PNC membranes using Chitosan natural polymer and low density polyethylene (LDPE) synthetic polymer that will be mixed with fullerene and graphene nanofillers.
- Investigating the mechanical properties and characterization of PNC
- Studying the different factors affecting the materials structural properties of PNC (physical properties, morphology)
- Investigating the possibility of using the prepared PNC in industrial applications such as filtration and packaging
- Determining the optimized mixture for the various factors used in fabricating the PNC membrane (temperature, cross-linking of CS, filler type and wt% of the fillers).

Chapter 2

LITERATURE REVIEW

2. Literature Review

2.1. Preface

The development of PNCs is rapidly emerging as a multidisciplinary research activity whose results could broaden the applications of polymers to the great benefit of many different industries. PNC are polymers (thermoplastics, thermosets or elastomers) that are reinforced with small quantities (less than 5% by weight) of nano-sized particles. PNCs represent a radical alternative to conventional filled polymers or polymer blends. In contrast to conventional composites, where the reinforcement is on the order of microns, PNCs are exemplified by discrete constituents on the order of a few nanometers. Their importance comes from providing value-added properties not present in the neat resin, without sacrificing the resin's inherent processability and mechanical properties, or by adding excessive weight [8]. Due to the unique properties of PNCs, they have been used in different applications including automobiles, aerospace, injection molded products, coatings, adhesives, fire-retardants, packaging Materials, optical integrated circuits, drug delivery, sensors, water filtration systems, dental, medical devices, tissue engineering applications, and packaging [8].

Polymer nanocomposite membranes present an interesting approach to improve the separation properties of polymer membranes because they possess properties of both organic and inorganic membranes such as good permeability, selectivity, mechanical strength, and thermal and chemical stability. The preparations and structures of polymer nanocomposite membranes, their applicability to gas separation and separation mechanism are reviewed. The applications of polymer inorganic nanocomposites membranes is dependent on the results obtained from researches, commercial sectors, existing markets and the improvement level of the nanocomposite properties. Furthermore, the relevance of their application in large scale, the capital to be invested, production costs and the profits should be taken into account. Therefore, there are several characteristics of membranes that are studied in this research including pore size, permeability and mechanical properties [8].

2.2. Membrane Characteristics

2.2.1. Pore Size

In the 20th century, membrane technology has emerged as one of the most promising technologies that have been used across a wide variety of disciplines ranging from filtration, gas and liquid permeability to biomedical applications [8]. Great research efforts in this technology as well as its applicability in commercial markets have been growing rapidly through different disciplines. The most crucial factors in such technology is choosing the high performance composing materials for particular application.

Currently available membranes are classified according to their pore size to microfiltration (MF) and ultrafiltration (UF) thin films. MF has the largest pore size (0.1–3μm) and typically rejects large particles and various microorganisms. MF fills in the gap between UF and granular media filtration. This MF range covers the lower portion of the conventional clays and the upper half of the range for humic acids. This is smaller than the size range for bacteria, algae and cysts, and larger than that of viruses. MF is also typically used for turbidity reduction, and removal of suspended solids.

On the other hand, UF thin films have pore sizes ranging from 0.01- 0.1μm as illustrated in Figure 2.1. UF thin films are mainly used to remove some viruses, color, odor, and some colloidal natural organic matter. In addition, nanofiltration (NF) thin films are relatively new and are sometimes called “loose” reverse osmosis (RO) thin films. They are porous thin membranes, but since their pore sizes are on the order of one nanometer or less, they exhibit performance between that of RO and UF thin films. Both processes (MF and UF) require low transmembrane pressure (1–30psi) to operate, and both are now used as a pretreatment to desalination technologies such as RO, NF, and electrodialysis [9-10].

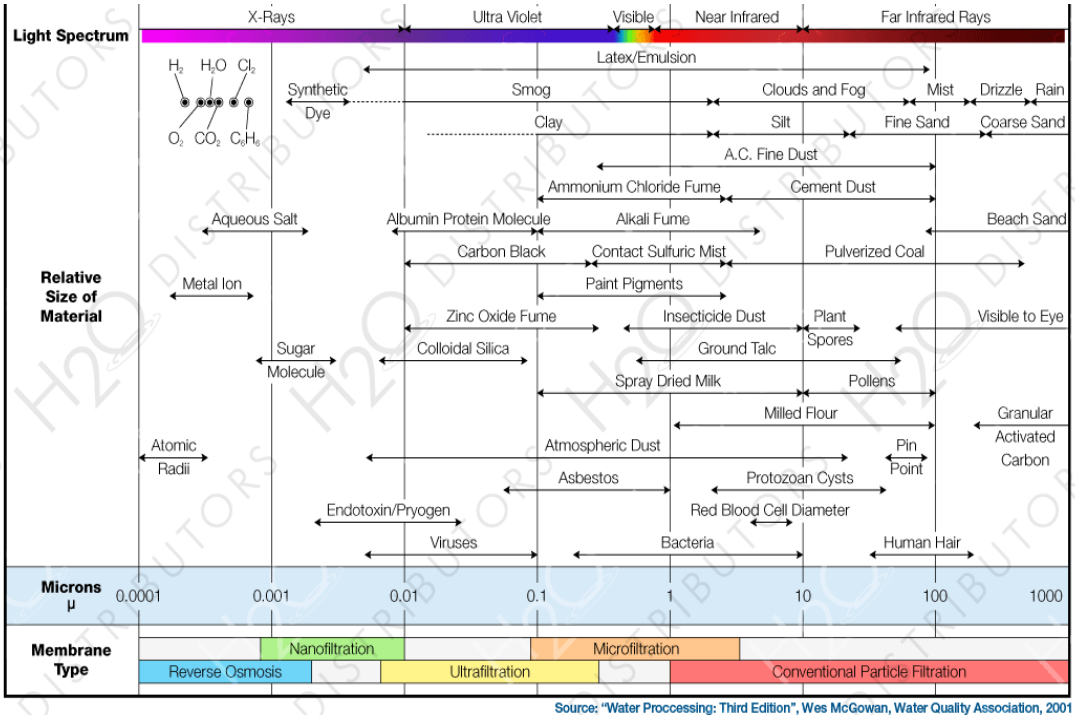

Figure 2.1 Membrane classification according to pore sizes [10]

Transport through the membrane takes place when a driving force is applied to the components in the feed. In most of the membrane processes, the driving force is either a pressure difference or a concentration (or activity) difference across the membrane [11].

2.2.2. Mechanical properties

Mechanical properties of polymeric membranes depend on a number of parameters, including the degree of crystallinity of the polymer and the presence of plasticizers within the polymer matrix. Increasing the crystallinity of a polymer generally enhances its elastic modulus and tensile strength and reduces its ductility because, the polymeric chains fold together and form ordered regions. Plasticizers are small molecules, such as residual solvents. They are inserted between macromolecular chains and weaken the intermolecular forces between them thus resulting in a softened and flexible polymeric matrix. They enhance the processability and mechanical properties of the polymers through lowering the melting and softening points and viscosity of the melts as shown in Figure 2.2 [12-13]. Moreover, mechanical properties are highly sensitive to the nature of the environment, such as the presence of water, organic solvents, oxygen and temperature. Increasing the

temperature induces generally a decrease in elastic modulus, a reduction of tensile strength and an increase of ductility due to the softening of the polymer chains [14].

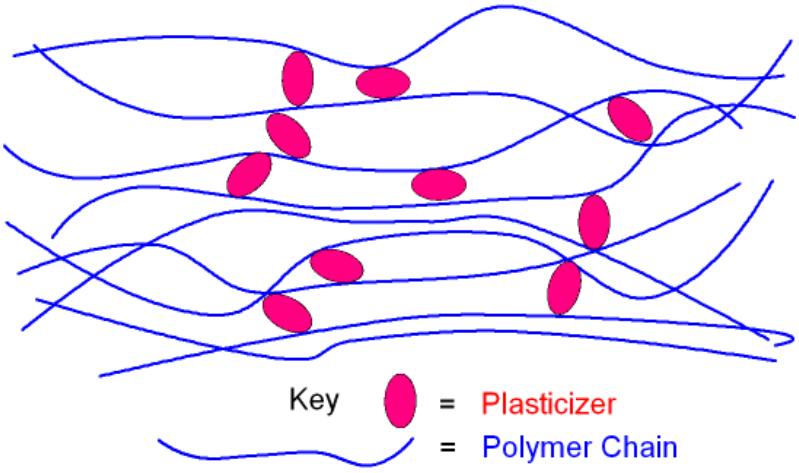

Figure 2.2 Plasticizers in polymer chains [15]

Recently, more attention has been witnessed to the use of natural polymers for sustainable development and environmental preservation. Polymers have attracted significant interest among the scientific community in a broad range of applications such as water treatment, separation membranes, food packaging, tissue engineering, and drug delivery. However, low mechanical properties of natural polymers restrict their use in those applications. Tensile strength, molecular weight and percentage elongation are mainly used to describe how mechanical properties are related to the chemical structure of the polymeric thin films. Tensile strength indicates the maximum tensile stress that the film can sustain whereas elongation is the maximum change in length of a tested specimen before breaking. These mechanical properties are crucial when using PNCs membranes for packaging applications for example. They vary with the nature of the polymer whether its chains are non-cross linked or cross-linked and also with the addition of nanofillers to the polymer matrix [16-17]. Undeniably, the most active area of food nanoscience research and development is packaging: the global nano-enabled food and beverage packaging market was more than 4 billion US dollars in 2008 and has been projected to grow to more than 7 billion US dollars by 2014, representing an annual growth rate of 12% [18].

2.2.3. Permeability

Permeability of thin films is a critical factor which directly affects their performance in many industries, including petrochemical, construction, water, gas, transport, electronics, medical and packaging applications. The process of permeation through polymeric membranes is a combination of dissolution and diffusion through the membrane. Dissolution is the process of absorption of particles in the polymer and depends on the affinity of the polymer for the absorbing molecule, and the volume available for absorption of the particles. Solubility determines the limit to the amount of particles that can be absorbed under any particular set of conditions [19]. Diffusion on the other hand, is the concentration gradient driven process whereby the absorbed molecules are transported within the polymer and diffusion properties are characterized via diffusion coefficients as shown in Figure 2.3. Diffusion is mostly calculated using Fick's first law of diffusion as illustrated in equation

$J = -D\frac{d\theta}{dx}$.....(1) [19]

J= steady state flux of diffusant per unit area

Ø = concentration

Ideal sorption of gases (including vapor) in a polymer follows Henry's law as illustrated in equation

C=SP..... (2) [20]

where the concentration adsorbed C is directly proportional to the pressure of the gas

C= concentration

P = Pressure

S = solubility parameter [20].

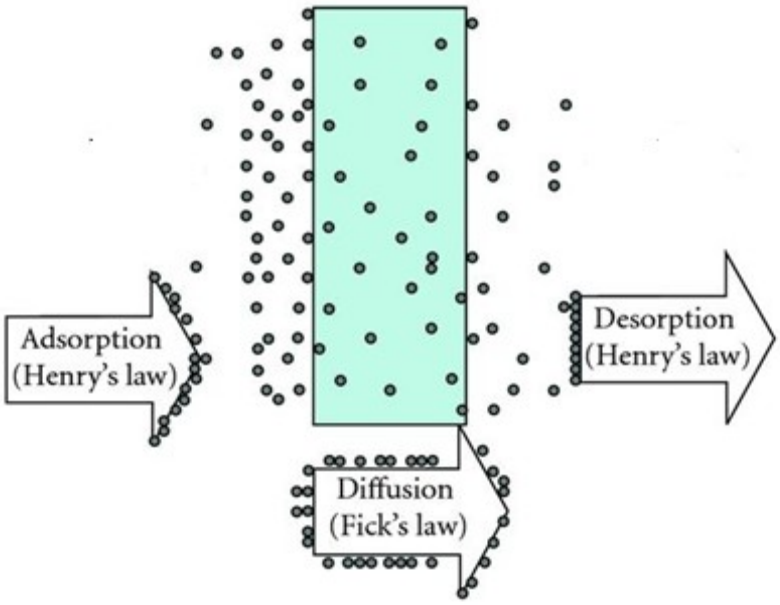

Figure 2.3 General mechanism of gas or vapor permeation through a plastic film [14]

There are a number of factors influencing the mass transport through membranes such as (i) polymer chemistry; (ii) the chemical composition of the polymer matrix; (iii) free volume; (iv) crystallinity and (v) temperature of the surrounding environment. Regarding polymer chemistry, polymers with polar chemical groups, such as epoxies or nylons, will have a strong affinity for polar molecules, including water. Such materials are known to be hygroscopic. In contrast, the uptake of polar species is much lower in non-polar polymer molecules, e.g. polypropylene. As for the second factor, polymer composition, which is related to the type of the polymers mixed together for example, has a strong influence on the solubility and diffusion properties of small molecules within the polymer matrix. Additionally, free volume is an intrinsic property of the polymer matrix and arises from the gaps left between entangled polymer chains and can be thought of as extremely small-scale porosity, however, free volume pores are dynamic and transient in nature since the size (and existence) of any individual free volume pore depends on the vibrations and translations of the surrounding polymer chains [21].

Moreover, crystallinity plays another important role in determining the permeability of polymeric thin films. Crystalline regions in polymers are more ordered than amorphous regions and free volume will thus be lower in these regions. It is often assumed that the crystalline region is impermeable and that the sorption depends only

on the volume fraction of the amorphous phase as shown in Figure 2.4 [22]. Furthermore, temperature has also an effect on the permeability and diffusion properties of small molecules within polymers matrices, hence, as the temperature increases, the mobility of the molecular chains increases and thermal expansion leads to a reduced density. Therefore, the free volume in the system will increase, leading to an increased solubility [23].

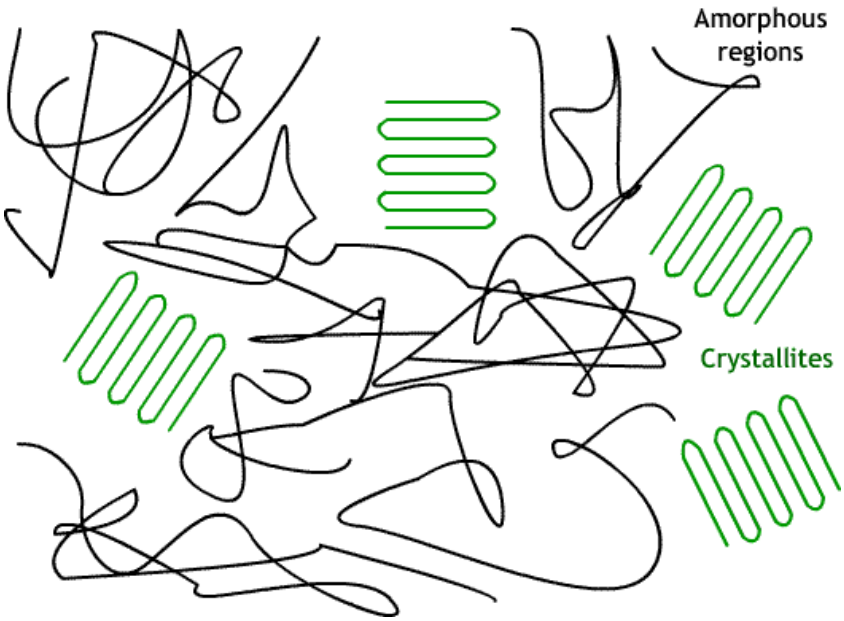

Figure 2.4 Small crystalline regions surrounded by amorphous polymer [24].

2.3. Membrane material

2.3.1. Synthetic polymeric membranes

Examples of typical MF and UF polymeric materials include low density polyethylene (LDPE), poly vinylidenefluoride (PVDF), polysulfone (PSU), polyacrylonitrile (PAN) and polyvinyl chloride (PVC) copolymers. PSU is also commonly used for UF thin films. MF thin films also include cellulose acetate (CA) and cellulose nitrate blends, nylons, and polytetrafluoroethylene (PTFE). RO thin films are typically either CA or PSU coated with aromatic polyamides. NF thin films are made from CA blends or polyamide composites like the RO thin films, or they could be modified forms of UF thin films such as sulfonated PSU [25-26].

Polyethylenes: Over 60 million tons of polyethene is manufactured each year making it the world's most important plastic. Its uses include thin film manufacturing for packaging and separation purposes [27]. Thin film fabrication is a development that began just 40 years ago[28]. More studies were performed by Mason et al. to investigate the diffusion of gases through membranes [29].

LDPE, Looking at the historical background of LDPE thin films, they gained a high market share particularly in food packaging industry as they did not transfer plasticizers to the packaged food [30]. LDPE is a thermoplastic made of ethylene monomers used for synthetic membrane preparation. It is opaque and robust enough to be virtually unbreakable and at the same time a quite flexible polymer. It is unreactive at room temperature although it is slowly attacked by strong oxidizing agents, and some solvents will cause its softening or swelling. Moreover, it has excellent resistance to diluted and concentrated acids, alcohols, bases and esters. In addition, it entails good resistance to aldehydes, ketones and vegetable Oils. Furthermore, it has easy processability properties, flexibility and high elongation modulus, which makes LDPE suitable for packaging materials such as foils, trays and plastic bags, both for food and non-food purposes. It is also used as protective coating on paper, textiles. However, despite LDPE's numerous advantages, it suffers from poor resistance to oxidizing agents and hydrocarbons [31].

PVDF thin films are commonly used in a variety of general filtration applications. PVDF plays an important role in various industries, such as pulp and paper, nuclear-waste processing and chemical processing, owing to its remarkable chemical and physical properties. Its strong chemical resistance against corrosive chemicals including acids, bases, oxidants and halogens makes it an excellent polymeric membrane material and popular among various research areas. As membranes, they are the most widely used in water treatment due to their ability to be controllably porous for MF and UF application. However, PVDF exhibits some complexity in thin film fabrication process due to the crystallinity of the polymer in addition to its low binding properties [32-33].

PSU, the third commonly used synthetic polymer is PSU, it has high degree of membrane asymmetry with larger pores stacked over the smaller micron-rated pores

resulting in a high flow rate during the filtration process. One of its major drawbacks is the resistance to flow is much less than conventional thin films [34].

There are also a number of frequently used thin films such as polyacrylonitrile (PAN). It has high resistance to fouling but one of its main disadvantages is its weak separation properties. PTFE on the other hand, has an unmatchable profile of unique properties which make it one of the most valuable and versatile engineering materials available. It has high thermal stability and exceptional electrical properties but exhibits weak tensile properties. Moreover, Nylon thin films are hydrophilic, eliminating the need for wetting agents that could be extracted when filtering aqueous solutions, flexible, durable, and tear resistant, and it can be autoclaved at 135ºC but unfortunately its pore sizes are limited up to 0.2µm [35].

Nevertheless, synthetic thin films are widely used as valuable scientific and technical tools due to their significant higher chemical and mechanical stability especially at elevated temperatures. Their selectivity is mainly determined by the porous structure according to their size, through the homogenous structure, or according to the solute solubility and diffusivity if the membrane is homogenous. However, they are not well defined in terms of their structure and function; they have only passive transport properties and are usually less selective and less energy efficient [8].

Moreover, the indiscriminate use of synthetic polymers in packaging and filtration without proper disposal management has led to mounting solid wastes, thereby causing severe environmental pollution. The major hurdle against the use of synthetic polymers is their non biodegradability, thus increasing the amount of waste. As a result of which petroleum based thermoplastic polymers are losing their importance due to waste disposal and non biodegradable problems. In India for example, plastic waste accounts to 3% by weight of a total of 80,000 metric tons of municipal solid waste generated daily [36]. In USA, however, out of 400,000 metric tons of garbage generated daily, plastics constitute 30% of its volume, and its disposal is causing new challenges [37]. In Egypt, 16.2 million tons of waste are produced annually, plastic waste is around 6 % of this waste [35].

There is a paradigm shift imposed towards fabricating thin films from biobased polymers, which are biodegradable, non toxic and therefore compatible with the

environment. Biodegradability is not only a functional requirement but also an important environmental attribute. The concept of biodegradability offers both user friendly and eco friendly advantages [38]. The increasing demand for renewable and bio-based materials and the shift in consumer's preference for eco-friendly packaging is driving the market for global biodegradable plastics. The global biodegradable plastics market in terms of volume is expected to grow from 664,000 metric tons in 2010 to 2330,000 metric tons by 2016, at an estimated compound annual growth rate (CAGR) of 20.24% from 2011 to 2016 as shown in Figure 2.5.

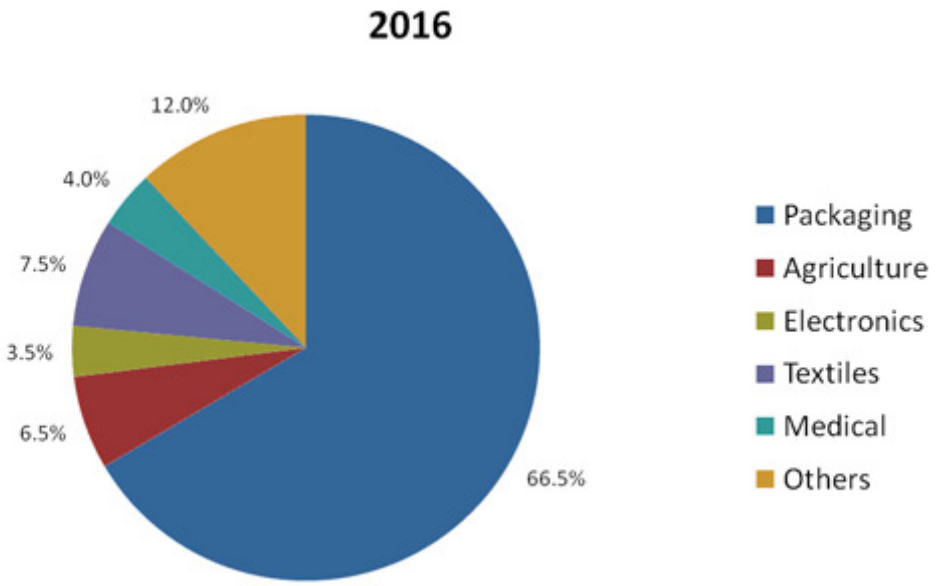

Figure 2.5 Global bio-based biodegradable plastics market by application.2016 [39]

Packaging forms the largest application market due to increased consumer awareness for sustainable packaging. The packaging application contributed to over 50% of the global biodegradable plastics market in 2010. Europe accounted for the major share for the global biodegradable plastics market estimated to be 40.6% in 2010. This was primarily due to the fact that focus on sustainability is significant in Europe, especially in the European Union. In this regards, Europe is the most regulated market especially when it comes to certifying and commercializing new plastic products. North America forms the second largest market for biodegradable plastics in the world. Industry participants with the most agreement and collaboration and significant product developments include Cardia Bioplastics Limited, Cereplast, Purac, and

Telles. In 2011, Cereplast Inc. has concluded a multi-million U.S. dollar distribution agreement with BioWorks for the distribution of Cereplast bioplastic resins in the Poland market [39].

There are three categories of biobased polymers as represented in Figure 2.6. The various naturally occurring biopolymers of use in composite film making formulations are broadly classified into: (i) polymers directly extracted from polysaccharides such as starch, cellulose, chitosan (CS), (ii) polymers produced by classical chemical synthesis using renewable biobased monomers, for example poly-lactic acid, a bioployester polymerized from lactic acid and (iii) polymers produced by microorganisms. Examples of the main polysaccharides having the ability to form thin films are starch, cellulose and CS [40].

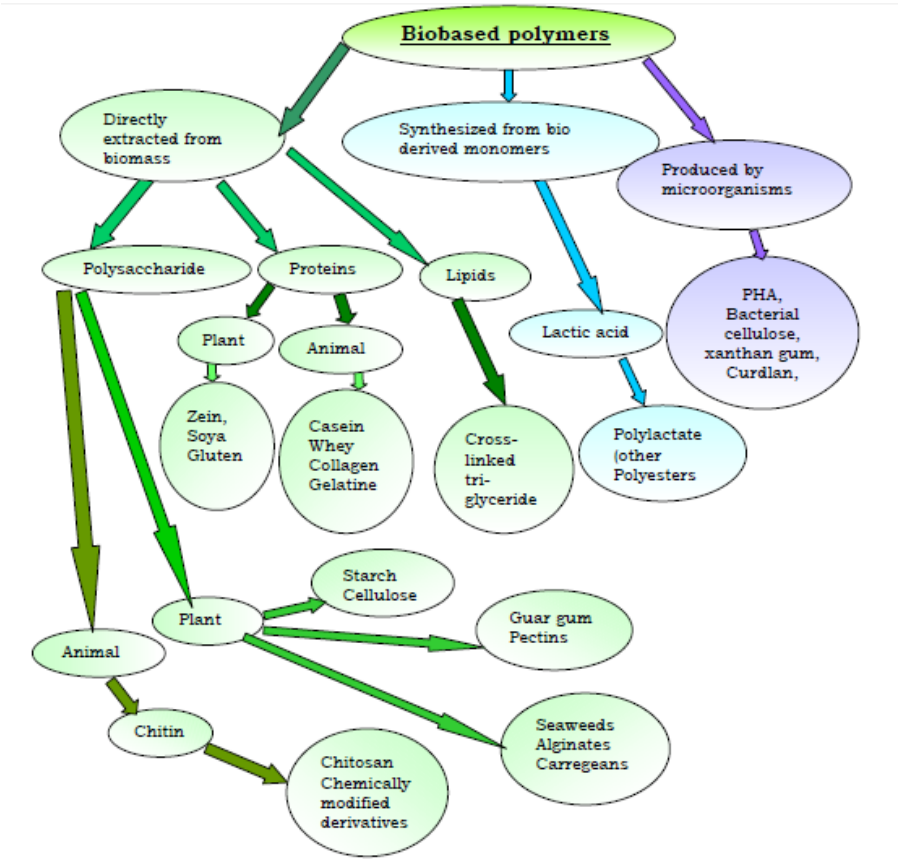

Figure 2.6 Three categories of biobased polymers [40]

2.3.2. Natural Polymeric membranes

Looking back to the early fabrication reports of membranes in 1963, Loeb and Sourirajan demonstrated asymmetric CA thin films which exhibited relatively high flux, low gas, moisture barrier properties and good salt rejection. They were asymmetric and exhibited NaCl rejection values of approximately 99.5% using a feed solution of 52,500 mg/L NaCl and flux values from 20 to 44 cm per day at feed pressures ranging from 10342 to 13789 Kpa [41].

Cellulose. among the naturally extracted polymers, cellulose is a naturally occurring polymer found in plants such as cotton. It is a linear, regular structure with an array of hydroxyl groups. It is rod-like material that is relatively inflexible, and tends to form strongly hydrogen bonded crystalline microfibrils and fibers, which makes thin films mechanically robust [42].

The degree of acetylation describes how many of the pendant OH groups (shown in Figure 2.7) on the cellulose are replaced with acetyl groups, CH_3CO. The degree of acetylation can range from 0 to 3 where 0 represents unreacted cellulose and 3 corresponds to completely substituted cellulose, also called cellulose triacetate (CTA). The degree of acetylation has a large effect on the resulting thin film properties. A high degree of acetylation gives high salt selection but low permeability. Lower degrees of acetylation yield thin films with lower rejection but higher flux. Commercial CA membranes used for RO applications have a degree of acetylation of about 2.7. This composition provides a good balance between salt rejection and permeate flux. However, on the negative side, thin films tend to hydrolyze over time, which decreases their selectivity. Also, they are extremely sensitive to changes in pH and are stable only in pH ranges of 4 to 6. Moreover, cellulose has lower percentage of nitrogen (1.25%) compared to CS (6.89%) [43].

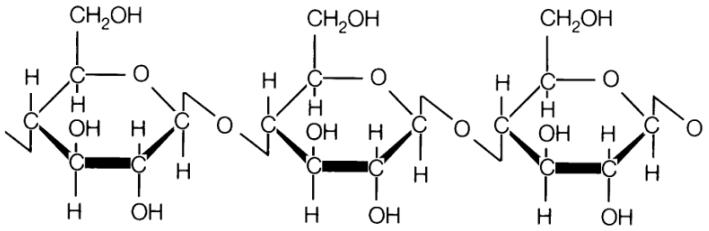

Figure 2.7 OH groups of Cellulose [41]

Cellulose acetate membranes had been the dominant choice for RO membranes until the development of thin film composite RO membranes in 1972. Based on aromatic polyamides thin film composite (TFC) membrane fluxes and rejections surpassed those of CA. Most TFC membranes are made with a porous, highly permeable support such as polysulfone, which is coated with a cross-linked aromatic polyamide thin film. The coating provides the salt rejection properties of the membrane [44]. Finally, salt rejection of CA membranes decreases as temperature increases. Therefore, feed water temperature typically does not exceed 35°C [44].

Starch, another natural polymer used for membrane preparation is starch. Research on starch based biodegradable plastics began in 1970s. Starch is a storage polysaccharide of cereals, legumes and tubers, and is widely available. It contains amylose and amylopectin, Starch has been used to produce biodegradable films to partially or entirely replace plastic polymers because of its abundant supply, low-cost, good processability, renewability, abundant, and ease of physical and chemical modifications, A number of film, sheet, and molded starch prototypes have been produced using conventional plastic processing equipment to demonstrate the feasibility and potential of these materials for the fabrication of consumer products. Moreover, according to Kaplan et al. it is possible to produce starch films through grafting of polymers. However, on the drawback side, it produces films but with poor mechanical properties. Moreover starch films exude water, and are not stable over a long time. An attempt to overcome these drawbacks has been to use Plasticizers to overcome brittleness of starch based films [45-47].

Chitin is the third natural polymer used to produce thin films. Chitin, poly(b-(1R4)-N-acetyl-D-glucosamine), which is the original source of CS, is the most abundant natural polymer second only to cellulose. The commercial source of chitin is the shells of crustaceans, mainly from crabs and shrimps as the byproducts of marine processing plants. CS, a N-deacetylated derivative of chitin, consists of linear b-1, 4-linked D-glucosamine (GlcN) and N-acetylglucosamine (GlcNAc) units as shown in Figure 2.8. The degree of deacetylation (%DA) generally dictates the physicochemical and biological properties of CS which is one of the most promising polymers for the preparation of thin films for various uses such as pervaporation, ultrafiltration, RO, gas separation, purification processes, antibacterial and drug delivery applications. CS, a relatively inert biomaterial with film forming ability, has been rapidly recognized for its potential in separation and purification technology in recent decades. Because of its hydrophilicity, biocompatibility, ease of modification, remarkable affinity to dyes, metals and proteins, CS thin films have become promising candidates for several applications including scaffolds, filtration membranes and packaging thin films[48-49].

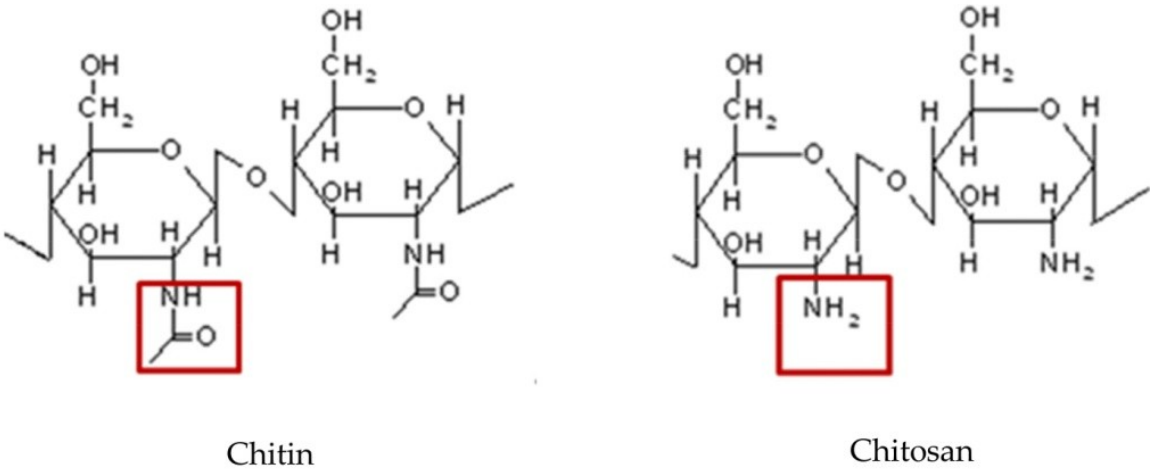

Figure 2.8 Chemical structure of chitin and chitosan [50]

CS membranes have been studied for a long time in food packaging due to its effective gas barrier property in dry conditions. Moreover, its excellent biocompatibility, non-toxicity, antibacterial and fungicidal properties and ease of film forming make it an attractive edible packaging material [51]. Later, researchers found that the sorption of water on CS thin films at high humidity causes the loss of its gas barrier property [52-53] This inspires the application of CS membranes for gas

separation. It is known that amines can serve as a carrier to facilitate the transport of acidic gases (e.g. CO_2) through membranes [53]. They can retard moisture migration and the loss of volatile compounds, reduce the respiration rate, and delay changes in textural properties. Such films have been used to coat different products such as mandarin, cherry and strawberries [54]. They are also excellent barriers to fats and oils, and have a high selective gas permeability ratio CO_2/O_2 as compared to conventional materials [55].

The mechanical characteristics of CS films depend on various parameters including the nature of the acid used in deacetylation (DA) and the concentration of CS. Acetic acid resulted in the toughest films when compared to malic, lactic, and citric acid. At DA below 20%, CS exhibits the highest structural charge density. CS displays polyelectrolyte behaviour related to long-distance intra- and intermolecular electrostatic interactions, which are responsible for chain expansion, high solubility and ionic condensation. For values of DA between 20-50%, hydrophilic and hydrophobic interactions are progressively counterbalanced. For DA over 50% electrostatic interactions are essentially short-distance interactions. Then, hydrophobic interactions due to the increase in the acetyl group content become predominant [40]. According to Sernivasa, CS with DA between 0-30% was the most useful in packaging applications. The increase in tensile strength is overcome by the addition of fillers whereas the increase in DA% of CS would decrease the tensile strength (the higher the DA% the lower the intermolecular interaction) of the films at low molecular weight. Moreover, the higher the DA% of CS, the more brittle and the less moisture absorption the films became, so 50 % was chosen to avoid brittle films [40].

There are three concentrations of CS, LMWC (low molecular weight chitosan), MMWC (medium molecular weight chitosan) and HMWC (high molecular weight chitosan). LMWC has higher permeability than that of HMWC and exhibits superior biological activities than HMWC. Moreover, LMWC had the highest bactericidal activity towards pathogenic bacteria. The increase in molecular weight of CS would increase the tensile strength and elongation as well as moisture absorption of the films, but they sacrifice permeability higher than that of high molecular weight HMWC and sacrifice superior biological activities and antioxidant activity [56]. Therefore, concentration of CS plays a key role in synthesizing the membranes.

2.4. Membrane Preparation

Membrane is defined as a barrier separating two phases and restricting the transport of various chemicals from one phase to the other preferably in a selective manner. A membrane can be homogenous or heterogeneous structure [57], and can carry a positive or negative charge or beneutral or bipolar. Transport through a membrane can be affected by convection or by diffusion of individual molecules, induced by an electric field or concentration, pressure or temperature gradient. The membrane's thickness may vary from 10 microns to few hundred micrometers. The principal types of membrane are shown in Figure 2.9 [57].

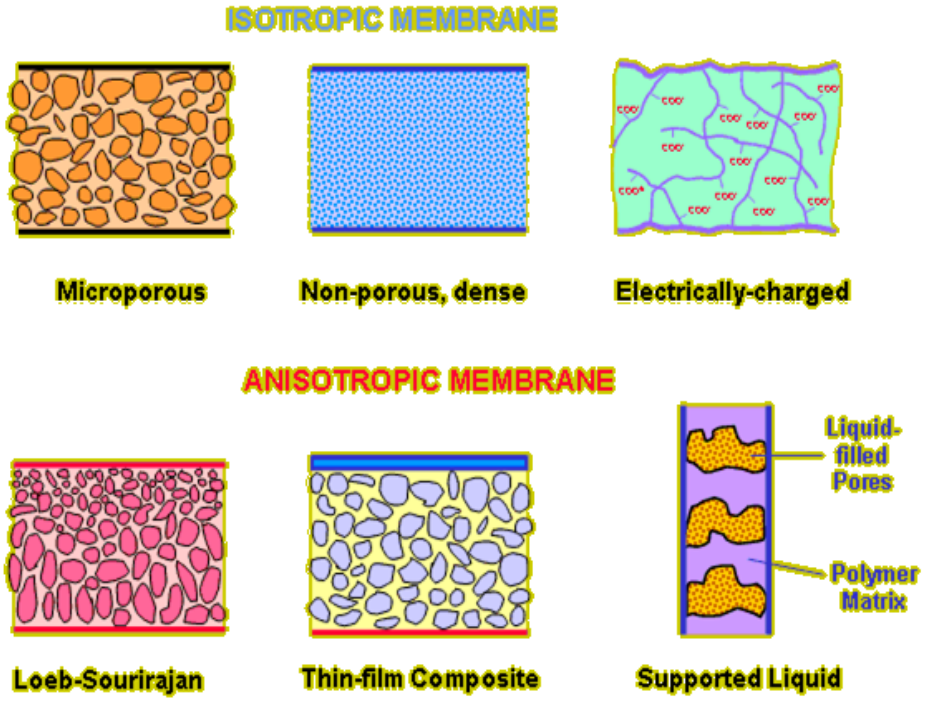

Figure 2.9 Types of membranes [57]

Polymeric membranes can be manufactured deliberately as porous or likely to be porous owing to defects, inclusions and different phases that leave pores within the polymer matrix. Isotropic thin films either lack pores or contain small pores. These films are prepared by solution casting followed by solvent evaporation or melt extrusion [58]. Anisotropic phase separation thin films are often called Loeb-Sourirajan membranes, referring to the researchers who developed these thin films. Loeb-Sourirajan membranes are produced via phase separation (inversion)

techniques, except that the pore sizes and porosity vary across the membrane thickness [59]. They consist of a dense layer of polymer on the surface of an increasingly porous layer [59]. Thin film composites usually consist of a highly porous substrate coated with a thin dense film of a different polymer. They are fabricated via several methods including phase separation, track etching, or expansion of films as will be discussed in the following section [58-59].

2.4.1. Phase separation

Phase separation (phase inversion) processes have been extensively applied to produce polymer membranes for separation processes and food industries. Phase separation process is suitable to produce the whole spectrum of membranes from MF, UF, NF and gas filtration membranes. Generally, they are produced by casting a film from a solution of polymer and solvent and immersing the cast film in a non solvent for the polymer. This casting solution is split into at least two phases: a polymer rich phase that forms the solid structure of the membrane, and a polymer poor phase that will be removed from the membrane to produce pores. After casting the polymer solution onto a flat surface, the formation of pores can be included by changing the composition of the solution. This process normally results in the formation of porous membranes as illustrated in Figure 2.10 depending on the material and the solvents used [58].

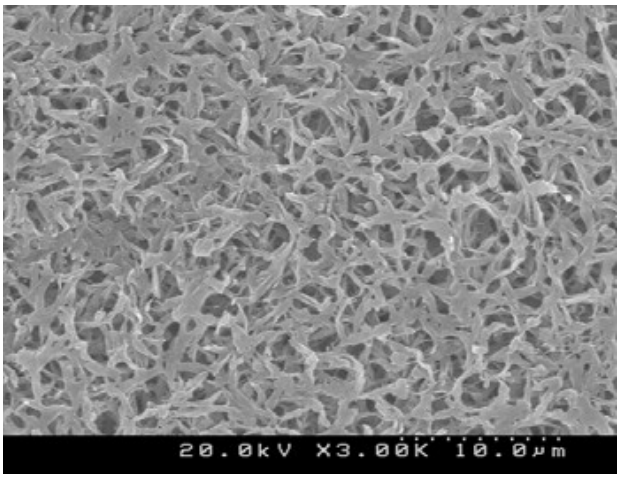

Figure 2.10 SEM image for porous structure of membranes prepared by phase separation method [58]

2.4.2. Track etched membrane

Another type of microporous membrane is the track-etched membrane. This type of membrane is prepared by irradiating a polymer film with charged particles that attack the polymer chains, leaving damaged molecules behind as illustrated in Figure 2.11. The film is then passed through an etching solution, and the damaged molecules dissolve to produce cylindrical pores, many of which are perpendicular to the membrane's surface [59].

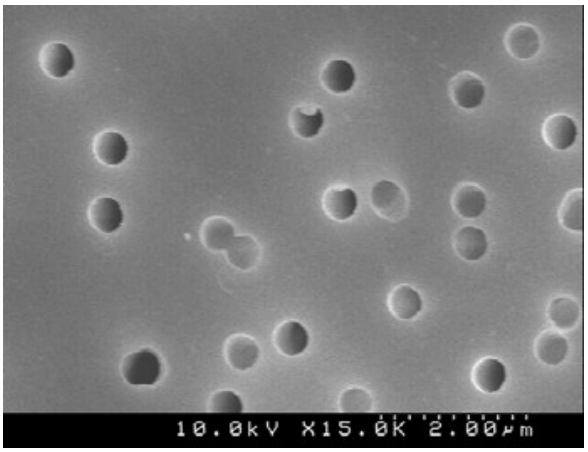

Figure 2.11 TEM image for microporous track etched membranes [59]

2.4.3. Expanded film membrane

A less common microporous membrane is an expanded-film membrane. They are oriented crystalline polymers with voids created by an extrusion and stretching process as shown in Figure 2.12. The material is extruded near its melting temperature using a rapid draw-down rate. Then, the extruded material is cooled, annealed, and stretched up to 300% of its original length. This stretching process creates slit-like pores ranging in size from 20 to 250nm [60].

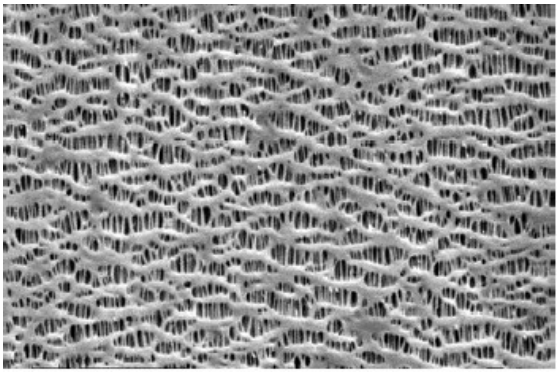

Figure 2.12 TEM image for microporous pore stretching like membranes [60]

2.4.4. Preparation of CS films

There have been different ways for preparing CS membranes. According to Muzarelli, CS solutions were prepared by dissolving about 1–2gm of CS in 100mL of 1% (v/v) aqueous acetic acid solution. All dried membranes were mounted on a stainless steel holding device and immersed in 2% NaOH aqueous solution for a given time to ensure the complete removal of residual acid from the membranes. These membranes were washed thoroughly in deionized water until a neutral pH, dried in air for 48 h and then in vacuum at 50–60 ºC for 24 h [61].

Kouchak work, on the other hand, provides another simple and efficient way to prepare CS/poly vinyl alcohol films with controllable network structure by solution casting. This selective method exhibited the features of simplicity, high-efficiency and controllability [62].

Moreover, CS thin film were also prepared by solution casting and solvent evaporation techniques. In brief, 1 wt.% CS solution prepared by dissolving CS powder in 2 wt.% acetic acid was cast as film on clean glass plate [63]. Finally, CS thin film with high porosity and good mechanical properties were prepared from CS using silica particles as porogen. By controlling the size of the silica particles (5, 10, and 15-40*n*m), the desired equal pore size can be easily achieved. Larger sizes of silica particles provide larger pore sizes and higher flow rates[64].

2.4.4.1. Cross-linking of CS membranes

Cross-linking is the most popular modification for CS thin films; it results in the formation of CS nanoparticles which exhibit unique properties at the nanoscale

regime compared to the non cross-linked CS. Factors affecting physical cross-linking of polymers vary from the type, concentration of the cross-linking agent, and the cross-linking time. Higher concentrations of cross-linking agent were reported to induce rapid physical cross-linking process. Generally, it leads to the decrease in polymer crystallinity and the shrinkage of crystal size. Moreover, the increase in length of the molecular chains between bonds upon cross-linking, decreased the pore volume and surface area leading to a growth in the pore size as shown in Figure 2.13, and a decrease in the tensile strength due to the decrease in surface area of the membrane [65].

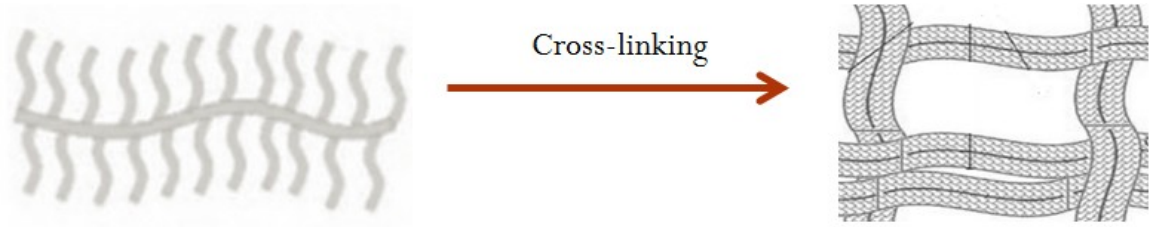

Figure 2.11 Formation of ionic cross-links between amino groups of chitosan and TPP groups [65]

Cross-linking of CS improve the mechanical properties of CS thin film, its abundant amino and hydroxyl groups enable nanoparticles formulation via both physical and chemical cross-linking. Covalent cross-linking is usually achieved by treatment of CS solutions by glutaraldehyde solution which reacts with the amino groups on CS chains to form Schiff bases [66]. Physical cross-linking of CS, on the other hand, is a typical non-covalent interaction, which can be realized by the association with negatively charged multivalent ions such as sodium tripolyphosphate (TPP) [67]. Physical cross-linking is more promising method since cross-linking is a reversible process and could largely avoid potential toxicity of the reagents [67]. Diverse efforts have been made to obtain CS nanoparticles via TPP cross-linking following the pioneering work of Calvo et al. A number of studies on the cross-linking reaction have been reported and shows that it is mainly influenced by the size and type of the cross-linker agent and the functional groups of CS. The smaller the molecular size of the cross-linker, the faster the cross-linking reaction, since its diffusion is easier [68].

However, concern over the disintegration of CS micro particles has led to their modification by cross-linking to make a rigid polymer to be used as a core material in controlled drug release research for example. For this purpose, a large number of studies on cross-linking with different agents involving bonds with CS amino groups have been reported [69-71]. Different studies shows that CS cross-linked with TPP has the highest mechanical resistance and chemical stability together with membrane flexibility compared to other cross-linking agents [72-73].

2.4.4.2. Addition of filler

Early1970s, minerals were only used in polymers as fillers commercially aiming to reduce the costs, since these fillers are heavier and cheaper than the added polymers. During the 1970s, there was a vertiginous and successive increase in the petroleum price during and after the 1973 and 1979 crises. These facts led to an expansion of the ceramic raw materials as fillers [74].

Nevertheless, only in the late 1980s was the great landmark in the polymer clay nanocomposite published by Toyota regarding the preparation and characterization of polyamide 6/organophilic clay nanocomposite to be used as timing belts in cars [74-76]. This new material, that only had 4.2 wt.%, had an increase of 40% in the rupture tension, 68% in the Young modulus and 126% in the flexural modulus as well as an increase in the heat distortion temperature from 65^{o}C to 152^{o}C in comparison with pure polymer [77].

2.4.4.3. Addition of nanofiller

The incorporation of nanoparticles into polymeric thin films have been a trend to overcome some of the existing disadvantages such as mechanical strength, chemical incompatibilities with process solutions and temperature limitations. Careful experimental studies in order to select the most appropriate type and composition of nanofillers added to polymeric thin film to fabricate PNCs. PNCs are a class of hybrid materials composed of an organic polymer matrix with dispersed inorganic nanofillers ,with unique properties, combining the advantages of the inorganic nanofillers (e.g., rigidity, thermal stability) and the organic polymers (flexibility, dielectric, ductility, and processability). The inorganic nanofillers have large surface area, leading to a dramatic increase in interfacial area. These nanofillers,

even at very low concentrations, can strongly change the macroscopic properties of the polymer [78-79].

Nanofillers include nanotubes, nanoparticles and nanosheets as shown in Figure 2.14 [80]. Nanoparticles have been widely used as reinforcements to enhance the physical and morphological properties of polymers. One of the most interesting reinforcement materials is Graphene which is considered as a promising nanofiller due to its excellent mechanical, thermal and electrical property, combining with its ultra-high surface area and economical sources. There are several structures of graphene including, 0-D Fullerenes made by wrapping a section of graphene sheet. Graphene has an affinity to organic compounds and polymers due to the presence of multi-pores, functional acids and OH groups on its surface. This enables polymers to be absorbed into the pores besides its high levels of stiffness and barrier effect [81].

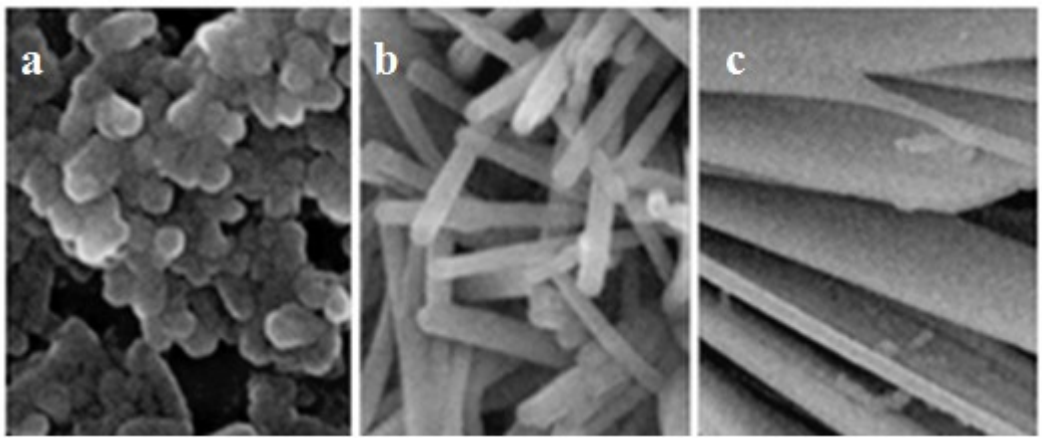

Figure 2.12 SEM image for (a) Clay nanoparticles (b) nanotubes and (c) nanosheets [82].

Many review articles have been devoted to polymer/nano porous nanofiller nanocomposites, few review articles focus on performance of polymer/mesoporous nanocomposites. Permeability is the main parameter that characterize the performance of a membrane material. High free volume natural polymers were lately introduced, providing very high permeability values [83]. The dispersal of nanofillers into the polymer matrix affects the barrier properties of a homogeneous polymer film in two specific ways. The first way is by creating a tortuous path for gas diffusion [84].

Because the filler materials are essentially impermeable inorganic crystals, gas molecules must diffuse around them rather than taking a (mean) straight line path that lies perpendicular to the film surface. The result is a longer mean path for gas diffusion through the film in the presence of fillers, as illustrated in Figure 2.15 [85].

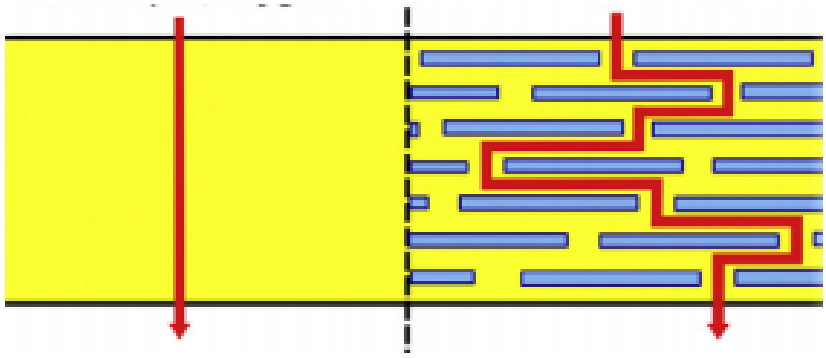

Figure 2.13 Illustration of the ‘‘tortuous pathway’’ created by incorporation of nanofillers into the polymer matrix [84].

In addition, filler particles can influence the molecular absorption behavior in two principal ways, where the solubility of the filler differs from the polymer matrix, and then the absorption can be either increased or decreased depending on the relative solubility of the molecule in the matrix and filler [85]. Most common inorganic filler particles (e.g. glass or carbon fibers, talc, clays, silica) are usually considered as impermeable in comparison to a polymer matrix. Inorganic nanoparticles such as Al_2O_3, TiO_2, ZrO_2, SiO_2 ZnO can be used for reinforcing or toughening polymeric materials [40]. Recently, these particles were incorporated into PVDF membranes and the effect on membrane properties including mechanical enhancement, hydraulic performance and fouling resistance was evaluated. Moreover, Nanoclay, which is of relatively low cost and commercially available, has been widely investigated as nanofiller for nanocomposite materials which have enhanced mechanical properties [85-86].

Moreover, many studies on the enhancement of the mechanical properties of polymeric membranes upon addition of nanofillers have been reported.. For example, tensile strength measurement results show an increase in the tensile modulus with $CaCO_3$ nanoparticles loading. Moreover, tensile strength and elongation at break show gradual improvement with the addition of up to 1 wt% of nanosized $CaCO_3$. Decreasing performance of these properties is observed when loading of more than 1

wt% of nano sized $CaCO_3$. The increase in tensile modulus must be caused by rigidity of the filler and strong interaction between the polymer and filler due to the large interfacial area between particles [33]. The enhanced composite modulus as a result of nanofiller loading has also been reported by several research groups.

2.5. Evaluation of membrane performance

2.5.1. Statistical analysis

Conducting an experiment is a procedure associated with many variables. Random patterns for doing the work will make it impossible to cover all variables and outcomes consistency. As a consequence, the need for an organized framework for doing experiments is a necessity. One factor at a time was the old trend used as an experimental framework methodology, which many researchers had relied on in the past [87]. It consists mainly of controlling all factors, fixing their values and varying one factor at a time. However, this method is considered invalid as does not consider the interactions between other variables; in addition, it needs a huge number of experiments to be performed, which is a waste of time and money . Unfortunately, many practitioners are still using this method which does not ensure obtaining valid results [87]. Accordingly, an alternative method was needed to design an organized framework with interaction consideration and minimum possible number of experiments which will draw valid conclusions. Design of experiments (DOE) is the alternative method that has gained an increasing attention. DOE saves time, money, and effort by providing valid results with a minimal number of experiments. It plays a crucial role in engineering design, development, and improvement of manufacturing processes. Developed products and processes from designed experiments have led to better performance, higher reliability, and lower overall costs. In addition, designed experiments are a reason for lead time reduction for engineering design and development activities [88].

In an experiment, built from the beginning using this design, purposeful changes could be made in the controllable variables of the system or process. In addition, observation of the resulting system output data and decisions could be made about which variables are responsible for the observed changes in output performance [87]. When designing experiments, there are controllable factors, uncontrollable factors, and responses. Controllable factors are the parameters set to predefined levels.

Uncontrollable factors are the ones that cannot be controlled in actual operations, but may be controlled during experimentation such as weather conditions or natural disasters. Responses are the output results obtained from experiments [89].

Typically, DOE has two main tasks: the first is setting efficient experimental design points i.e. building an efficient design with a minimum number of distinct runs or experiments. Distinct runs are the most important runs settings of the experiment at which response behavior is best tracked; therefore, valid conclusion could be drawn, and a valid model of the response could be obtained. The second task is analyzing the factors involved within the experiments and showing the most important ones i.e. knowing the most affecting factors on the response [88].

Moreover, DOE has three main branches; experiments with dependent, independent, and hybrid factors. Experiments with dependent factors are concerned with factors having certain levels that are interacting in an experiment and are independent from each other affecting the response in a certain way. Several experimental designs are available in this case including factorial, Box-Wilson Central Composite, and Orthogonal designs. Factorial design is a type of design where runs are performed at all possible combination of factors' levels [88]. Box-Wilson Central Composite Design, on the other hand, is known as central composite design. It contains an imbedded factorial design, in addition to center points, which is increased with a group of star points. The main reason behind adding star points is to allow curvature estimation. Finally, orthogonal design is distinguished with its ease of use for allocating factor levels and their efficiency. In the orthogonal design, factors' settings involve allocating levels by using an orthogonal array designed by Taguchi. It is based on a standard table containing a number of levels in columns and a number of factors in rows arranged in a way defined by Taguchi to get the number of experiments and combinations; factors with required level in each particular experiment, minimizing the number of experiments needed when comparing to full factorial design [89].

The Response Surface Methodology (RSM) is also extremely useful as an automated tool for model calibration and validation, especially for modern computational multi-agent large-scale social-networks systems that are becoming heavily used in modeling and simulation of complex social networks. It is a collection of mathematical and

statistical techniques useful for modeling and analysis of problems in which a response of interest is influenced by several variables, where the objective is to optimize the response. The response surface is usually presented graphically to help visualizing the shape of the response; the contours of the response surface are plotted as shown in Figure 2.16. In the contour plot, lines of constant response are drawn in the x1, x2 plane. Each contour corresponds to a particular height of the response surface [90].

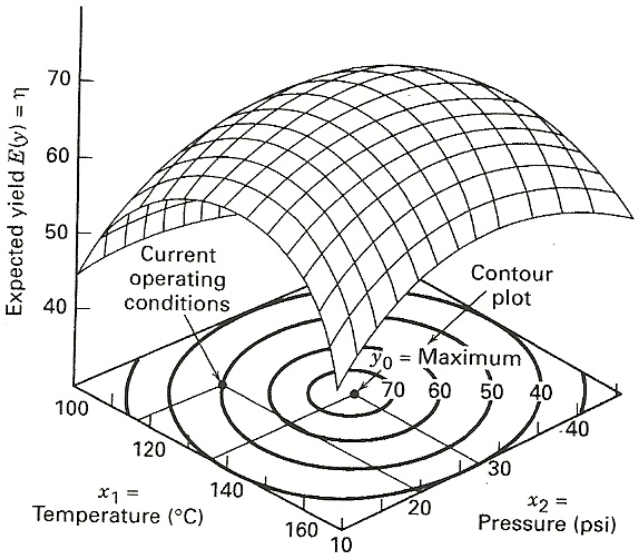

Figure 2.14 A contour plot of a response surface [90]

In most RSM problems, the form of the relationship between the response and the variables is unknown. It consists of the experimental strategy for exploring the space of the process or independent variables, empirical statistical modeling to develop an appropriate approximating relationship between the yield and the process variables, and optimization methods for finding the values of the process variables that produce desirable values of the response. Thus, the first step in RSM is to find a suitable approximation for the true functional relationship between (y) and the set of independent variables. The response might be well modeled by a linear function of the independent variables, then, the approximation function is the first order model. If there is a curvature in the system, then a polynomial of higher degree must be used such as the second order level. It is unlikely that a polynomial model will be a reasonable approximation of the true functional relationship over the entire space of

the independent variables for a relatively small region [91]. RSM is a sequential procedure, when there is a point remote from optimum such as the current operating conditions shown in Figure 2.17, there is a little curvature in the system and the first-order model will be appropriate. RSM leads the experimenter rapidly and efficiently along a path of improvement toward the general vicinity of the optimum. Once the region of the optimum has been found, a more elaborate model such as the second - order model is employed [91].

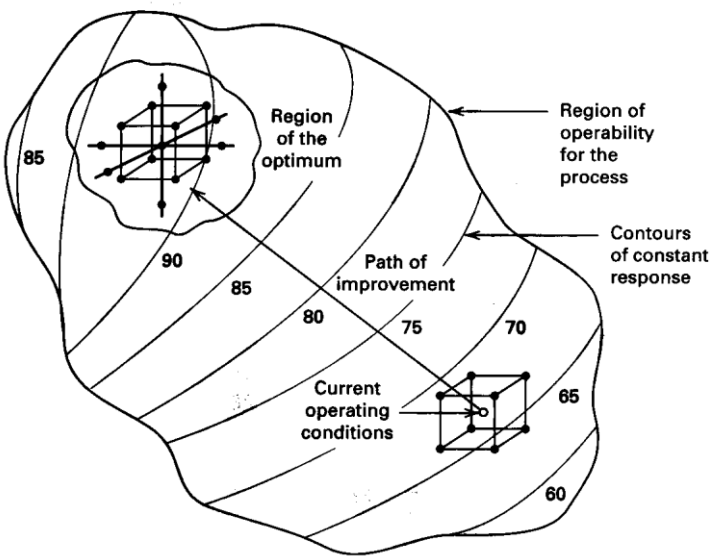

Figure 2.15 Sequential nature of RSM [91]

Design-Expert 9.0.1 software offered by Stat-Ease Inc, is one of the best specialized software in experimental design as it is used by many specialized researchers in this area. Typically, there is an algorithm in the software that is applied in all methods till reaching the most feasible model fit; using Design-Expert. The application of this algorithm helped reaching a final model with appropriate fitting equation, minimum possible error, and lack of fit. The flowchart shown in Figure 2.18 explains the steps of the algorithm. For validating the model, a step was added to the algorithm "Extend the model with new points. It was followed by a removal of outlier step to minimize any noise affecting the model. The *Decision* of an adequate model or not was based on the model analysis; represented in "Fit Summary", "ANOVA", "Case statistics", and "Graphical displays", obtained from Design-Expert output. Model verification is making sure that the model performs as intended; i.e. ensuring that no mistakes have

been made in implementing the model. However, no computational model will be 100% free of errors. A properly structured good software; Design-Expert, will increase level of certainty in the model [89]. Typically what are tested are the proper implementation of the algorithm and the minimum model content of errors, mistakes, or bugs. Model validation is concerned with whether the model is representing and imitating the performance of a real world system. The ultimate goal of model validation is to make the model useful in the sense that it provides accurate information about the system being modeled, and to make the model actually used. This is achieved when the model predictions are almost matching experimental data. The model verification is done to the "adequate model" obtained after the "Model reduction (outliers' elimination)" step in the algorithm; where it is checked for errors, and the algorithm proper implementation. The next step was added to the algorithm to validate the model; where additional experimental data were added to check the model prediction adequacy or the truly imitation of real word system [89].

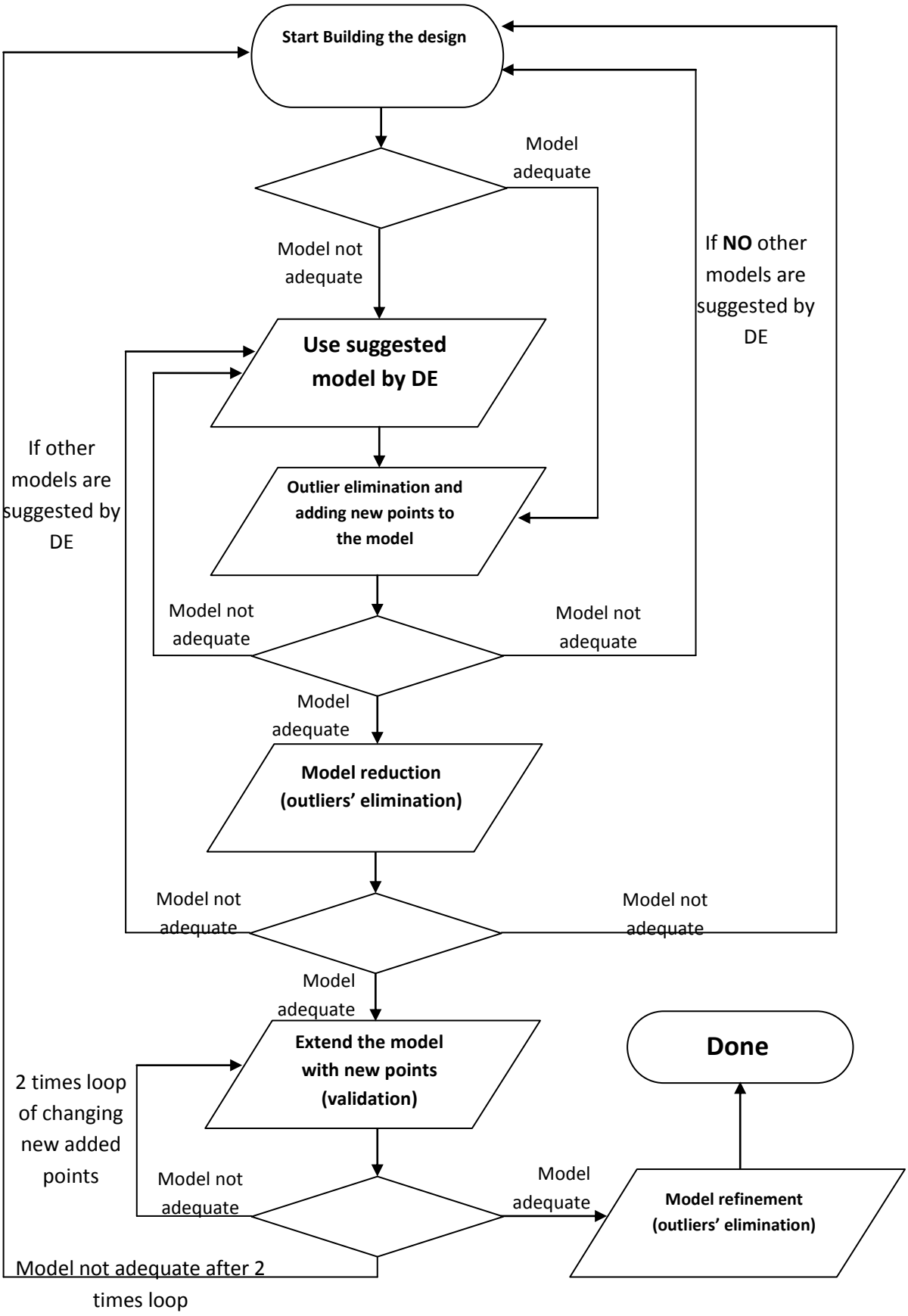

Figure 2.18 Steps of the software algorithm [89]

Mead and Pike used RSM in agronomy and product development in 1975. Moreover the utility of RSM in toxicological studies has been demonstrated by Carter et al. RSM involves the development of mathematical models and equations that relate the biological response to the concentrations of the agents used. The model indicates the relative importance of each agent in producing the response. In addition, RSM can predict the response that would occur if combinations of concentrations different from those investigated experimentally were used [91].

2.5.2. Finite Element Analysis

The understanding of gas mass transport through thin films has become increasingly important in technological applications. Permeation is a mass transport process in which molecules transfer through the polymer from the 'exterior' environment to the 'interior' environment as mentioned earlier. The model the diffusion of molecules through the material is driven by concentration gradients. The driving force for mass transport includes diffusivity and permeability. According to Fick's laws, the diffusion flux is proportional to the negative gradient of concentrations. It goes from regions of higher concentration to regions of lower concentration. The measurement of diffusivity is very complicated, so finite elements analysis (FEA) will be used to calculate diffusion numerically [92].

Abaqus is a software application used for modeling and analysis of mechanical components and assemblies, mass diffusion analysis and visualizing the finite element analysis result. Abaqus/Standard provides modeling of steady-state diffusion of one material through another, using governing equations that are extension of Fick's equations, to allow for non uniform solubility of the diffusing gas in the base material. Permeability is also defined in this software as a function of void ratio which is related to the pore size in the thin film. The basic solution variable is the "normalized concentration (C/S), where *C* is the mass concentration of the diffusing material and *S* is its solubility in the base material. To select the right membrane for a given gas separation is very challenging as the criteria is quite complex. The first choice is usually based on favorable flux and selectivity for a given gas which are determined by FEA [93].

In addition to gas permeation simulation in polymeric membranes, much progress has been attained on the theories whereby the mechanisms of transport are described. Amooghin *et., al.* presented an algorithm for direct determination of diffusion coefficient. It determines diffusion coefficient by two approaches: first, through the traditional time lag method, and second, considering the concentration dependent system. A comprehensive mathematical model was developed and solved for CO_2 gas permeation through a nonporous polymeric membrane. The results shows that considering the concentration dependent system (CDS) for diffusion coefficient led to the small deviation of about 13%, while the deviation of 360% by the concentration independent system (CIS) was acquired. Finally, a reasonable conformity between the predicted values based on concentration dependant method and experimental data was perceived [94].

Sablani et al. reported that polymer-layered silicate nanocomposites improved the gas barrier properties of food packaging polymers. They developed a computer simulation model using the commercial software, COMSOL Multiphysics to analyze changes in oxygen barrier properties in terms of relative diffusivity, influenced by volume fraction, aspect ratio, intercalation width, and orientation angle of nanoparticles. Diffusivity increased as the rotational angle increased. It also increased drastically as θ changed from 15° to 30°. Nanoparticles with exfoliation configuration exhibited better oxygen barrier properties compared to intercalation. The finite element model developed in this study provides insight into oxygen barrier properties for nanocomposite with a wide range of structural parameters[95].

On the other hand, Morehouse et al. used finite element modeling to predict the uni-axial deformation of microporous phase inversion membranes. Pore area, pore aspect ratio, and stress were studied as part of the modeling work. In order to adequately predict the change in pore shape due to the deformation two separate models were constructed. The models were formed in ABAQUS, a finite element solver commonly used for deformation modeling. One model predicts the initial phase of membrane deformation in which pores transition from a random alignment with respect to the direction of stretching to a uniform alignment in the direction of stretching. The second model is used to predict the deformation of the membrane pore structure after all pores have been aligned in the direction of stretching [96].

Chapter 3

MATERIALS AND METHODS

3. Materials and Methods

3.1. Materials

3.1.1. Materials for Fabricating Synthetic Polymer (LDPE) Thin Films

Figure 3.1 shows Low density polyethylene (LDPE) in the form of pellets as received. It has hardness = 68 Shore, density= 0.919 g/cm^3 MW = 28000, Tm around 120 °C. Tg < -100 °C. it was purchased from AG trading, Egypt. Xylene (anhydrous, ≥ 99%) purchased from Sigma Aldrich was used as a solvent for LDPE.

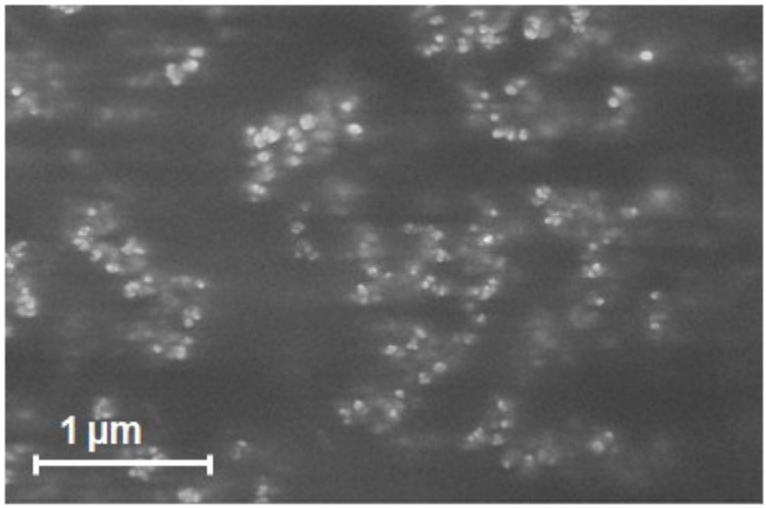

Figure 3.1 SEM for LDPE Pellets

3.1.2. Materials for Fabricating Natural Polymer (CS) Thin Films

Shrimp shells were purchased from the Egyptian local market. Chitin was extracted from the shells, and the shells were deproteinized by boiling them repetitively in a solution of 1N sodium hydroxide (NaOH) in multi-sequential steps as shown in Figure 3.2. They were demineralized using 1N hydrochloric acid (HCl). Chitin was partially deacetylated using 50% NaOH to obtain chitosan [97]. Pure, commercial-quality chitosan, MW 60,000-120,000, Chitosan, ≥93% (w/w), was purchased from Primex. Chemicals used for dissolving chitosan were purchased from Sigma Aldrich. These included NaOH; HCl; acetic acid (Ac-OH, 99% purity); ethanol (99.5% purity), which was used for chitosan film fixation; sodium tripolyphosphate (TPP), used to synthesize chitosan nanoparticles; phenolphthalein (phph, 99% purity), used as an

indicator for NaOH in testing liquid permeability of thin films; and methanol (99.9% purity), used for cleaning glassware.

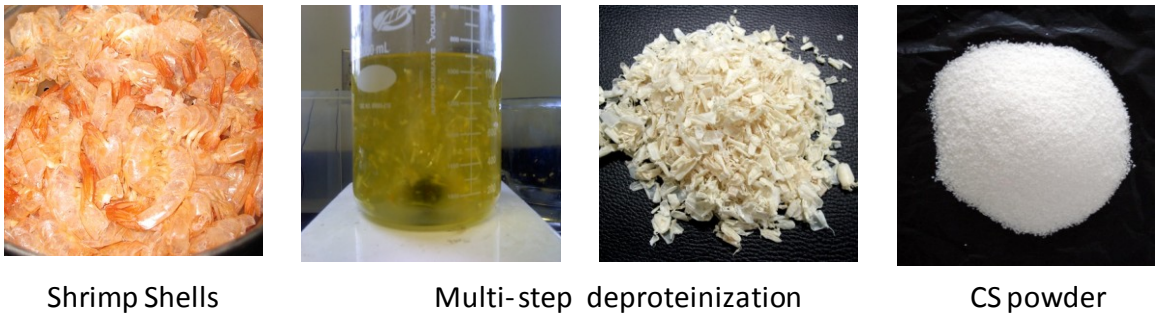

Figure 3.2 Preparation steps of shrimp shells to produce Chitosan [97]

3.1.3. Nanofillers for Fabricating LDPE, CS Thin Films

G-nanofiller shown in Figure 3.3(a) (Sky Spring Nanomaterials, Inc. USA), and F-nanofiller shown in Figure 3.3(b) (Carbon 60, 99.5+%, SES Research, USA), were used to produce the PNC thin films. Graphene is carbon atoms, densely packed together into a honeycomb shaped crystal lattice. Fullerenes are an allotrope (physical arrangement of atoms) of carbon distinct from both graphite and diamond. The difference in morphology (Flaky vs spherical) and nano clusters size between F and G had a significant effect on the tensile and barrier properties of the membranes. he decades since the discovery of fullerene have been fruitful ones. The similarities between fullerenes and graphene lie in their molecular structures.

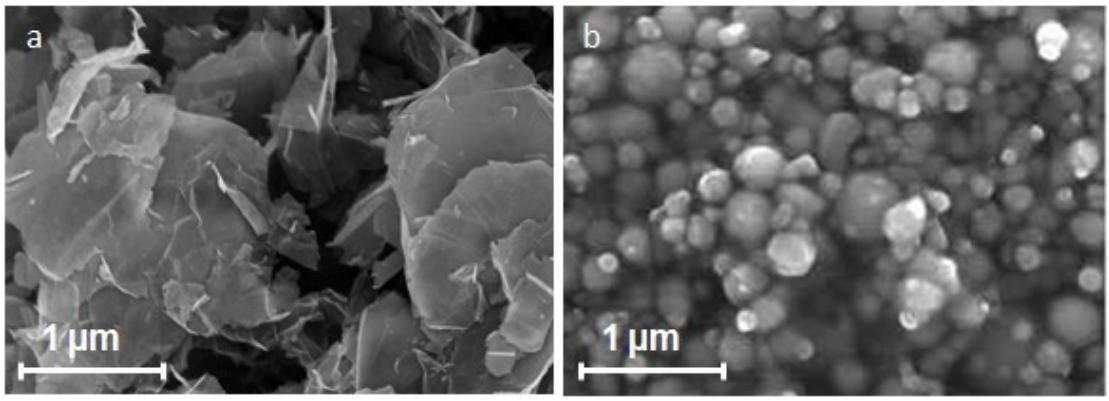

Figure 3.3 SEM Image for (a) G-nanofiller (b) F-Nanofiller

3.2. Thin Film Processing

3.2.1. Synthetic Polymer (LDPE)

To prepare the LDPE thin films, 20g of LDPE pellets was dissolved in 200mL of xylene solvent at room temperature. The mixing of F and G with LDPE occurred with constant stirring for 24hrs with a VWR® Standard Analog Shaker, to form a clear homogeneous solution. The LDPE/F and LDPE/G filtrate were poured into two separate flattened containers and left to dry at room temperature to form thin films with a 2 mm thickness, as shown in Figure 3.4.

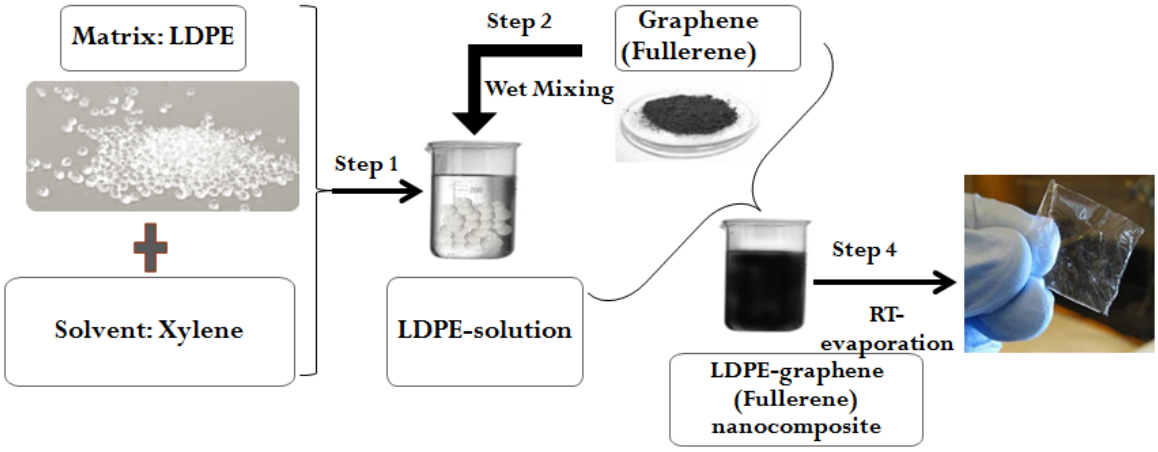

Figure 3.4 Fabrication of LDPE Membrane

3.2.2. Natural Polymer

To prepare the CLCS thin films, 0.2g of CS was dissolved in 2% acetic acid at room temperature with continuous stirring. A cross-linking agent (TPP) was added to the CS solution.

3.2.2.1. Cross-linking of Chitosan

0.033gm TPP was dissolved in 11mL distilled H_2O and was added by drops onto the CS solution during the homogenization at 10,000 rpm for 30 min using a Polytron homogenizer PT 10-35GT.

3.2.2.2. Addition of nanofiller

CLCS and NCLCS solutions were mixed with two nanofillers (F and G) with 0.1, 0.5, 1 wt. % by solvent mixing. Mixing occurred with constant stirring for 60 min with a VWR® Standard Analog Shaker to form a clear homogeneous solution. The solutions were used to produce non cross-linked CS nanocomposites (NCLCS/G and NCLCS/F), as well as the cross-linked CS nanocomposite (CLCS/G and CLCS/F) thin films. The NCLCS and CLCS filtrate were poured into two separate flattened containers and left to dry at room temperature to form CS thin films with 0.2mm thickness. The dry thin films obtained from the NCLCS and CLCS solutions are shown in Figure 3.5. The same procedure was used for the CLCS/G, CLCS/F, NCLCS/G, and NCLCS/F. The as received F and G diameters were 10µm and 15µm respectively. Upon sonication and forming a solution the F and G were transformed to clusters of size 2nm and 10 nm respectively [98].

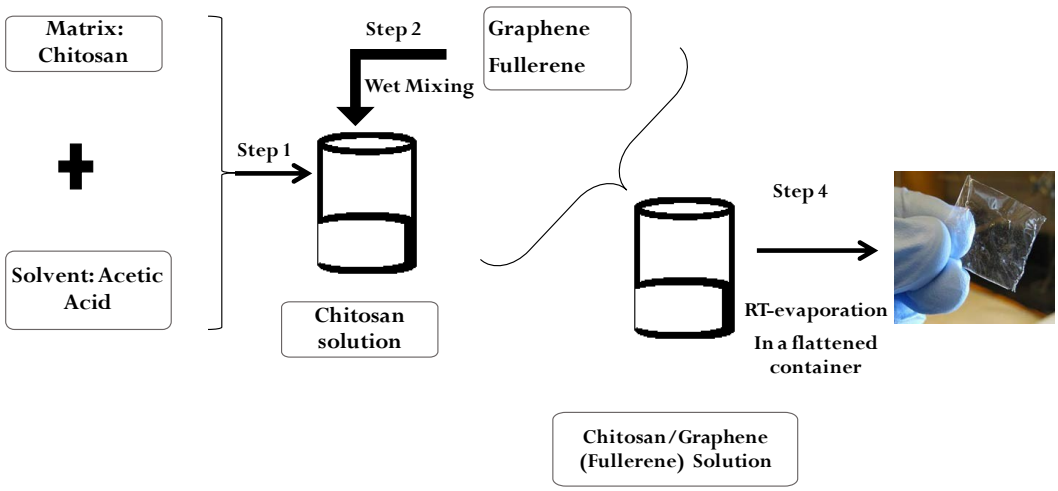

Figure 3.5 Fabrication of CS Membrane

3.3. Process Selection Procedure

The overall goal of process selection was performed to illustrate how systematic selection procedures can be used to select the optimum materials for a given component by analyzing the material performance requirements for a given

application. The material performance requirements can be divided into three broad categories: functional requirements, processability requirements, and reliability requirements. In this work the fabrication of membranes requires a proper knowledge of materials properties, design concepts and their interactions. The large number of available materials, together with the complex relationships between the various selection parameters, often makes the selection process a difficult task. When selecting materials, a large number of factors should be taken into account. These factors range from mechanical to electrical to physical properties. The main concerns in this work are the mechanical (yield strength) and physical properties (e.g. controlling porosity) due to the packaging and filtration applications for the fabricated membranes.

3.3.1. Digital Logic Method

The determination of relative importance of performance goals was made using the digital logic (DL) method. Evaluations were arranged such that only two properties were considered at a time. Every possible combination of properties or performance goals was compared and no shades of choice were required, only a "yes" or "no" decision for each evaluation was considered. To determine the relative importance of each property or goal, a table was constructed, the properties or goals were listed in the left hand column, and comparisons were made in the columns to the right. The properties selected to compare the different membrane materials were porosity, toxicity, biodegradability, biocompatibility, antimicrobiability, yield strength and ductility.

Comparing two properties or performance goals, the more important goal was given a numerical value of one (1) and the less important was given zero (0). The total number of possible decisions was

$$N = n(n-1)/2 \quad (1),$$

where n is the number of properties or goals under consideration.

A relative emphasis coefficient or weighting factor for each goal was obtained by dividing the number of positive decisions for each goal over the total number of possible decisions (N) [99].

3.3.2. Weighted Property Method

In most applications, the selected material should satisfy more than one functional requirement. In this method, each material requirement (or property) was assigned a certain weight, depending on its importance to the performance of the design. This method attempts to quantify how important each desired requirement was by determining a weighting factor, and then quantify how well a candidate material satisfies each requirement by determining a scaling factor [99].

3.3.3. Scaled Properties

For scaling candidate material properties, each property was scaled so that its highest numerical value did not exceed 100. When evaluating a list of candidate materials, one property was considered at a time. The best value in the list was rated as 100 and the others scaled proportionally. For properties like corrosion or wear loss, weight gain in oxidation, or density, a lower value was more desirable. In such cases, the lowest value was rated as 100 [99].

3.3.4. Performance Index

After ranking and scaling of alternatives, candidates that have the most promising performance indices can each now be used to develop a detail design. The material performance index was calculated according to the equation[99].

$$\gamma = \Sigma Bi\alpha i \quad \text{.....(2)}$$

where, γ is Performance index, Bi is Scaled property and αi is Weighing Factor

3.4. Characterization of the Fabricated Thin Films

The morphology, pore size, liquid permeability, gas permeability, melt flow index (MFI), thermo gravimetric analysis (TGA) and mechanical properties of thin films were determined using different techniques including scanning electron microscopy (SEM), porosimeter (micrometrics ASAP 2020), Gas permeability tester (GDP-E Brugger Feinmechanik GmbH), melt flow indexer (A Ray-Ran Co. England melt flow

systems), TGA analyzer Q series (Thermo Fisher Scientific, USA), and Instron universal testing machine (100KN, Instron, England).

3.4.1. Scanning Electron Microscopy (SEM)

LDPE, NCLCS and CLCS thin films and their nanocomposite counterparts reinforced with F and G- nanofiller were analyzed using a SEM (FESEM, Leo Supra 55 – Zeiss Inc., Germany). High standard zoom secondary electron (SE2) lens was used with a range of 6-8 KV to prevent deteriorating the polymeric thin film. The SEM samples had to be clean, dry, with a conductive surface, which was grounded. The thin films were cut to 1cm x 1cm and mounted on carbon tape to reduce charging with a small aperture [100]. Image J analysis software was used to determine the pores size, shape and distribution before and after tensile testing as a function of variable temperatures[101] .

3.4.2. Pore Size Characterization

The porosimeter was employed for determining the average pores size as a function of variable temperatures for LDPE, NCLCS and CLCS thin films and their nanocomposite counterparts reinforced with F and G- nanofillers. The pore size tests were carried out by using a porosimeter (Micrometrics ASAP 2020 version 1.00 software) that included powerful data reduction to provide a variety of reports including pore volume, pore size, and pore surface area [102]. It was used to determine the pore size, pore volume and surface area of the internal pores of LDPE, NCLCS and CLCS and their nanocomposite thin films.

3.4.2.1. Procedure for Pore Size Measurements

The samples were cut into 1mm pieces and placed in a specified glass tube that was fixed into the apparatus as shown in Figure 3.6. The instrument has two independent vacuum systems allowing simultaneous preparation of two samples and the analysis of the other. The technique depends on condensing nitrogen gas in the pores and derives pore volume from quantities of gas converted to liquid.

Figure 3.6 Porosimeter for Pore Size Measuring

3.4.3. Liquid Permeability Characterization

Liquid permeability of thin films was tested by passing the NaOH solution through an inlet into a glass beaker containing a phenolphthalein indicator, which changes the color of the solution in the presence of NaOH from colorless to pink. A prototype composed of two polymeric parts, the top part (solution inlet) and the bottom part (solution outlet) as shown in Figure 3.7 was carefully designed and fabricated.

3.4.3.1. Procedure for Liquid Permeability Measurements

The setup was designed to have both top and bottom parts with central cylindrical holes in order to allow for the diffusion of NaOH solution passing through the thin film which was placed horizontally between the top cover and the bottom cup. The time taken for the NaOH solution to pass through the porous thin film onto a glass beaker containing phenolphthalein indicator determined the permeability of each CS thin film.

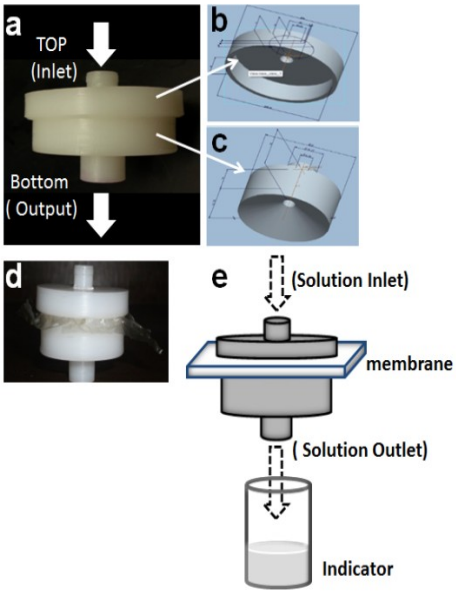

Figure 3.7 A Schematic Illustration of the Designed Set Up Composed of Two Polymeric Cylindrical Parts for Measuring Liquid Permeability of All Fabricated CS Thin Films [97]

3.4.4. Gas Permeability Characterization

Gas permeability determination was performed using a permeability testing apparatus Type GDP-E (Brugger Feinmechanik GmbH) as shown in Figure 3.8. The apparatus has a fast and exact display even for very low permeability up to 0.5mL/m^2 d bar. Thin films were analyzed to determine the permeability, diffusion and solubility constants of the gas in the film. In this work, oxygen gas was used to proof the porosity of the prepared thin films. The oxygen permeability tests were performed three times for each sample to ensure reproducibility. The test was performed three times at intervals of three weeks to ensure the stability of the fabricated thin films and to be certain that time had no effect on the permeability of the thin film.

Figure 3.8 Gas Permeability Tester

3.4.4.1. Procedure for Gas Permeability Measurements

The external computer evaluates data recorded by the GDP-E. Test results are written using Access software to allow data export. After setting predefined evacuation periods within the range of 10 seconds through 48 hours, the test was executed automatically. The permeation of the test specimen may be determined within a temperature range of -20 °C through 60 °C.

3.4.5. Finite Element Analysis

The input data for ABAQUS software included the geometry of the membrane, which was constructed with a specific thickness, after which the material properties were specified. These included diffusivity and the solubility of oxygen gas through the fabricated membranes [92]. The input data varied according to the material it would diffuse in, whether pure polymer or polymer reinforced nanocomposite. The first step was constructing the membrane followed by assigning each material to the solid homogenous section. This was followed by specifying the steady state mass diffusion and then specifying a time increment and a time period for the step. Abaqus/Standard then proceeded through the step accordingly. The boundary conditions were applied at the inlet to the nodes in the mass diffusion element to prescribe values of normalized concentration as shown in Figure 3.9. This was followed by applying a surface

concentration flux, as concentration fluxes were the only loads that could be applied in a mass diffusion analysis step. Finally, meshing was optimized to assure convergence of the solution when choosing the DCC3D8 element (the 8-node convection/diffusion brick). There were no applicable element controls for this type of element [92]. The normalized concentration output shown in Figure 3.9 was measured through the thickness of the one-layer membrane (2mm). The normalized concentration of the diffusing molecules passes through a diffusion pathway from high concentration at the inlet to lower concentration at the outlet. The output was calculated at three different temperatures (23, 30, 60 ºC).

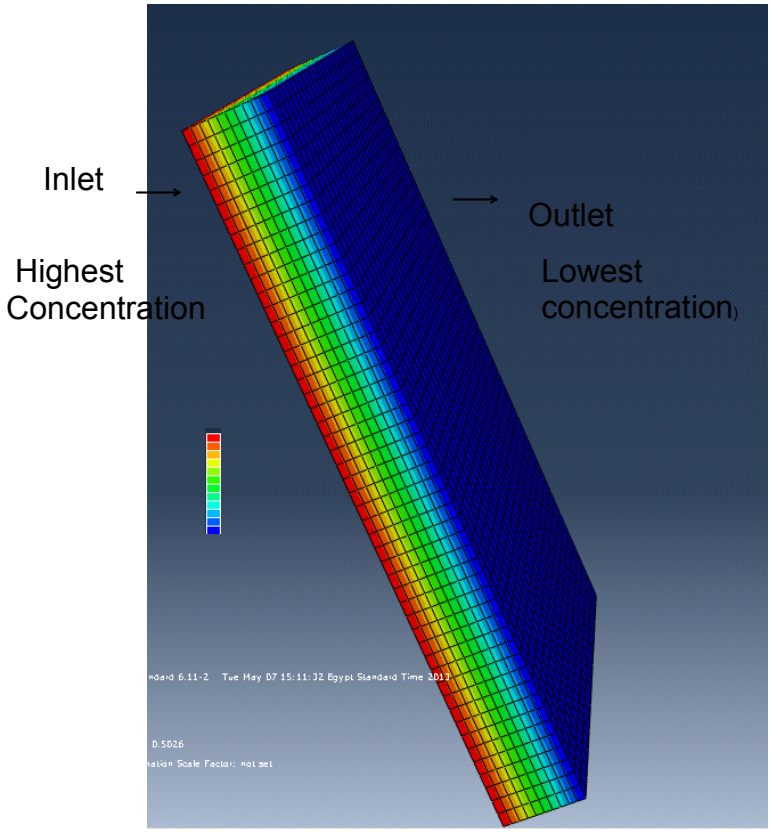

Figure 3.9 Inlet and outlet normalized concentration through the membrane thickness

3.4.5.1. Procedure for Finite Element Analysis

ABAQUS requires the following input data:

- Diffusivity behavior through the command DIFFUSIVITY, Isotropic
- Solubility properties using the SOLUBILITY command
- Mechanical properties (density, conductivity, specific heat) if needed

- TYPE=TEMP to define temperature dependence
- LAW=Ficks
- INITIAL CONDITIONS TYPE=CONCENTRATION
- NSET or node number, initial normalized concentration value at the node(s)
- Steady state, defined as the point in time when all normalized concentrations change at less than a user defined rate.
- Load magnitude of a concentrated concentration flux, controlled by referring to an amplitude curve.
- The membrane constructed with a specific thickness followed by specifying several materials and their properties including diffusivity and solubility.
- Assigning each material to the solid homogenous section
- Specifying the initial step and step 1 (mass diffusion, steady state) with iterations of increment sizing to reach convergence of the solution. The boundary conditions are specified at the initial step.
- Applying a surface concentration flux load as concentration fluxes are the only loads that can be applied in a mass diffusion analysis step
- Meshing optimized to assure convergence of the solution when choosing DCC3D8 the 8- node convection/diffusion brick. There was no applicable elements control for this mesh element.

3.4.6. Melt Flow Index (MFI)

The viscosity of NCLCS and CLCS thin films and their nanocomposite counterparts reinforced with F and G nanofillers were measured using a melt flow indexer (MFI) (A Ray-Ran Co. England melt flow systems) as shown in Figure 3.10. In this technique, a stainless steel cylinder was placed on top of the thin film and then placed inside a column. The selection of the cylinder's weight was in accordance with ASTM D-1238 and the weight was selected to be 2.16 kg at 210 ºC [103].

3.4.6.1. Procedure for Melt Flow Index (MFI) Measurements

Four grams of polymer sample was packed properly inside the extruder barrel to avoid formation of air pockets. A piston was introduced, which acted as the medium responsible for the extrusion of the molten polymer. The sample was preheated for a specified amount of time. After preheating, a specified weight was introduced to the piston. Examples of standard weights are 2.16 kg and 5 kg. The weight exerted a force

on the molten polymer and it immediately started flowing through the dye. A sample of the melt was taken after a desired period of time and was accurately weighed. For flow rate consistency, it was important to make sure that the extrudate was free of voids. The weight of the resulting material strips was measured every 0.5 min. The specified flow range to drive the melt through the column was in g/10 min.

Figure 3.10 Melt Flow Indexer

3.4.7. Thermo Gravimetric Analysis (TGA)

Thermo gravimetric analysis (TGA) experiments were carried out to determine the variation in the thermal degradation temperature of the thin films using a TGA analyzer Q series (Thermo Fisher Scientific, USA). A Heating rate of 20 °C/min was used to raise the temperature of 10-14mg samples from room temperature up to 700 °C under nitrogen purge flow rate of 50mLmin^{-1}.

3.4.7.1. Procedure for TGA Measurements

The nitrogen gas valve and the TGA release valve were opened. The sample pan was cleaned and carefully placed with tweezers onto the sample platform. The instrument was tared. The sample was then placed in the center of the sample pan as shown in Figure 3.11. The appropriate inputs were entered into the Q50-TGA program as

dictated by the experiment parameters. Then the run started. Once the run was finished, the pan was carefully cleaned with a propane torch.

Figure 3.11 Thermo Gravimetric Apparatus

3.4.8. Mechanical Properties Characterization

The yield tensile strength and % elongation (ductility) of the previously prepared CS membranes and nanocomposites was evaluated through an axial tensile test. The test was conducted using an Instron universal testing machine with 100KN capacity. To insure the axial uniform load distribution on the membrane-thin sheets, a fixture was designed as a transition between the flat grips of the machine and the thin films as shown in Figure 3.12. The % elongation for all CS membranes at three different temperatures (23, 30, and 60 °C) was also measured during tensile testing. The guidelines for the dimensions of the membrane samples were cut in accordance with ASTM Standard Method D 882-91 [104]. The initial grip separation was set at 30 mm. The tensile tests were conducted at a preselected strain of 0.4mm/mm for the NCLCS and 1.8 for the CLCS membranes. The testing was performed at the preselected strain values to insure that testing occurred within the uniform plastic deformation. A strain rate of 10mm/min was employed for all tested samples. The tensile behavior of the fabricated membranes was tested as a function of temperature at 23, 30 and 60^{o}C to investigate the influence of stretching of the membranes as a function of the operating temperatures on the pore size and shape.

Figure 3.12 Instron Testing Machine

3.4.9. Statistical Analysis

For better interpretation of data and to derive the representative conclusions about the influence of the various parameters on the membrane properties, a statistical analysis was performed using Design Expert software [105]. The parameters included in the statistical analysis are illustrated in Table 3.1. The output of Design Expert (9.0.1) included three responses: tensile strength, diffusion time, and pore size. The analysis of variance shows the parameters that have significant effect. The significant factors have values with low p-value (Probability>F) where p was less than 0.0001 [105].

Table 3.1 The Factors and their combinations used for the statistical analysis

A	Temperature (23, 30, 60 ºC)
B	Polymer (NCLCS-CLCS)
C	Type of filler (Graphene, Fullerene)
D	Wt. % of filler (0.1, 0.5, 1 %)
AB	Interaction between temperature and type of polymer
AC	Interaction between temperature and type of filler
AD	Interaction between temperature and wt. % of filler
BC	Interaction between type of polymer and type of filler
BD	Interaction between type of polymer and wt.% of filler
CD	Interaction between type of filler and wt. % of filler

Response surface methodology (RSM) was useful in this work, as it modeled three different responses: tensile strength, pore size and diffusion time. The eventual objective of RSM was to determine the optimum operating conditions for the membrane fabrication. Fitting and analyzing response surfaces was greatly facilitated by the proper choice of factorial design as it provides distribution of data points, allows model adequacy, provides precise estimates of model coefficients, provides a good profile of the prediction variance throughout the experimental region, provides reasonable robustness to insure simplicity of calculation of model parameters [87].

3.4.9.1. Design of Experiments Steps

There are several steps that are required to perform an experimental design using response surface method including problem statement (fabrication of polymer nanocomposites with controlled porosity), choice of the factors listed in Table 1 and their corresponding levels, choice of response variable(s): tensile strength, pore size, and diffusion time. Baseline experimentation (phase I experiments) are initial random experiments performed according to a literature review. They provide experience about the factors included, determine important ones to be investigated further, and exclude minor ones [89].

3.4.9.2. Choice of Experimental Design

Generally, there are two main steps required to complete the design. The first step was considered with obtaining a set of reasonable candidate points to be used in the selection of design points. It should be based on the model order wished to be used. It was recommended to use one of the following models based on practice: Linear, quadratic, cubic or special cubic model. Quadratic models would include vertices, overall centroid, and edge of centers, axial points, and constraint plane centroid. In this work, quadratic model was used as a starting model; as it was a mid-way between linear and higher degree models allowing the formation of several other models without wasting much runs. Moreover, Quadratic models were recommended as a starting initial model when the case was not simplex [89].

The second step was the usage of a convenient method to select and identify points and their coordinates in the constrained design space. Typically, there are various designs; each having its algorithm such as: Distance based, extreme vertices,

CONAEV, D-optimal, and others. Extreme vertices design was formed by the combination of upper and lower bounds constraints [90]. A set of points within the constrained region were suggested by McLean and Anderson to be used as the basis for the design including overall centroid, points at the center of the edges, faces. However, Myers and Montgomery recommended the usage of one of the two other methods as they are most commonly used in practice [91].

Distance based design was based on the technique of uniform spreading of design points over the feasible region. The algorithm that was utilized; for points selection, was based on a simple criterion of putting points to cover the boundary of the region then adding interior points only when these points are farther from the points already in the design. In other words, it was a point's choice using coordinate exchange to achieve the maximum spread throughout the design region. However the selected points using this technique might not be sufficient for model coefficients estimation, nor an estimate of pure error or lack of fit could be provided. Therefore, this type was excluded from the selection of this work also [91].

D-optimal design is called "D-optimal design" or sometimes other alphabetic letters are used based on the optimality criteria. However, this design was used to select points for any mixture design in a constraint region. This type of design needs a set of reasonable candidate points from which it chooses the design points. It works mainly by the selection of a set of points minimizing the variances of model regression coefficients by adopting the technique of loading up vertices points. In addition, it should be noted that when the number of variables increases, the likelihood of choosing interior points in a design with a reasonable number decreases. Therefore, the tendency to use designs other than the D-optimal, such as the distance based, was not recommended. Specifically, when the number of variables was four or more, the usage of D-optimal criterion was recommended. This was due to the fact that distance criterion lean to choose interior points in a feasible region and thus the variances of the model regression coefficient are not minimized; for that reason experimenters are more oriented to use D-optimality because the concept of minimizing variances was pleasing. For example, for the same region, D-optimality would place 2 internal points and distance criterion 4. In addition, distance criterion was not recommended for physical experiments, which was the case in this work. Moreover, D-optimality was a powerful tool in the identification of the most crucial variables. Therefore, for all the reasons mentioned and the fact we are dealing in this work with four variables

in a physical experiment, D-optimal design was adopted in this work. However, a common problem with D-optimal design that it depends heavily on the number of runs. In other words, if a different number of runs were adopted in several trials the results would differ significantly [89].

3.4.9.3. Performing the Experiment (Phase II Experiments)

The stage prior to the main experimental design (phase II experiments) included several modifications. Firstly, testing was performed to check whether wet or dry mixing would be the optimum for fabricating the membranes. The second important modification was choosing the optimum cross linking agent. Decisions concerned with process variables (processing temperatures and speed) were taken into account at this stage.

3.4.9.4. Output of Design Expert

The output of Design Expert contains four sections: Fit Summary, ANOVA, Diagnostic Case Statistics, and graphical display. "Fit Summary" was used mainly for the comparison between different model types fitting the input data. In addition, it gives initial information about the adequacy of a certain model. It contains all the important parameters needed for the comparison: sequential p-value, lack of fit p-value, adjusted R-squared, and predicted R-squared. The selection was based on the lowest sequential p-value, highest values of lack of fit p-value, adjusted, and predicted R-squared values, as explained above. The sequential p-value shows the accumulating improvement in the model fit as terms of the intended model are added, which should be the minimum value among others. That was, lack of fit p-value should be the maximum among all values. When prob>F value, <0.05 indicates a high lack of fit, revealing that variation in model points significantly differs from variations in the replicated points. This was not desired and could lead to an inadequate model. That was, if a model shows lack of fit, it should not be used to predict the response [87]. The ANOVA table of permeability and relative moisture shows that the filler type has a significant effect. They have low p-values (Prob>F) where it was less than 0.0001. This was an indication that these factors are affecting the model as they are significant factors. However, the effect was not extended to harm the model as a whole; rather, a good result of lack of fit (low lack of fit) shows a positive indicator, revealing that a variation in model points does not differ from variations in the replicated points [87].

Chapter 4

RESULTS AND DISCUSSION

4. Results and Discussions

In order to study the overall parameters of fabricating PNC membranes, a process selection procedure was performed using the digital logic method to select the most suitable polymer (synthetic or natural) for applications in filtration and packaging. This was followed by complete pore size morphology, physical and mechanical (tensile strength, % elongation) characterization of the PNC membranes. The effect of increasing operating temperature on the PNC membrane pore size, tensile strength and barrier properties of PNC membranes were also studied. Moreover, an evaluation of the diffusion performance of the PNC membranes was performed using finite element analysis (FAE). Finally, a statistical analysis was performed to find the optimum tensile strength, pore size and diffusion time of particles through the PNC membrane according to a variety of factors (type of polymer, type and wt.% of filler).

4.1. Process selection procedure

4.1.1. Digital logic (DL) Results

The performance goals selected included the most important characteristics for the thin films in packaging and filtration applications [8]. Controlled porosity and yield tensile strength were the major factors that influenced the selection of the membrane material.

4.1.2. Weighted Property Results

To further select the suitable properties, the weighing factor of the two selected performance goals (from DL method) were calculated as shown in Table 4.1. Controlled porosity had the highest weighing factor followed by tensile strength according to the usage of membranes in filtration and packaging [99].

Table 4.1 Positive decisions and weighing factor of performance goals

Goals	Positive decisions	Weighing Factor
Controlled porosity	7	0.28
Ductility	4	0.16
Biodegradable	4	0.16
Biocompatible	0	0
Antimicrobial	1	0.04

Yield Tensile strength	5	0.2
Carcinogenic	1	0.04
Non Toxic	3	0.12
Total	25	1

4.1.3. Weighing Factor (αi) Results

The selected membrane materials in this theoretical work were nylon, LDPE, PTFE and Chitosan, as they are the most commonly used ones in literature for packaging and filtration purposes [18]. The two most important factors that have the highest weighing factors were controlled porosity, and yield tensile strength according to the DL method calculated previously as shown in Table 4.2. The data included in Table 4.2 were based on previously published data [8].

Table 4.2 Performance goals with highest weighing Factors [8]

	Controlled pores (nm)	Yield Tensile strength (MPa)
LDPE	200	95
Nylon	125	65
PTFE	60	57
CS	20	73

4.1.4. Scaled properties (βi) Results

The two significant performance goals (controlled porosity and tensile strength) were scaled. The smallest pores obtained were 20 nm upon using chitosan. The controlled pores of chitosan were rated 100, since the main objective of this work was to increase the barrier properties of membranes. Barrier properties were improved upon achieving small pore size in the fabricated membranes. Regarding the tensile strength, chitosan membranes were rated 100, since a higher tensile strength was a desirable property in membranes [99]. Table 4.3 shows the scaling of the two performance goals.

Table 4.3 Scaling of properties of selected membranes

	Controlled pores (nm)	Yield Tensile strength(MPa)
LDPE	10	100
Nylon	16	68
PTFE	33	60
CS	100	76

4.1.5. Performance Index (γ)

The LDPE, Nylon, PTFE, CS performance indices were calculated according to equation $\gamma = \Sigma Bi\alpha i$ (2) [99].The maximum performance index was for chitosan followed by LDPE as shown in Table 4.4. The two polymers were selected in fabricating the PNC membranes.

Table 4.4 Performance index of performance goals

	Controlled pores (nm)	Yield Tensile strength (MPa)	$\gamma = \Sigma \beta i \alpha i$
L DPE	2.8	20	22.8
Nylon	4.48	13.6	18.08
PTFE	9.24	12	21.24
CS	28	15.2	43.2

LDPE and CS were selected for the fabrication of synthetic and natural PNC membrane respectively. LDPE was selected rather than PTFE and nylon as it had the highest tensile strength after CS. Moreover, applications for LDPE products are growing. It is extensively used as an overwrap film for towels and tissues, a film for bakery goods, meat, coffee, frozen foods, liquid packaging (milk cartons and bag-in-box applications), liners, bags, and shrink film for books [106]. Additionally, the tensile strength of LDPE membranes could be further enhanced by the addition of nanofillers such as G and F. Liquid and gas permeability techniques for LDPE were performed to check the effect of same nanofillers on barrier properties of fabricated membranes.

In preparing natural PNC membranes, chitosan was selected due to its potential as a natural material. It is biodegradable, biocompatible and has relatively low toxicity. One of CS's most important features is the ability to be shaped into different forms

such as fibres, hydrogels, beads, sponges, and films [43]. It is used for numerous agricultural food preservation applications such as biomedical and biotechnological applications such as food packaging [107]. Of greatest importance is the film-forming property of chitosan, which makes it a potential industrial source as food preservative or coating material in drug manufacturing. CS has been used in the preparation of membranes and has also been incorporated into other packaging materials to be used for preserving and extending the shelf life of foods [65].

Chapter 4

SYNTHETIC POLYMER (LDPE)

4.2. Synthetic polymer (LDPE) characterization

4.2.1. Pore Size Morphology of LDPE membranes and their nanocomposites

Effective characterization of the morphology was an important factor in establishing structure – property relationships for the membranes. The SEM examination of LDPE was illustrated in Figure 4.1. It clearly revealed the microporous structure of LDPE membrane with pore sizes ranging from 0.2 to 0.8μm. The porous network structures of LDPE were observed in several SEM images that were characterized. They were found to be stable at room temperature. The porous network was formed due to the semi crystalline structure of the polymer and the linear molecular structure of repeating CH_2-CH_2 units [106].

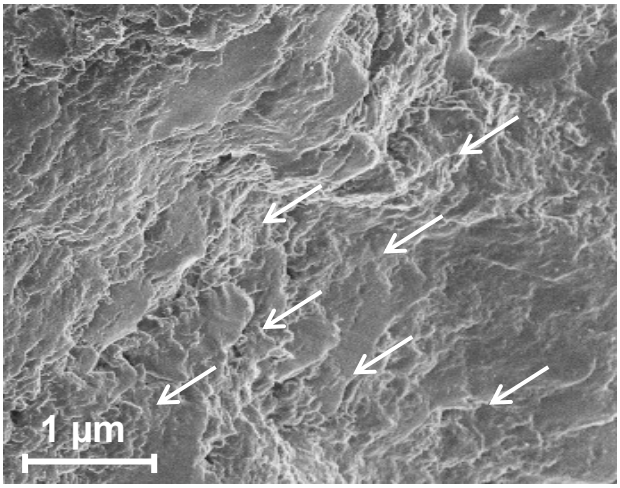

Figure 4.1 SEM image for LDPE (arrows point at pores)

The SEM images of LDPE/F nanocomposites shows the morphology of F clustered within the LDPE matrix. The increase in wt.% F from (0.1 wt.% to 1 wt.%) was clearly shown in Figure 4.2(a, b). On the other hand, the SEM images of LDPE/G nanocomposites shows the flaky-like morphology of G with randomly aggregated clusters between the polymer chains as shown in Figure 4.2(c, d). Upon the addition of 1 wt.% G, Clusters of G-nanofiller were formed causing agglomerations as shown in Figure 4.2(d) within the polymer according to Checchetto *et., al.* [108].

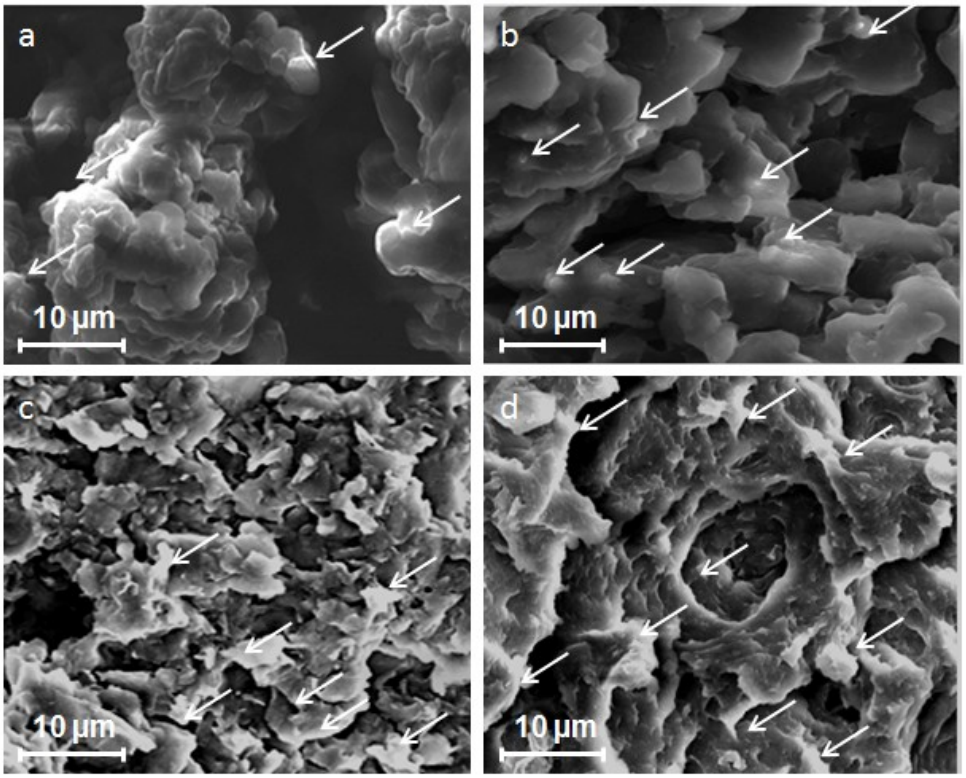

Figure 4.2 SEM images for (a) LDPE/0.1wt.% F, (b) LDPE/1wt.% F, (c) LDPE/0.1wt.% G and (d) LDPE/1wt.% G (arrows point at F and G respectively)

4.2.2. Pore Size Determination of LDPE membranes and their nanocomposites

The pore sizes of the LDPE membranes were calculated by two methods: (i) using Image J analysis commercial software version 1.48, it allowed the calculation of individual pore sizes from the recorded SEM images [102]. (ii) using ASAP 2020 software version 1.00 of the porosimeter's instrument, which normally determines an average pore size of the features and not an individual pore size. The results observed indicated an average pore size of 0.2µm.

The pore size of the LDPE membranes as determined from the Image J analysis of the SEM images was illustrated in Figure 4.3. It shows the effect of increasing the wt.% of F and G nanofillers on the pores' size of the LDPE membranes. At 0.1wt.% F, the pore size was 0.18µm. However, by increasing the wt.% of F to 0.5, 1%, the pore size reached 0.17µm, 0.16µm respectively.

On the other hand, at 0.1wt.% G, the pores' diameter was 0.14µm. However, by increasing the wt.% of G to 0.5,1wt.%, the pore size reached 0.12µm and 0.1µm respectively.

The reduction in pore size at F addition was smaller than at G addition due to difference in size and morphology between F and G nano clusters. The flaky like structure of G nano clusters filled most of the open spaces between chains producing effective blocking as mentioned by Nguyen et al.[79].

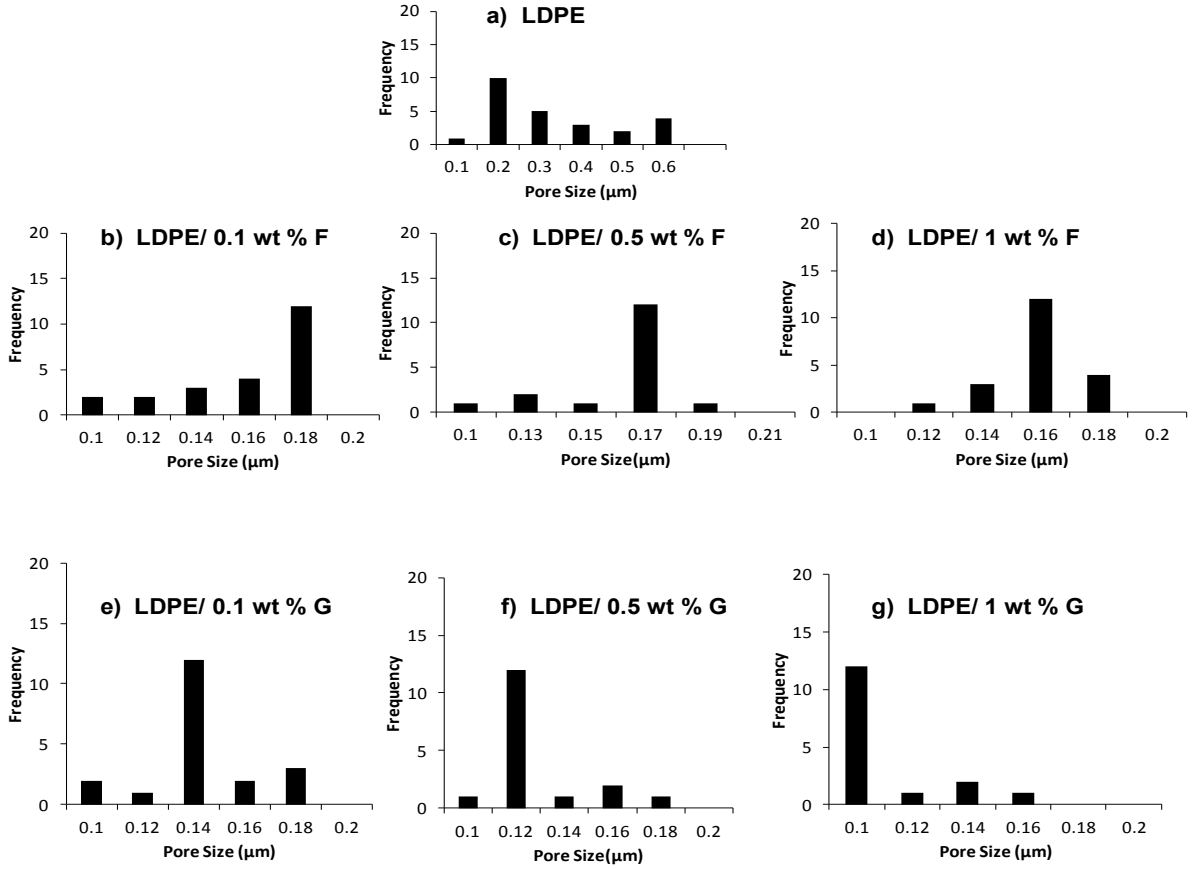

Figure 4.3 Pore size distribution for the different LDPE and nanocomposites membranes using Image J analysis

The average pore size of the LDPE nanocomposite membranes determined using the porosimeter were shown in Table 4.5. The increase in wt.% of nanofiller within the LDPE polymer chains slightly reduced the pore size of the LDPE membranes' pores as highlighted in the Table 4.5. The average pore size decreased from 0.2μm to 0.1μm. The results shown in Table 4.5.were in good agreement with those presented in Figure 4.3.The barrier effect of nanofillers was published by Hosseinkhanli *et., al.* [109]. He highlighted the effectiveness of nanofiller addition in hindering the mass diffusion through the fabricated films thus decreasing the pore size of PNC membranes, which was in agreement with the results shown in Table 4.5.

Table 4.5 A comparison between different LDPE and nanocomposite membranes as a function of pore size at room temperature measured by porosimeter.

LDPE membranes	Average pore size (μm)	Stdv	Mean	CV (Stdv/mean)	Pore size % decrease
LDPE	0.2	0.02	0.27	0.07	
LDPE/0.1 wt.% F	0.17	0.05	0.17	0.29	15
LDPE/0.5 wt.% F	0.16	0.02	0.17	0.12	19
LDPE/1 wt.% F	0.16	0.02	0.17	0.12	20
LDPE/0.1 wt.% G	0.15	0.01	0.15	0.06	25
LDPE/0.5 wt.% G	0.12	0.01	0.10	0.1	40
LDPE/1 wt.% G	0.10	0.03	0.11	0.27	50

4.2.3. Liquid Permeability of LDPE membranes and their nanocomposites

In order to measure the permeability of the fabricated LDPE and nanocomposite membranes, diffusion rate of NaOH was measured through each membrane. It was measured by calculating the diffusion time as a function of nanofiller content as shown in Figure 4.4. The NaOH diffusion time was 3 hrs through the LDPE pores due to the large pore diameter of LDPE. Furthermore, the NaOH diffusion rate at 0.1wt.% LDPE/F decreased. This was indicated by an increase in the diffusion time to 4.5 hrs. Upon, increasing the wt.% F, the diffusion rate decreased and the diffusion time increased to 6hrs. as shown in Figure 4.4.

A similar behaviour occurred with the addition of 0.1wt.% G to LDPE membranes. The diffusion rate decreased. The further increase of wt. % G decreased the diffusion rate manifested by the increase of diffusion time to 7hrs.

From the previous results, one can conclude that the addition of F and G- nanofillers within the LDPE matrix affected the NaOH diffusion rate. Diffusing molecules worked their way around impermeable particles, increasing path lengths, reducing mass transport rates and improving barrier properties [109]. The barrier effect of F was less than G as explained in section 4.2.2.

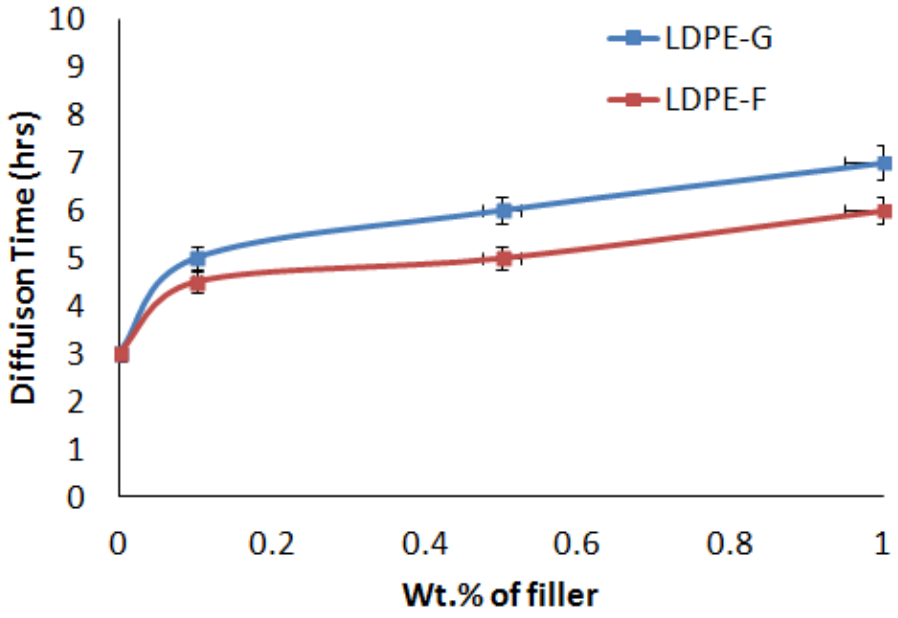

Figure 4.4 Liquid permeability for LDPE nanocomposite membranes as a function of F and G

4.2.4. Gas permeability of LDPE membranes and their nanocomposites

It is observed in Figure 4.5 that the rate of oxygen transmission through the LDPE and nanocomposite membranes is a function of the nanofiller content. Upon addition of F-nanofiller to the LDPE membrane, there was a decrease in gas transmission rate from (125 to 122cm^2/cm^2 d bar) due to filling the open spaces between LDPE chains by F-nanofiller. The increase in wt.% F to 1 wt.% further decreased the oxygen transmission to 120 cm^2/cm^2 d bar .

A significant decrease of oxygen transmission rate with the addition of G-nanofiller was observed in Figure 4.5. There was a decrease in gas transmission rate from (125 to 118cm^2/cm^2 d bar and further decrease to 114cm^2/cm^2 d bar). This agreed with Checchetto *et., al.* findings [108]. He found that addition of G-nanofiller reduced the permeability by approximately a factor of two, compared to that of the pure LDPE

membrane for all the examined gases and also concluded that gas transport through the nanocomposite membrane obeys the solution–diffusion mechanism [108-110].

The addition of F and G-nanofillers decreased the oxygen transmission rate by 4 % and 8 % respectively. This variation was due to the difference in between F and G nano cluster size and morphology [79].

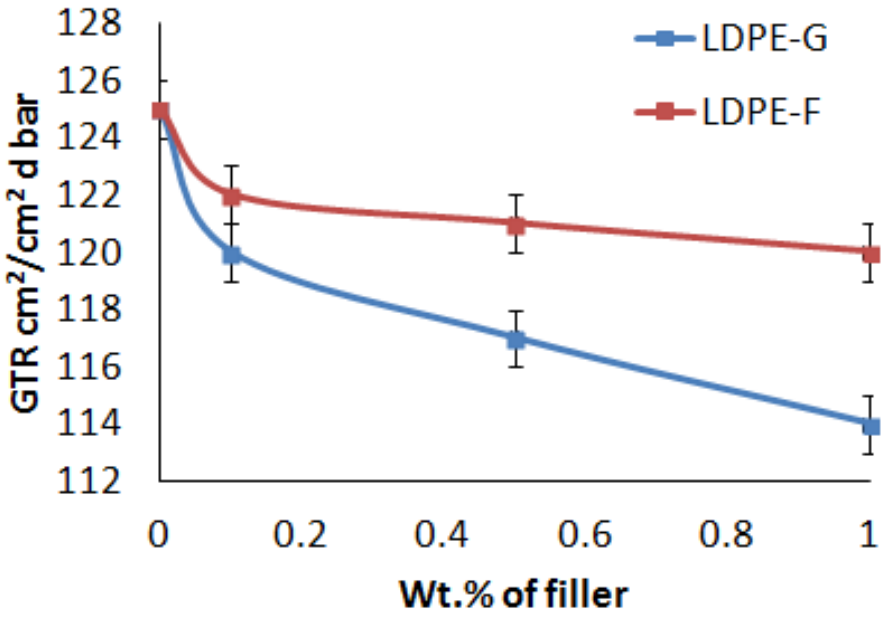

Figure 4.5 Oxygen transmission rate for LDPE nanocomposite membranes as a function of F and G

4.2.5. Melt Flow Index (MFI) of LDPE membranes and their nanocomposites

It is observed in Figure 4.6 that the MFI of the LDPE and nanocomposite membranes is a function of the nanofiller content. The addition of 0.1 wt.% F decreased the MFI of the LDPE/F nanocomposite (increased the viscosity of the LDPE melt significantly). The increase in wt.% F decreased the MFI (from 2 to 1 g/10min) as illustrated in Figure 4.6. Lower melt flow indices (i.e. higher viscosity) can be attributed to higher shear force needed between F-nanoparticles and LDPE. The viscosities of all the LDPE/F nanocomposites samples increased with increasing wt.% F (MFI decreased with increasing wt.% F). This was most probably due to the

formation of clusters leading to less dispersion and higher shear force within the polymer matrix.

The decrease in MFI upon addition of G-nanofiller decreased from 2 to 0.7 g/10min. By comparing MFI of F and G, MFI of LDPE/1wt.% G decreased by 60% compared to the MFI of LDPE/1wt.% F, which decreased by 50% , owing to the fact that F-nanofiller cluster size was significantly smaller than that of G- nanofiller [111].

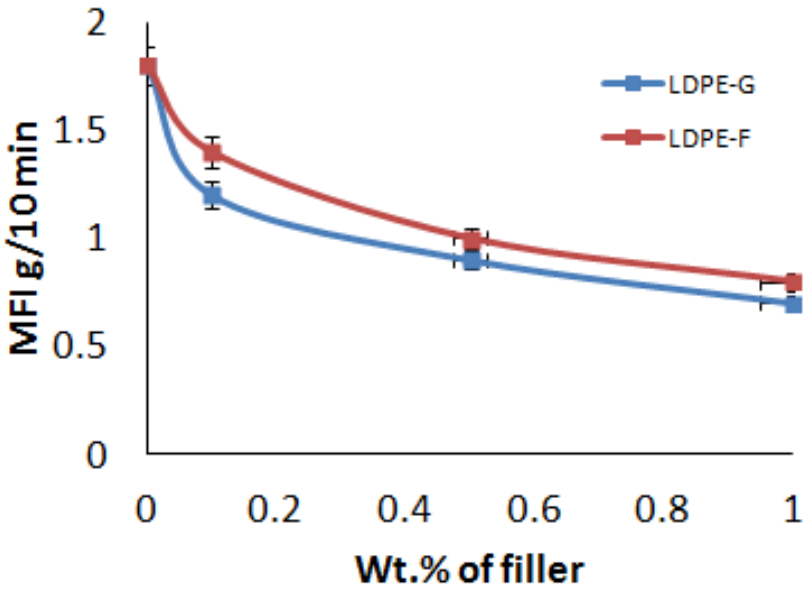

Figure 4.6 Melt flow index for LDPE nanocomposite membranes as a function of F and G

4.2.6. Thermo Gravimetric analysis of LDPE and their nanocomposites

TGA of LDPE and nanocomposite thin films is outlined in Figure 4.7. The temperature is a function of nanofiller content. It can be revealed that the addition of F-nanofiller led to a remarkable improvement of LDPE thermal stability (from 100 ºC to 300 ºC). while the addition of G-nanofiller enhanced the thermal stability (from100 to 250 ºC).

The F and G-nanofillers acted as a physical cross link which limited the movements of the macromolecular chains of LDPE during glass transition. It can also be noticed that the addition of F-nanofiller led to an improvement of the LDPE thermal stability with a higher % (200 %) compared with addition of G (170%) due to the small nano

cluster size of F- nanofiller that allowed easier dispersion within LDPE matrix. The increased stabilization effect with F-nanofiller, could be attributed to the increased interfacial interactions between the F-nanofiller and the LDPE chains and to the fine dispersion of F within the LDPE matrix [112].

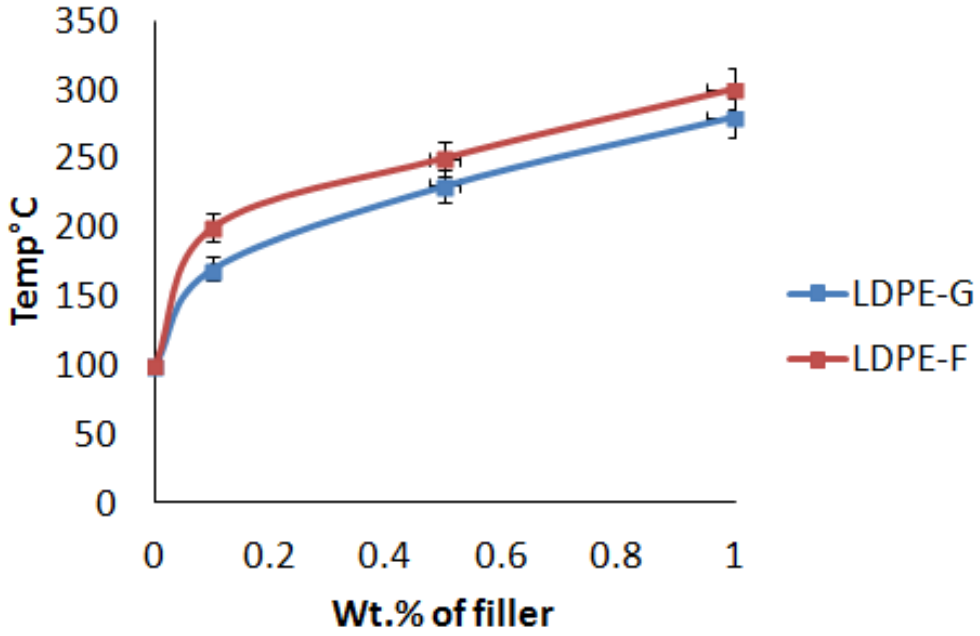

Figure 4.7 Temperature vs Wt.% of filler for LDPE nanocomposite membranes as a function of G and F

4.2.7. Mechanical Properties of LDPE membranes and their nanocomposites

The presence of F and G-nanofillers within LDPE matrix offered resistance to the movement of the polymer chains which led to an enhancement in the mechanical strength. This is an agreement with the findings of Checchetto *et., al.* where the enhancement of tensile properties depended strongly on the properties of the filler, and the nanofiller-matrix interface [108]. The tensile strength vs strain% of the LDPE/F thin films was summarized in Figure 4.8. It is obvious that the addition of F had a significant effect on the tensile behavior of LDPE. The tensile strength increased with increasing in wt.% F. The average tensile strength for LDPE thin film was 20 MPa, which gradually increased to 32 MPa for 0.1 wt.% F and further to 45 MPa at 1 wt.% of F. This corresponded to an overall enhancement of 125%.

On the other hand, the tensile strength gradually increased to 38 MPa for 0.1 wt.% G and further to 52 MPa at 1 wt.% of G. This corresponded to an overall increase in strength up to160% with 1 wt.% G addition. The higher % of enhancement accompanied with G could be due to the restacking of G nano clusters in the polymer matrix [113]. Moreover, it was reported that the tensile strength of LDPE increased by a factor of 2.5 with the addition of G nanofiller [114].

On the other hand, the % elongation decreased gradually as the wt.% F or G increased as shown in Figure 4.8(a, b) respectively. The increase in wt % of F,G decreased the elongation by 20 %. These observations may be attributed to the stiffening action of the nanofiller by restricting the chain movement of LDPE during tensile testing [108]. The % elongation was also affected by the volume fraction of the added nanofiller, the dispersion of the nanofiller within the matrix, and the interaction between the nanofiller and the matrix at the interface [115].

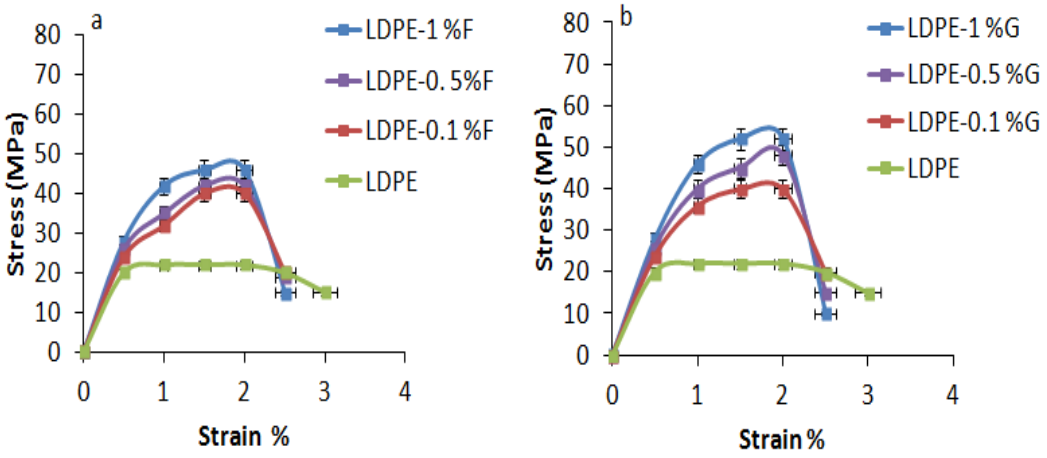

Figure 4.8 Stress - strain curve for LDPE and LDPE nanocomposite membranes a) wt.% F b) wt.% G

4.2.8. Effect of increasing temperature on the tensile properties of LDPE and nanocomposite membranes

The results mentioned in the previous sections were recorded at room temperature. However, in order to study the effect of temperature on the tensile strength of LDPE microporous membranes, all tests were repeated on all fabricated LDPE nanocomposite membranes at 30 ºC and 60 ºC. The results revealed that upon increasing the temperature from 23 ºC to 30 ºC for the LDPE with 1 wt.% F and G,

there was a decrease in the tensile strength by 15% and 13% respectively as shown in Figure 4.9(a, b). While, at 60 ºC the tensile strength decreased by 44 % and 42 % respectively as shown in Figure 4.9(c, d) and Table 4.6. This was due to the increase in pore size of LDPE nanocomposite membranes upon heating. The coarsening in pore size shown in Table 4.6 was due to the free movement of LDPE chains upon increasing temperature [116].

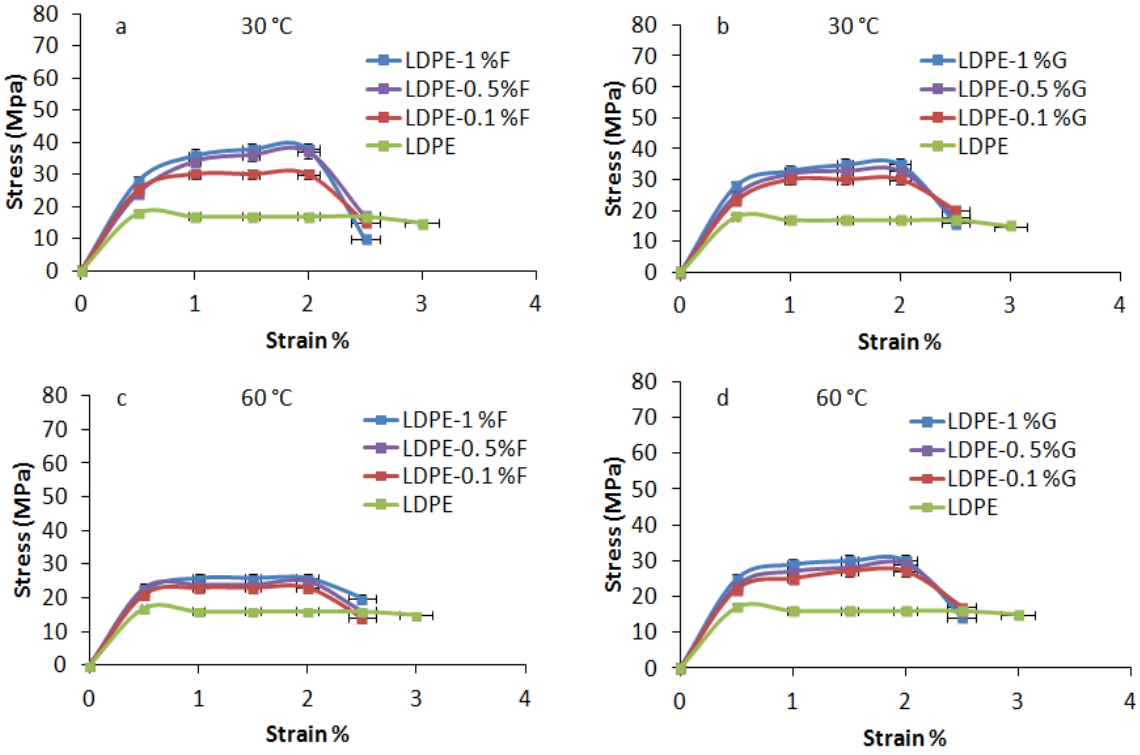

Figure 4.9 Stress-strain curve for LDPE and nanocomposite membranes with a) wt.% F at 30 °C. (b) wt.% G at 30 °C. c) wt.% F at 60 °C and (d) wt.% G at 60 °C.

Chapter 4

NATURAL POLYMER (CS)

4.3. Natural polymer (Chitosan) characterization

The addition of nanofillers either F or G caused a 50% reduction of pore size of LDPE membranes (0.1μm). However, this large pore size was not suitable for using the membranes in packaging and filtration applications. So, CS polymer was used in the fabrication of the membranes to reach a smaller pore size and avoid the passage of gas particles, viruses and bacteria. The main challenge behind manufacturing novel CS nanocomposites mesoporous membranes lied in controlling their pore size to achieve precise separation capabilities of pollutants and therefore decrease the amount of pollution. It has been shown that the pore size has a major effect on the properties of polymeric membranes. In the current work, the pore size varies according to the type (F versus G) and the amount (wt.%) of the added nanofillers materials to the CS polymer solution. Moreover, the variation of the pore size was affected by changing the chemical nature of the CS membranes by physical cross-linking of the CS membranes with TPP as a cross-linking agent.

4.3.1. Pore Size Morphology of CS membranes and their nanocomposites

The SEM images of NCLCS and CLCS were illustrated in Figures 4.10(a) and (b) respectively and clearly revealed a difference in the morphology between both images and the appearance of new porous network structure in case of CLCS after cross-inking with TPP as can be seen in Figure 4.10(b). The porous network structures were not observed in NCLCS and thus indicate the successful cross-linking of CS chains as has previously been reported [117]. These porous network structures of CLCS have also been observed in many SEM images and were found to be stable at room temperature. A possible explanation for these porous networks was that the amino groups of CS react with the negative groups of TPP, thus establishing ionic interaction between CS chains. In addition, the effect of cross-linking could be explained as follows: the increase in length of the molecular chains upon cross-linking decreased the pore volume and surface area leading to a growth in the pore size [118].

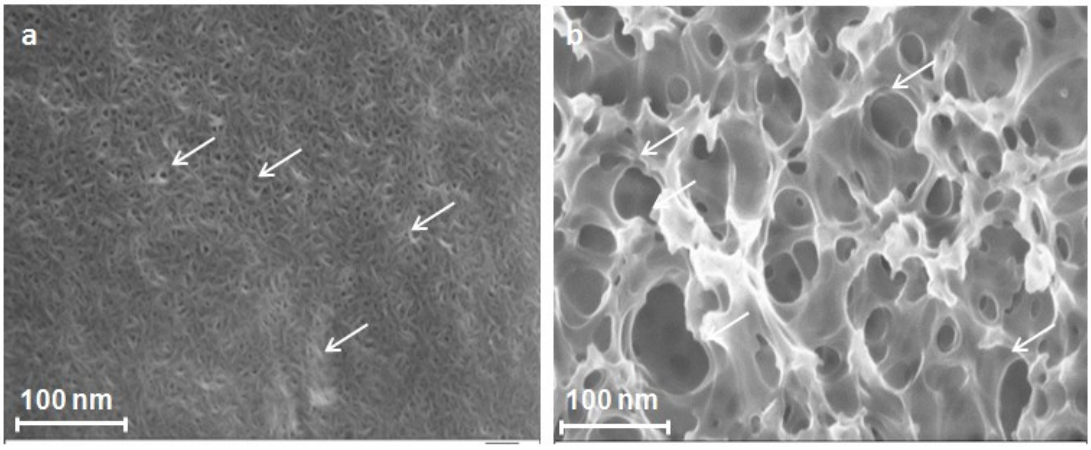

Figure 4.10 SEM images for (a) NCLCS and (b) CLCS membranes, respectively. (Arrows point at pores)

Upon adding F and G-nanofillers, separately, to NCLCS and CLCS solutions during the preparation step of the CS membranes as discussed in section 3.2.2.2., SEM images revealed significant changes in the pore size morphology of CLCS membranes as compared to NCLCS as illustrated in Figure 4.10(a). The SEM image of NCLCS shows a wide distribution of pores, while upon adding F and G-nanofillers with different wt% (0.1 and 1%), the pore size decreased as shown in Figure 4.11(0.1 and 1% with F and G for NCLCS),. This observation had a direct effect on the barrier properties of the CS membranes as will be discussed in the following section. One could also see that the morphological change upon addition of F and G-nanofillers can be better manifested in the case of CLCS (Figure 4.12). The pore size decreased significantly upon the increase of F and G-nanofiller up to 1 wt.%.

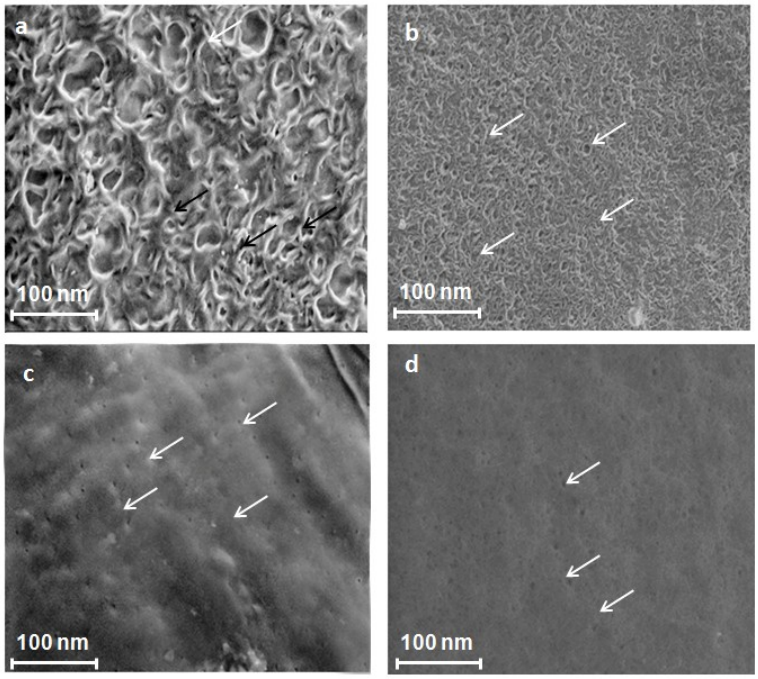

Figure 4.11 SEM images for (a) NCLCS/0.1wt.%F and (b) NCLCS/1wt.% F. (c) NCLCS/0.1wt.%G and (d) NCLCS/1wt.%G. (arrows point at pores)

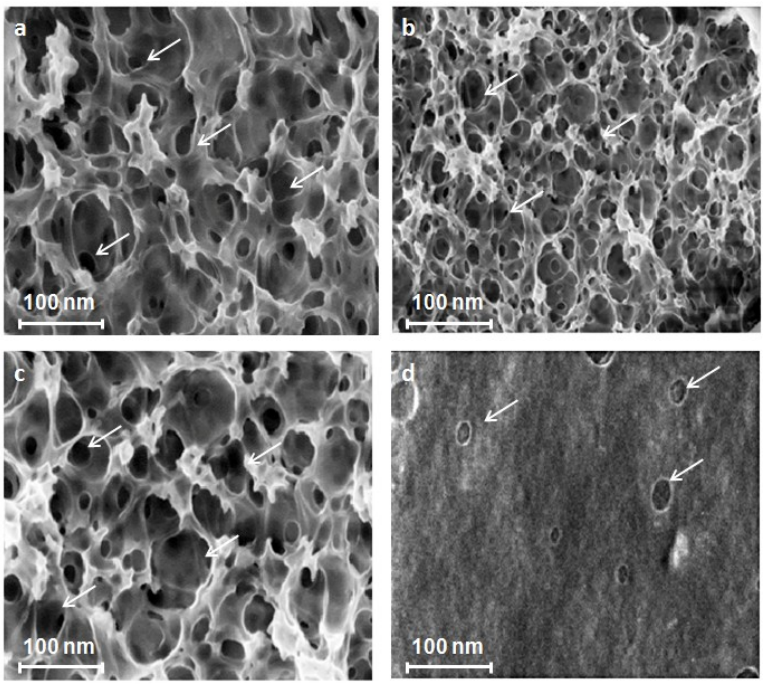

Figure 4.12 SEM images for (a) CLCS/0.1wt.%F and (b) CLCS/1wt.%F. (c) CLCS/0.1wt.%G and (d) CLCS/1wt.%G. (arrows point at pores)

4.3.2. Pore size determination of CS membranes and their nanocomposites

The pore sizes of the CS membranes were calculated by two methods: (i) using Image J analysis commercial software, several SEM images (large scale images and zoom-in areas) were used in the calculations in order to get correct data about the pore sizes. Although the contrast and resolution of the SEM images are not ideal to determine an accurate pore size especially in case of 2D surfaces such as the CS membranes, (ii) using ASAP 2020 software, the results observed from the software indicated an average pore size of the PNC membranes. However, the results obtained from both methods (i and ii) were complementary to each other. there were some differences due to the selected number of spots per image were not exact enough for quantifying the pore size.

The pore size distribution of the CS membranes as determined from the Image J analysis of the SEM images was illustrated in Figure 4.13. The NCLCS membranes had pore size of 10nm while the pore sizes in CLCS membranes were approximately 30nm with few pore sizes ranging from 40 to 50nm. The previous results were comparable to the average pore size obtained using ASAP2020 in Table 4.7. The average pore sizes for NCLCS and CLCS membranes were 10 and 30nm respectively.

The influence of adding F and G-nanofillers decreased the pore sizes in both NCLCS and CLCS membranes. However, the G-nanofiller was more effective in closing the pores as will be observed in section 4.3.2.1. and 4.3.2.2.

4.3.2.1. Pore size of NCLCS membranes with F-nanofiller

NCLCS/0.1wt.% F pores were obviously visible in the SEM image as shown in Figures 4.11(a) and 4.13(c) with pore size mostly 5nm. However, by increasing the wt.% F to 0.5 and 1wt.%, the pore size reached mostly 3nm and 4nm respectively as shown in Figures 4.13(d) and 4.13(e). Thus, by comparing the pore sizes of the NCLCS membranes prepared versus NCLCS/0.1wt.%F and NCLCS/1wt.% F, there was a decrease in the pore size by 50% (with 0.1wt.% F) and 60% (with 1wt.% F), respectively. This was most probably due to the dispersion of F-nanofillers in between the CS polymer chains resulting in

reducing the pore size in CS membranes. The reduction in pore size due to addition of nanofillers agreed with the influence of the exfoliated clay-based PNC, where nano clay reduced the pore size of polymers [117]. The average pore size of NCLCS membranes determined using ASAP2020 were shown in Table 4.7.,where the average pore size for NCLCS/0.1wt.% F was 5nm and decreased to 4nm at 1 wt.% F. The results were similar to the pore size distribution by Image J analysis, where nanofillers decreased the pore size of the membranes.

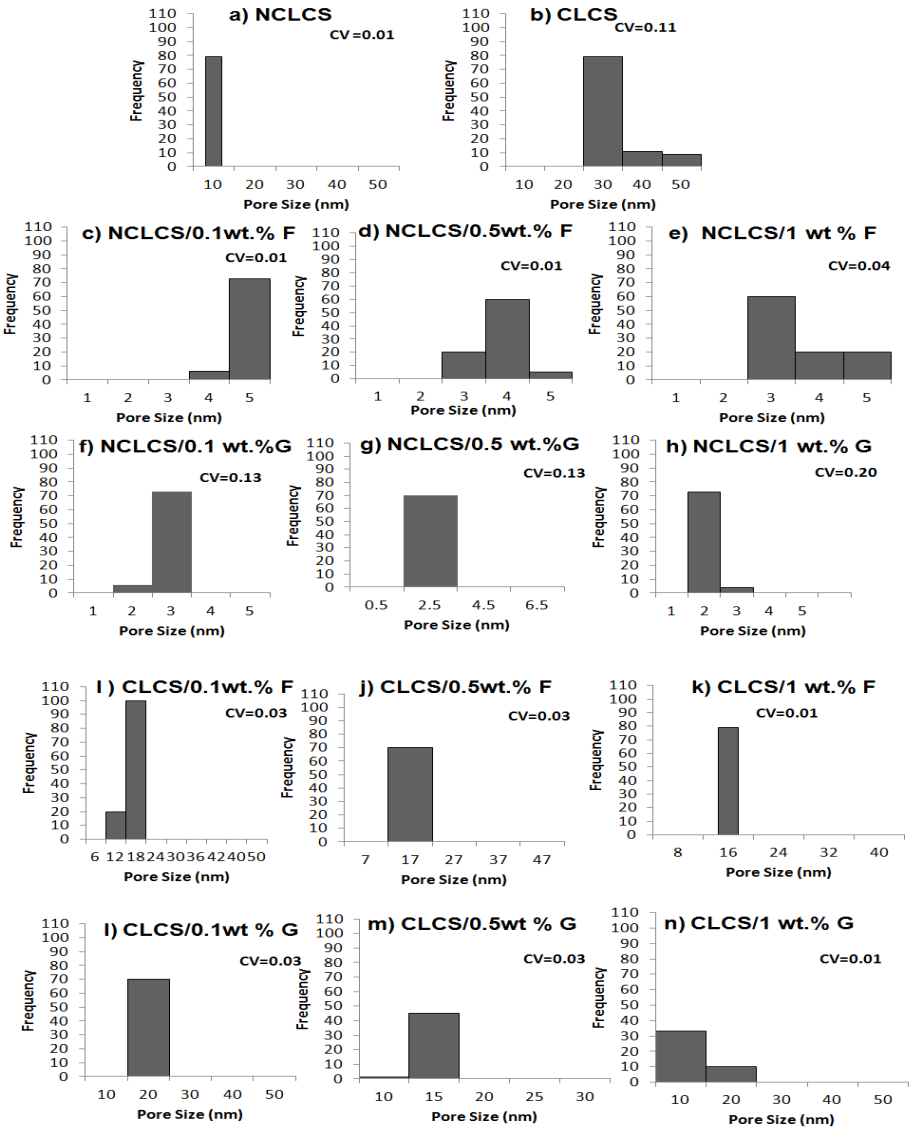

Figure 4.13 Pore size distribution for different CS membranes using Image J-analysis.

Table 4.6 A comparison between the different CS membranes and their pore size at temperature measured by porosimeter.

CS membranes	Average pore size (nm)	Stdv	Mean	CV (Stdv/mean)	Pore size % decrease
NCLCS	10	0.03	9.68	0.00	
NCLCS/0.1 wt F	5	0.03	4.48	0.01	0.50
NCLCS/0.5 wt F	4.5	0.03	4.48	0.01	0.55
NCLCS/1 wt F	4	0.03	3.44	0.01	0.56
NCLCS/0.1 wt G	3	0.03	2.40	0.01	0.70
NCLCS/0.5 wt G	2.5	0.03	2.4	0.01	0.75
NCLCS/1 wt G	2	0.04	0.31	0.11	0.80
CLCS	30	0.02	24.18	0.00	
CLCS/0.1 wt F	22	1.12	21.94	0.05	0.26
CLCS/0.5 wt F	21	0.03	17.4	0	0.3
CLCS/1 wt F	20	0.03	17.4	0	0.33
CLCS/0.1 wt G	16	1.03	23.34	0.04	0.46
CLCS/0.5 wt G	14	1.03	23.3	0.04	0.53
CLCS/1 wt G	10	0.05	8.65	0.01	0.66

4.3.2.2. Pore size of NCLCS membranes with G-nanofiller

Since the structure and chemical nature of the nanofiller was expected to affect their dispersion within the polymer matrix, G-nanofiller has been used as another nanofiller to be able to compare its effect as nanofiller on the CS membranes' properties. Table 4.7, Figure 4.11(c, d) shows the effect of increasing the wt.% of G-nanofiller on the pore size of the NCLCS membranes. At 0.1wt.% G, the pores are quite visible with a pore size of 3nm However, by increasing the wt.% to 1wt.% G, the pore size reached 2nm as can be seen in the SEM image in Figures 4.11(d) and 4.13(h). The 0.5wt.% G shows a pore size of (2.5nm) as illustrated in Figure 4.13(g). Thus, by comparing the pore sizes of the NCLCS membranes versus NCLCS/0.1wt.% G and NCLCS/1wt.% G, there was a decrease in the pore size by 70% (with 0.1wt.% G) and 80%

(with 1wt.% G), respectively. This was mainly due to the barrier effect of G-nanofiller morphology and size. The average pore size results for NCLCS/G membranes in Table 4.7 were similar to the pore size distribution. So far, it was shown that the nanofiller wt.% played a crucial role in controlling the pore size of CS membranes.

4.3.2.3. Pore size of CLCS membranes with F-nanofiller

To compare the effect of the F-nanofiller on the properties of CLCS membranes, F was added to CLCS solutions in different wt%. Table 4.7, Figures 4.12(a, b). and 4.13(i, k) shows the effect of increasing wt.% of F-nanofiller on the pores of CLCS membranes. At 0.1wt.% F, the pores were quite visible mostly at 22nm in the SEM image in Figure 4.12(c). However, the increase of F nanofiller to 1wt.% slightly reduced the pore size to 17nm as shown in Figure 4.12(b). Thus, by comparing the pore sizes of the CLCS membranes versus CLCS/0.1wt.% F and CLCS/1wt.% F, there was a decrease in the pore size by 26% (with 0.1wt.% F) and 43% (with 1wt.% F), respectively. There was a slight difference in pore size decrease % according to average pore size measurement (33% with 1wt.%F) in Table 4.7.

4.3.2.4. Pore size of CLCS membranes with G-nanofiller

Table 4.7, Figures 4.12(c, d), 4.13(l, n) suggested the effect of increasing the wt.% of G nanofiller on the pores of the CLCS membranes. At 0.1wt.% G, the pores were visible mostly 20nm in the SEM image in Figure 4.12(c). However, the increase of G-nanofiller to 1wt.% reduced the pore size to mostly 10nm with few larger pores as shown in Figure 4.12(d). Thus, by comparing the pore sizes of the CLCS membranes versus CLCS/0.1wt.% G and CLCS/1wt.% G, there was a decrease in the pore size by 33% (with 0.1wt.% G) and 66% (with 1wt.% G), respectively. There was a slight difference when calculating the % of pore size decrease using average pore size at 0.1 wt.% G as shown in Table 4.7. The reduction in pore size was 46%. This was mainly due to the barrier properties of CLCS membranes which were significantly altered by the addition of G-nanofiller that altered the diffusion path of penetrant molecules as reported by Bharadwaj *et., al.* [119].

4.3.3. Liquid Permeability of CS membranes and their nanocomposites

In order to measure the permeability of the fabricated CS membranes and their nanocomposite membranes as described in section 3.4.3.1. It was measured by calculating the diffusion time as a function of nanofiller content. NaOH diffusion rate was measured through each CS membrane. The diffusion time through the NCLCS pores was 16hrs. The NaOH diffusion rate increased through CLCS membranes and the diffusion time decreased to 11hrs. due to the coarsening of pore size in CLCS membranes.

The addition of F and G-nanofillers decreased the diffusion rate of NCLCS and CLCS membranes due to blocking of pores. The NaOH diffusion rate deceased in NCLCS/0.1wt.% F and the diffusion time increased to 12hrs. Moreover, increasing the wt.% F-nanofiller decreased the diffusion rate manifested by the increase in diffusion time to 15hrs due to the increase of barrier effect of F-nanofiller. The same behaviour occurred upon the addition of F-nanofiller to CLCS membranes.

Furthermore, the addition of 0.1wt.% G to NCLCS membranes lowered the diffusion rate and increased the diffusion time to 20hrs due to the barrier effect of G-nanofiller. Upon increasing wt.% G to 1wt.%, a further decrease in diffusion rate occurred. The same behaviour occurred upon the addition of G-nanofiller to CLCS membranes.

From the above, one can conclude that the addition of F and G-nanofillers within the CS matrices decreased the NaOH diffusion rate through the fabricated CS membranes. The barrier effect of F-nanofiller was less than that of G due to the difference in shape and diameter size of each nanofiller [79]. This was as illustrated in the suggested scheme in Figure 4.14.

The figure shows the cluster effect of G-nanofiller on the CS pores that led to their accumulation inside the pores of the CS membranes. This decreased the pore size of the CS membranes, whereas F- nanofiller was dispersed inside the pores to an extent that allows higher permeability compared with G nanofiller. The pores in the scheme

in Figure 4.14 were scaled according to the obtained experimental pore sizes in Table 4.7.

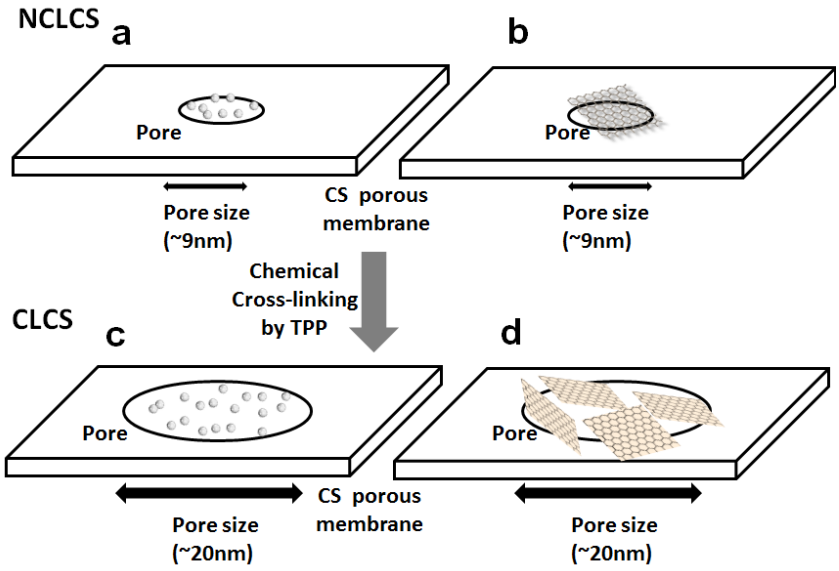

Figure 4.14 A Schematic illustration of CS membranes and their pore sizes before and after physical cross-linking by TTP and after addition of F (a, c) and G (b, d) nanofillers at 23°C.

4.3.4. Gas permeability of CS membranes and their nanocomposites

It is observed from Figure 4.15 that the rate of oxygen transmission through the CS and nanocomposite membrane is a function of the nanofiller content. The oxygen transmission rate through NCLCS membranes was lower than CLCS. The oxygen transmission rate of CLCS reached 75cm^2/cm^2 d bar compared to that of NCLCS membranes (70cm^2/cm^2 d bar). Upon addition of both F and G-nanofillers, the oxygen transmission rate decreased in both NCLCS and CLCS nanocomposite membranes and the permeability decreased.

From the diagram, it is clear that addition of F-nanofiller to the NCLCS membranes resulted in a decrease of oxygen transmission rate through the NCLCS and CLCS membranes up to 1 wt.% F reaching 55cm^2/cm^2 d bar and 65cm^2/cm^2 d bar respectively .

For the G-addition, a continuous decrease in oxygen transmission was persistent up to 1 Wt.% G for both NCLCS and CLCS membranes reaching 50cm^2/cm^2 d bar and 60cm^2/cm^2 d bar respectively .

The addition of G-nanofiller had a superior effect on the oxygen transmission rate compared to the F-nanofiller. The G-nanofiller decreased the rate by 29% compared to that of F-nanofiller (21%). The pore spaces were saturated with addition of G-nanofiller , while the morphology of F clusters had a less blocking effect.

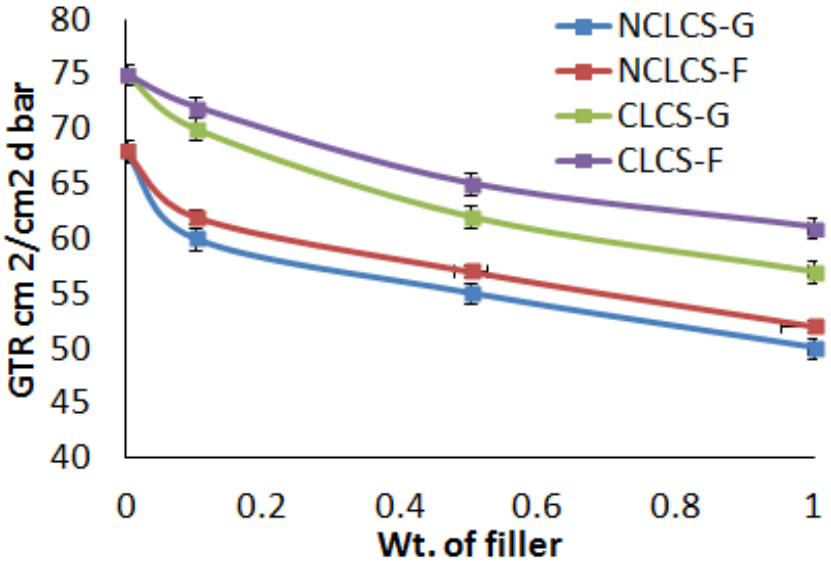

Figure 4.15 Oxygen transmission rate for different CS nanocomposite membranes.

In an attempt to highlight the possible filtration applications of the fabricated mesoporous CS membranes; sea salt (with a pore size of 35nm) could be filtered using membranes CLCS membranes. Oil smoke (with a pore size of 30nm) could be filtered using CLCS/0.1% F membranes. On the other hand, smoke from combustion (with a pore size of 10nm) could be filtered using NCLCS. Atmospheric dust (with a pore size of 1nm) could be filtered using CLCS/0.5% G membranes. Oxygen and nitrogen (with a pore size of 0.5nm) could be blocked using NCLCS/0.5% or 1% G [10]. A further confirmation of liquid and gas permeability characterization results was performed using finite element through mass diffusion analysis using Abaqus.

4.3.5. Finite Element analysis (FEA) for CS membranes and their nanocomposites

Abaqus/Standard provided modeling of steady-state diffusion of particles through the fabricated membranes Fick's Law. Steady-state mass diffusion analysis provided the steady-state solution directly: the rate of change of concentration with respect to time was omitted from the governing diffusion equation in steady-state analysis. The basic inputs in the model were solubility and diffusivity. Ficks' equations allowed for non uniform solubility of the diffusing particles in the membrane. The basic solution variable was the normalized concentration (Ø=c/s), where c was the mass concentration of the diffusing particles and s was its solubility in the membrane [92]. After incorporating all the input data to Abaqus software, the output (normalized mass concentration) was calculated at the specified nodes for both NCLCS and CLCS membranes as shown in Figure 4.16.

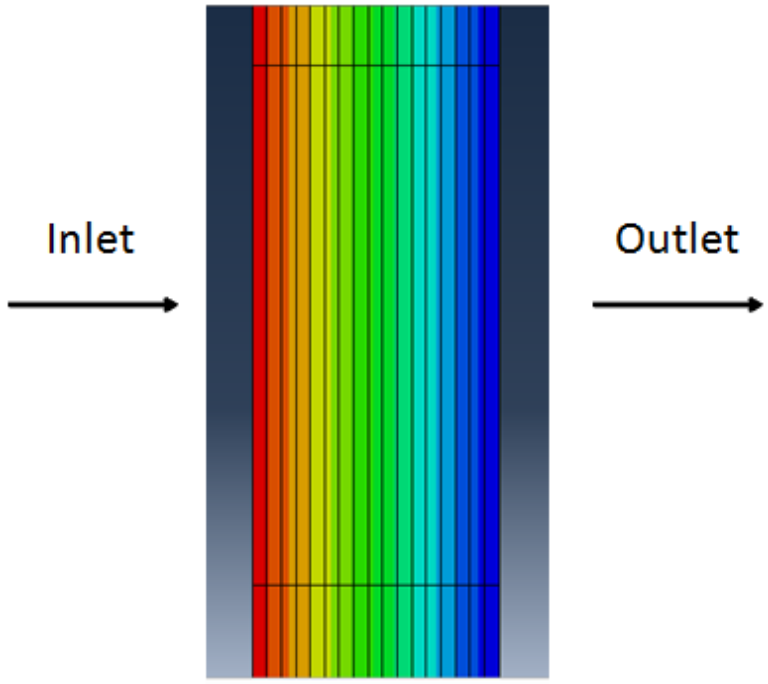

Figure 4.16 Inlet and outlet normalized concentration through the membrane thickness

Figure 4.17 Shows the variation of normalized concentration across the NCLCS membrane thickness as a function of nanofillers. There was a decrease in normalized mass concentration with the increase in the wt.% of F and G-nanofiller. The presence of nanofillers hindered the mass diffusion. The normalized concentration dropped at the addition of 1 wt.% F (500 to 100 c/s) and the same behaviour occurred upon addition of G-nanofiller. The normalized concentration decreased from 500 to 10 c/s. This highlighted lower diffusion rate of particles through NCLCS/G membranes and higher diffusion in NCLCS/F membranes, which agreed with experimental results in section 4.3.4.

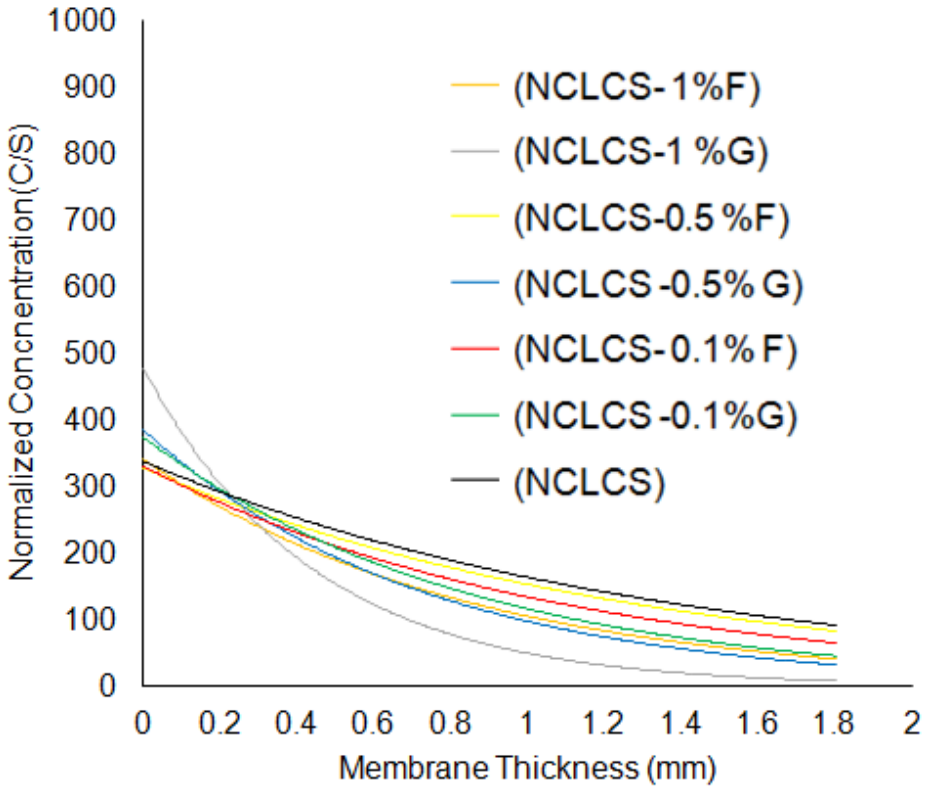

Figure 4.17 Normalized mass concentration for NCLCS/G, F with different wt.% of filler

Figure 4.18 shows the variation of normalized concentration across the CLCS membrane thickness as a function of nanofillers. The pore size of CLCS membranes was coarser than that of NCLCS membranes. There was an increase in normalized concentration as the pore size increased [120]. The coarser pore size allowed the passage of particles through the pores. There was a decrease in normalized mass concentration with the increase in the wt.% of F and G-nanofiller. The normalized concentration dropped at the addition of 1 wt.% F (900 to 300 c/s) and the same behaviour occurred upon addition of G-nanofiller. The normalized concentration decreased from 900 to 2 c/s. However, there was a sudden drop in normalized concentration at CLCS/1 wt.% G and CLCS/0.5 wt.% G membranes at 0.2 mm thickness compared to gradual decrease in normalized concentration for the rest of the membrane conditions. This was most probably attributed to the flaky shape morphology and large size of G nano clusters that saturated the pores immediately.

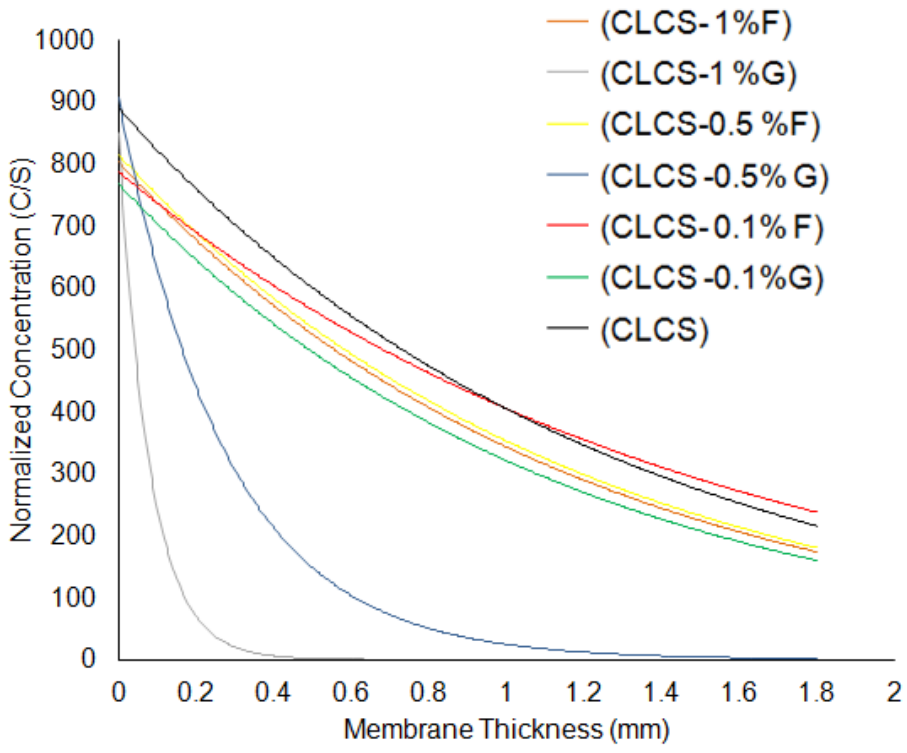

Figure 4.18 Normalized mass concentration for CLCS/G, F with different wt.% of filler

The mass diffusion decreased with the addition of F and G-nanofillers. The blocking effect of G was higher than F due to the difference of nano cluster size and morphology as explained in section 3.1.3. Similar study was reported by Hedenqvist *et., al.* [121]. He developed a mass transfer model based on an integration algorithm to include concentration dependent diffusivities that has been applied to water diffusing in multi-layer polyesters. Hedenqvist concluded that the polymers can exhibit a huge range of mass transport properties depending on type of polymer and type of filler [121].

4.3.6. Melt flow Index {MFI) of CS membranes and their nanocomposites

It is observed that MFI is a function of the nanofiller content as shown in Figure 4.19. Cross-linking of CS membranes decreased viscosity thus increased the MFI of the CLCS membranes (55 g/10 min) compared to NCLCS (45 g/10 min) as revealed in Figure 4.19. The improved MFI was attributed to the intramolecular cross-linking, leading to a decrease in viscosity due to volume contraction of the polymer coils [122]. The increase in MFI shortened the fabrication time for the membranes thus saving time and money and facilitates the processability due to the low viscosity [123].

The addition of F, G-nanofillers decreased the MFI in both CLCS and NCLCS as illustrated in Figure 4.19. Lower melt flow indices (i.e. higher viscosity) can be attributed to higher shear force formed between F, G nanoparticles and the CS polymer. The MFI of NCLCS/1 wt.% F decreased by 22 %. While, the MFI of NCLCS/1 wt.% G decreased by 33 %. The same behaviour was observed in CLCS/G and F. The MFI of CLCS/1 wt.% F and CLCS/1 wt.% G decreased by 20% and 30% respectively.

MFI was influenced by F-nanofiller cluster size (2-3m) which is much smaller than that of G (8-10nm). Moreover, the spherical shape of F clusters might have limited the residual stresses and shear stresses formed at the polymer -nanofiller interface. This resulted in a decrease of MFI in NCLCS, CLCS/F nanocomposites but with a lower rate than the decrease of MFI in NCLCS, CLCS/G [123].

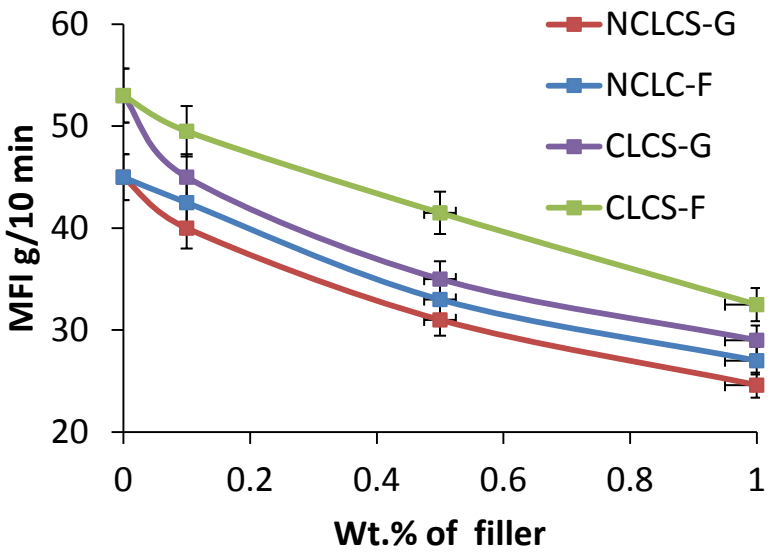

Figure 4.19 Melt flow index for CS nanocomposite membranes as a function of F and G

4.3.7. Thermo Gravimetric Analysis (TGA) of CS membranes and their nanocomposites

TGA of CS and nanocomposite membranes is outlined in Figure 4.20. The temperature is a function of nanofiller content. There has been a significant improvement by 20°C (from 250 to 270 °C) in the thermal stability of CLCS membranes compared to NCLCS membranes as revealed in Figure 4.20, which was mainly attributed to the addition of TPP. A possible explanation was that TPP has increased the chain length by connecting more CS chains together, thus decreasing the CS chain mobility, and increasing the glass transition temperature (Tg) as suggested by Muzzarelli et., al. [124]. The CS chain interactions fixed the individual chains strongly in position and resisted deformations and matrix breakup. The thermal stability was probably due to increased hydrogen bonding interaction between CS chains due to cross-linking effect [124].

It can be concluded that the addition of F,G nanofiller led to a remarkable improvement of both NCLCS,CLCS thermal stability as illustrated in Figure 4.20. It can be revealed that the addition of F nanofiller to NCLCS membranes increased the temperature by 50% . On the other hand, the addition of 1 wt.% G increased the temperature by 24%. The addition of 1 wt.% F to CLCS membranes increased the temperature by 48% and the addition of 1 wt.% G increased the temperature by 37%.

This enhancement in NCLCS and CLCS membranes could be explained by the barrier effect of F,G which resulted in the improvement of the resistance to thermal degradation and hindered the diffusion of the decomposition products from the bulk polymer onto the gas phase. This stabilization effect could be attributed to the increased interfacial interactions between the F,G nanofiller and CS [124]. F-nanofiller cluster size (2-3m), which is much smaller than that of G (8-10nm) explained the superior thermal stability upon adding F-nanofiller. The smaller cluster size of F compared to G-nanofiller increased the interfacial interactions between CS polymer and nanofiller [98].

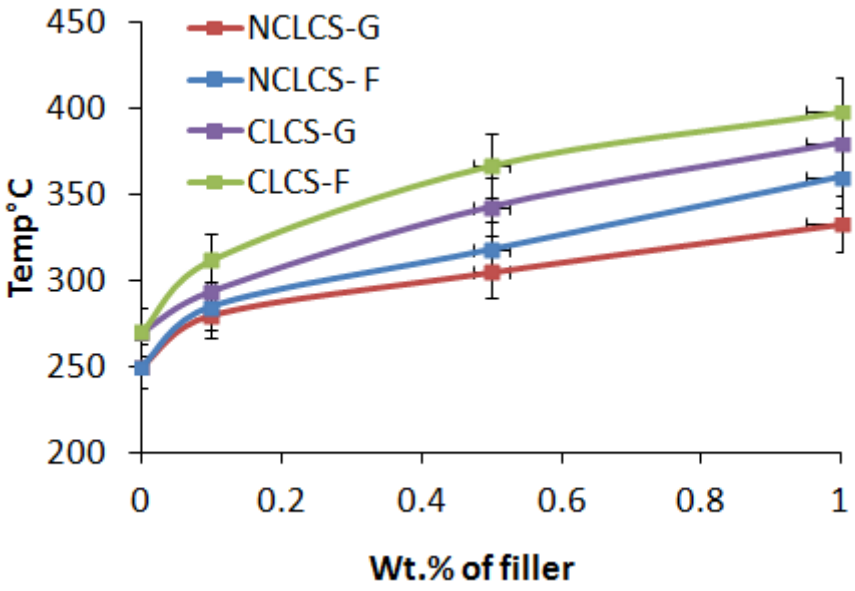

Figure 4.20 Temp vs wt.% of filler for CS nanocomposite membranes as a function of F and G

4.3.8. Tensile properties of CS membranes and their nanocomposites

CLCS and NCLCS nanocomposite membranes with F and G-nanofillers were fabricated, and their tensile properties were investigated. The influence of the membrane chemical structure on the tensile strength and % elongation was studied. Physical cross-linking of CS by TPP and the addition of F and G-nanofillers were found to be crucial factors affecting the tensile strength and % elongation of the fabricated CS membranes. In the following subsections, the influence of the membrane crosslinking condition with and without nanofillers on the tensile behaviour of the films was displayed.

4.3.8.1. Tensile Behaviour of NCLCS and CLCS membranes

The tensile behavior versus strain of the plain NCLCS and CLCS membranes is shown in Figure 4.21. It clearly revealed higher tensile strength of 24 MPa for the NCLCS compared to 2.8 MPa for the CLCS membranes. CLCS membranes had coarser pore sizes compared to NCLCS. The formation of ionic cross-links between amino groups of CS and TPP groups decreased the surface area of the polymer leading to an increase in the surface area of the membranes' pores [125]. The decrease in tensile strength could be attributed to the coarse pore size formed in the CLCS, which promoted pore size growth and coalescence resulting in premature failure, which agrees with the work done by Muzzarelli *et., al,* [126]. However, in NCLCS membranes, the pore size was smaller. Therefore, the stability of the pores against growth and coalescence due to the increased hydrogen bonding interaction between the CS chains, could have resulted in the enhanced tensile strength [127].

The correlation between elongation and cross-linking of polymers was not as straight-forward as was the relation between cross-linking and tensile strength. The elongation increased from 0.5 to 2 % upon cross-linking as shown in Figure 4.21. At first, crosslinking dramatically increased elongation since the structure of the overall material changed from individual chains linked only with van der Waals forces to covalent bonds, which are few but strong. The polymer acts as a single molecule as soon as the covalent bond occurs. Additional crosslinking continues to strengthen the response of the polymer and allows the retention of chain segments for elastic deformation. However, above a certain degree of crosslinking, the material ceases to elongate [128]. A further explanation of the relationship between crosslinking and increasing % elongation can be attributed to the more flexible molecular structure resulting from ionic cross-linking [129].

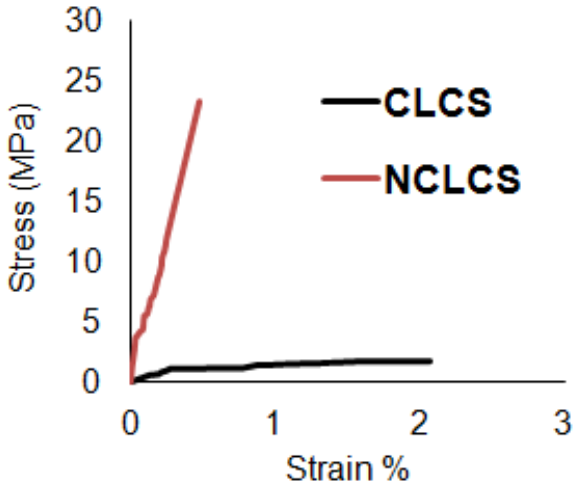

Figure 4.21 Stress-strain curve for NCLCS and CLCS membranes

4.3.8.2. Effect of F and G nanofiller content on the tensile properties of NCLCS membranes

Figure 4.22 reflected the effect of addition of nanofillers (F or G) to CS matrices membranes. On using F as a nanofiller in NCLCS, the tensile strength increased from 24MPa for the plain matrices up to 45MPa with increasing F-content up to 1 wt.%. with an average of 46% as illustrated in Figures 4.22(a). The increase in tensile strength upon addition of F-nanofiller was most probably due to the rigidity of the F nanofiller and the strong interaction between the CS polymeric chains within. The clusters of F-nanofiller were dispersed within the CS polymeric chains as reported by Shlykov *et., al.* [130]. They reported that F improved the tensile strength of polymers to 30-40 % [130-131].

On the other hand, addition of G-nanofiller, the tensile strength of NCLCS/0.1 wt.% G displayed was about 30MPa, which shows an increase in the tensile strength compared to NCLCS (24MPa). The strength was further increased by adding 1wt. % of G up to 40MPa as shown in Figure 4.22(b). Accordingly, increasing G-content up to 1 wt.% to the NCLCS matrices resulted in 40% increase in tensile strength. It was reported by Chaharmahali *et., al.* that G improved the tensile strength of polymers to 29%. The enhancement was easily explainable with the large aspect ratio and high interfacial contact area of G-nanoparticles with the polymers [132].

The increase in tensile strength with the addition of different wt.% of G suggested that G-nanofiller was mechanically dispersed into the NCLCS during the wet mixing process forming a carbon network in the polymer structure. Moreover, the compatibility of the hydrogen bonds in CS with the carbonyl functional group in G nanoparticles caused an observed enhancement in tensile strength [133].

However, the higher tensile strength upon addition of F-nanofiller was attributed to the small clusters of F-nanofiller that were better dispersed within the CS polymeric chains.

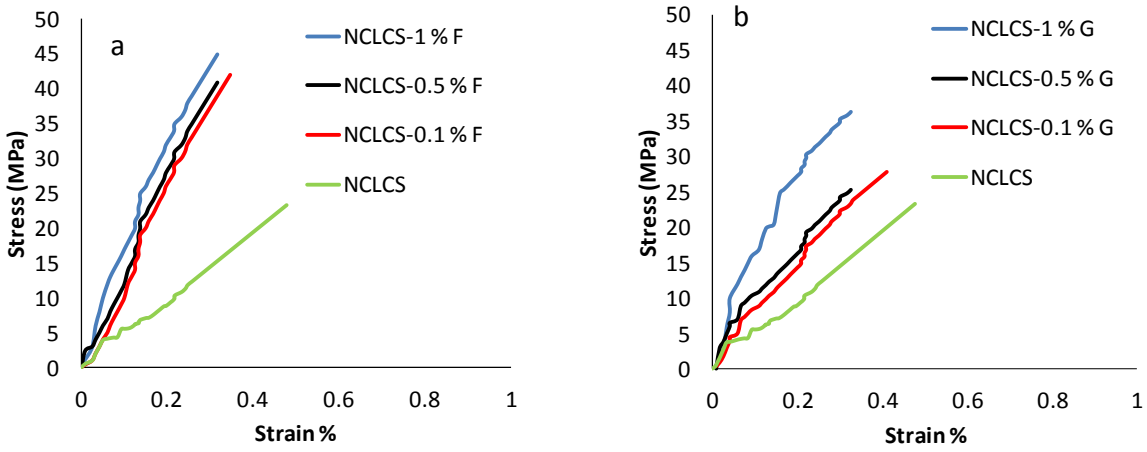

Figure 4.22 Stress-strain curve for NCLCS matrices as a function of increasing the wt.% of (a) F and (b) G.

The reduction in the ductility of the composite with increase in the F and G-nanofillers was due to increase in the deformation of a rigid interfacial interaction between F,G and the polymer matrix. The rigidity of bonding between F,G and NCLCS matrix led to a weak % elongation, as illustrated in Figure 4.22(b). However, upon comparing the % elongation in NCLCS/F membranes and NCLCS/G membranes, one would conclude that the same behaviour occurred and the composite was tending towards brittle behaviour [134].

4.3.8.3. Effect of F and G nanofiller content on the tensile properties of CLCS membranes

The addition of nanofillers (F or G) to CLCS matrices membranes enhanced their tensile strength. The tensile strength of CLCS/0.1 wt.% F displayed about 10MPa. The tensile strength was further increased by adding 1wt. % of F up to 20MPa as shown in Figure 4.23(a).

The tensile strength of CLCS/0.1 wt.% G displayed 9MPa, which shows an increase in the tensile strength compared to CLCS (2.8MPa). The tensile strength was further increased by adding 1wt. % of G up to 17MPa as shown in Figure 4.23(b). Accordingly increasing G-content up to 1 wt.% to the CLCS matrices resulted in 80 % increase in tensile strength, while caused a decrease of 20 % in elongation due to the rigidity of the nanocomposite [134].

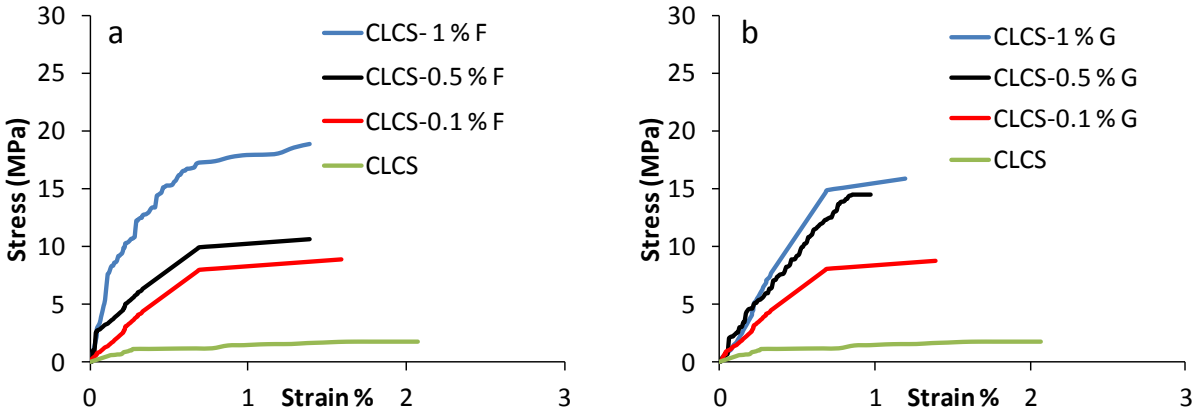

Figure 4.23. Stress-strain curve for CLCS with different wt.% of (a) F and (b) G

However, the higher tensile strength upon addition of F-nanofiller was attributed to the small clusters of F-nanofiller that were better dispersed within the CS polymeric chains.

4.3.8.4. Effect of increasing temperature on the tensile properties of CS membranes

The results referred to in the previous sections were recorded at room temperature. However, in order to study the influence of temperature on the tensile strength and % elongation of the CS mesoporous membranes as a function of the cross-linking and the nanofillers content, the tensile testing of the fabricated membranes were carried out at two more different temperatures of 30 and 60^{o} C. The tensile strength and pore size for all CS membranes were measured at a preselected strain of (ε = 0.4% for NCLCS - 1.8% for CLCS membranes) and listed in Table 4.8. It is worth mentioning that these tensile strength results were recorded prior to membrane failure.

It was clear from the listed results in Table 4.8. that the NCLCS tensile strength was higher than that of the CLCS, while the average pore size for the NCLCS was lower than that of the CLCS. Increasing the temperature resulted in the decrease of tensile of NCLCS membranes by 8% and 20 % and an increase in the pore size by 30% and 90% at 30 and 60^{o}C, respectively as shown in Table 4.8. This could be due to the increase in the movement of CS chains leading to enlargement of the pore sizes in the different CS membranes [133].

Upon the addition of 0.1wt.% F to NCLCS membranes there was a decrease in tensile strength of 30 % and 20 % and an increase in pore by size 70 % and 100% at 30 and 60^{o}C, respectively. Upon the addition of 1wt.% F to NCLCS membranes there was a decrease in tensile strength of 45 % and 53 % and an increase in pore by size 62 % and 91% at 30 and 60^{o}C, respectively as shown in Table 4.7. The same behaviour of decreasing tensile strength with an increase in pore size, was observed in CLCS membranes upon the addition of F-nanofiller. However, the decrease of tensile strength is larger than that of NCLCS as explained in section 4.3.8.1.

On the other hand, upon the addition of 0.1wt.% G to NCLCS membranes there was a decrease in tensile strength of 10 % and 30 % and an increase in pore by size 22 % and 66 % at 30 and 60^{o}C, respectively. Upon the addition of 1wt.% G to NCLCS membranes there was a decrease in tensile strength of 5 % and 28 % and an increase in pore by size 50 % and 50 % at 30 and 60^{o}C, respectively as

shown in Table 4.7. The same behaviour was observed in CLCS membranes upon the addition of G-nanofiller. Although the tensile strength decreased as a result of pore enlargement, still the tensile strength of NCLCS/1 wt.% G at 60ºC (29 MPa) was considered a reliable membrane, suitable for packaging applications even at elevated temperatures according to Siracusa *et., al.* [134]

Table 4.7 Tensile strength for CS membranes at 23, 30, 60 °C

Temperature	23°C		30°C		60°C	
Membranes	T.S. * MPa	P.S.* nm	T.S. * MPa	P.S.* nm	T.S. * MPa	P.S.* nm
NCLCS	24.0	10.6	22.8	13.4	19.4	15.4
NCLCS-0.1%F	40.0	2.6	27.5	4.4	19.9	5.2
NCLCS-0.5%F	43.0	2.5	30.5	4.1	20.2	4.9
NCLCS-1%F	45.0	2.4	36.0	3.9	21.1	4.6
NCLCS-0.1%G	30.8	1.8	27.2	2.2	24.2	3.0
NCLCS-0.5%G	35.3	1.1	32.5	1.6	26.2	2.5
NCLCS-1%G	40.1	0.0	38.8	1.0	29.8	2.0
CLCS	2.8	19.3	1.2	29.5	0.8	33.3
CLCS-0.1%F	9.0	18.1	8.6	26.4	7.9	29.4
CLCS-0.5%F	18.0	17.2	11.5	18.2	11.5	26.4
CLCS-1%F	20.0	16.0	17.3	4.5	15.2	25.1
CLCS-0.1%G	10.9	15.3	8.6	17.0	5.2	20.0
CLCS-0.5%G	14.2	9.2	10.1	11.5	7.4	15.2
CLCS-1%G	17.0	4.0	13.2	5.0	10.2	7.0

* T.S. Tensile Strength, *P.S. Pore size

4.3.8.5. Effect of increasing temperature on barrier properties of CS membranes using FEA

The increase in temperature had a direct effect on the mass diffusion. High diffusion rates occurred at low % of nanofillers as a function of increasing temperature. Table 4.9 and 4.10 shows the effect of increasing temperature on the normalized concentration of both NCLCS and CLCS and their nanocomposite membranes along

the membrane thickness. It is clear from Tables 4.8 and 4.9. that the increase in temperature from 23 ºC to 30 ºC and 60 ºC revealed higher (normalized concentration) diffusion due to increase in the pore size.

The normalized concentration at 0.2mm in NCLCS was 767 (C/S) which increased to 777 (C/S) at 30 ºC. The same behaviour was displayed upon raising the temperature up to 60 ºC. A normalized concentration of 797 (C/S) was measured as shown in Table 4.8.

The normalized concentration, in Table 4.9. for CLCS membranes at 0.2 mm distance was higher (780 (C/S)) than that of NCLCS membranes (767 (C/S)), which agreed with the exhibited increase of pore size upon cross-linking. The similar effect of increasing temperature was illustrated in Table 4.9, for CLCS membranes at 0.2mm distance; the increase of normalized concentration from 780 (C/S) to 800 (C/S) at 30 ºC was followed by an increase to 840 (C/S) at 60 ºC. This established the correlation between pore size increase and the increase in temperature. The similar behaviour was reported by Morehouse *et., al.* [96], where the increase in temperature increased the normalized concentration of the membranes due to increase in pore size with stretching the membranes.

Table 4.8 Normalized Concentration for NCLCS membranes at 23, 30, 60 °C

23°C	Normalized Concentration *(C/S)						
*D. (mm)	NCLCS	NCLCS-0.1% F	NCLCS-0.5 %F	NCLCS-1%F	NCLCS-0.1%G	NCLCS-0.5% G	NCLCS-1%G
0	850	850	850	850	850	850	850
0.2	767	766	764	763	765	762	754
0.4	684	682	678	676	680	674	658
0.6	601	598	592	589	595	586	562
0.8	518	514	506	502	510	498	466
1	435	430	420	415	425	410	370
1.2	352	346	334	328	340	322	274
1.4	269	262	248	241	255	234	178
1.6	186	178	162	154	170	146	82
1.8	103	94	76	67	85	58	0
30°C	Normalized Concentration (C/S)						

D.(mm)	NCLCS	NCLCS-0.1% F	NCLCS-0.5 %F	NCLCS-1%F	NCLCS-0.1%G	NCLCS-0.5% G	NCLCS-1 %G
0	850	850	850	850	850	850	850
0.2	777	776	774	773	776	774	773
0.4	694	692	688	686	692	688	686
0.6	611	608	602	599	608	602	599
0.8	528	524	516	512	524	516	512
1	445	440	430	425	440	430	425
1.2	362	356	344	338	356	344	338
1.4	279	272	258	251	272	258	251
1.6	196	188	172	164	188	172	164
1.8	113	104	86	77	104	86	77
60°C	Normalized Concentration(C/S)						
D. (mm)	NCLCS	NCLCS-0.1% F	NCLCS-0.5 %F	NCLCS-1%F	NCLCS-0.1%G	NCLCS-0.5% G	NCLCS-1 %G
0	850	850	850	850	850	850	850
0.2	797	796	794	793	796	794	793
0.4	714	712	708	706	712	708	706
0.6	631	628	622	619	628	622	619
0.8	548	544	536	532	544	536	532
1	465	460	450	445	460	450	445
1.2	382	376	364	358	376	364	358
1.4	299	292	278	271	292	278	271
1.6	216	208	192	184	208	192	184
1.8	133	124	106	97	124	106	97

*C/S normalized concentration, C mass concentration of diffusing material, s solubility in the base material, D distance in mm.

Table 4.9 Normalized Concentration for CLCS membranes at 23, 30, 60 °C

23°C	Normalized Concentration* (C/S)						
*D. (mm)	CLCS	CLCS-0.1%F	CLCS-0.5 %F	CLCS-1%F	CLCS-0.1%G	CLCS-0.5%G	CLCS-1 %G
0	850	850	850	850	850	850	850
0.2	780	778	788	776	775	756	750
0.4	710	706	726	702	700	662	650
0.6	640	634	664	628	625	568	550
0.8	570	562	602	554	550	474	450
1	500	490	540	480	475	380	350
1.2	430	418	478	406	400	286	250
1.4	360	346	416	332	325	192	150
1.6	290	274	354	258	250	98	50
1.8	220	202	292	184	175	4	0
30°C	Normalized Concentration (C/S)						
D.(mm)	CLCS	CLCS-	CLCS-0.5	CLCS-	CLCS-	CLCS-	CLCS-1

		0.1%F	%F	1%F	0.1%G	0.5%G	%G
0	850	850	850	850	850	850	850
0.2	800	798	808	796	795	776	770
0.4	730	726	746	722	720	682	670
0.6	660	654	684	648	645	588	570
0.8	590	582	622	574	570	494	470
1	520	510	560	500	495	400	370
1.2	450	438	498	426	420	306	270
1.4	380	366	436	352	345	212	170
1.6	310	294	374	278	270	118	70
1.8	240	222	312	204	195	24	20
60°C	Normalized Concentration (C/S)						
D.(mm)	CLCS	CLCS-0.1%F	CLCS-0.5 %F	CLCS-1%F	CLCS-0.1%G	CLCS-0.5%G	CLCS-1 %G
0	850	850	850	850	850	850	850
0.2	840	838	848	836	835	816	810
0.4	770	766	786	762	760	722	710
0.6	700	694	724	688	685	628	610
0.8	630	622	662	614	610	534	510
1	560	550	600	540	535	440	410
1.2	490	478	538	466	460	346	310
1.4	420	406	476	392	385	252	210
1.6	350	334	414	318	310	158	110
1.8	280	262	352	244	235	64	60

*C/S normalized concentration, C mass concentration of diffusing material, solubility in the base material, D distance in mm.

Chapter 4

STATISTICAL ANALYSIS

4.4. Statistical Analysis

In order to find the optimum and most desirable membranes for filtration and packaging applications, statistical analysis was performed. The input for the analysis was the experimental results of the collective properties (porosity and tensile strength) of CLCS and NCLCS with different wt.% Of G and F at 23, 30, and 60°C. The experimental results used are mentioned in sections 4.3.2, 4.3.3 and 4.3.8. The Results for LDPE characterization were not included in the statistical analysis due to lack of significant improvement of barrier properties of LDPE membranes.

RSM was useful in applying the statistical analysis as it modeled three different responses: i) tensile strength, ii) pore size and iii) diffusion time. The responses were influenced by several parameters including temperature (23, 30, and 60°C), polymer (CLCS and NCLCS), nanofiller type (F and G) and wt.% of the nanofiller (0.1, 0.5, and 1 wt.%). It is worth mentioning that the input data for tensile strength were prior to membrane failure. The ultimate objective of RSM was to determine the optimum operating conditions for the membrane fabrication [91].

4.4.1. Design Summary

The first step was to enter all input experimental results shown in Table 4.10 to the Design Expert software. When using response surface designs, it was necessary to check the normality assumption before obtaining the results. It was important to ascertain whether data show a serious deviation from normality [91].A check of normality assumption was made by plotting a normal probability plot. A check on the assumption of constant variance was also performed before analyzing the input data [90]. (normality and variance checks are in Appendix 1.)

Table 4.10 Input experimental results

Temperature	23°C			30°C			60°C		
Membranes	T.S. * MPa	P.S. * nm	D.T.* hrs	T.S. * MPa	P.S. * nm	D.T.* hrs	T.S. * MPa	P.S. * Nm	D.T.* hrs
NCLCS	24	10.6	16	22.8	13.4	11	19.4	15.4	8
NCLCS-0.1%F	40	2.6	17	27.5	4.4	12.5	19.9	5.2	9.5
NCLCS-0.5%F	43	2.5	18	30.5	4.1	13	20.2	4.9	11
NCLCS-1%F	45	2.4	18	36	3.9	14	21.1	4.6	12
NCLCS-0.1%G	30.8	1.8	20	27.2	2.2	13	24.2	3	11
NCLCS-0.5%G	35.3	1.1	24	32.5	1.6	24	26.2	2.5	24
NCLCS-1%G	40.1	0	25	38.8	1	25	29.8	2	25
CLCS	2.8	19.3	11	1.2	29.5	6.5	0.8	33.3	5
CLCS-0.1%F	9	18.1	12	8.6	26.4	8	7.9	29.4	6
CLCS-0.5%F	18	17.2	14	11.5	18.2	10	11.5	26.4	7
CLCS-1%F	20	16	15	17.3	4.5	10.5	15.2	25.1	7.5
CLCS-0.1%G	10.9	15.3	13	8.6	17	8.5	5.2	20	8
CLCS-0.5%G	14.2	9.2	16	10.1	11.5	10.5	7.4	15.2	9
CLCS-1%G	17	4	19	13.2	5	12	10.2	7	10

*T.S. Tensile Strength, *P.S. Pore size,* D.T. Diffusion Time

4.4.2. Analysis of Variance

The main aim for this experiment was investigating the effect of F and G- nanofillers and temperature on the tensile strength, porosity, and diffusion time on CS nanocomposites membranes. There were 2 replicates to each data point to ensure that the data was correct. The 48 runs were entered in random order. This randomized test sequence was necessary to prevent the effects of unknown nuisance variables and avoid contaminating the results. To be more objective in this work, an analysis was performed to test the differences between the mean of each factor at every specified response. The appropriate procedure for testing the equality of several means was the analysis of variance (ANOVA) [87]. The ANOVA was suitable for analysis of these types of experiments. The name analysis of variance was derived from partitioning of total variability into its component parts. It states that the total variability in the given data as measured by the total corrected sum of squares can be partitioned into a sum

of squares of the differences between the treatment average and the grand average plus a sum of squares of the differences of observations within treatments from the treatment average. A further step in this method was calculating the mean square of the treatments and the error. F is the ratio of the mean square of the treatments to the mean square error. In this work, the ANOVA shows that the mean square of treatments is larger than the error mean square and the p value can be computed (if it is less than 0.0001 than the factor is significant) [91]. The factors and their interactions highlighted in Table 4.11 are the significant ones.

Table 4.11 ANOVA for the three responses for selected membranes

	F	P value	F	P value	F	P value
A-Temp	35.62	< 0.0001	46.26	< 0.0001	45.38	< 0.0001
A^2	6.7	0.015	17.69	0.0002	26.34	< 0.0001
B-Polymer	118.42	< 0.0001	337.43	< 0.0001	47.03	< 0.0001
C-Filler	0.1	0.75	57.37	< 0.0001	34.88	< 0.0001
D-% of filler	23.35	< 0.0001	40.92	< 0.0001	24.72	< 0.0001
AB	1.49	0.23	12.12	0.002	0.12	0.735
AC	3.53	0.07	3.21	0.083	3.56	0.069
AD	2.79	0.06	2.57	0.074	1.69	0.196
BC	1.29	0.26	10.54	0.003	1.93	0.175
BD	0.85	0.48	6.58	0.002	2.64	0.069
CD	0.15	0.93	12.61	< 0.0001	7.65	0.0007

* F. Ratio of mean square, P. Probability

The Design Expert output chart shown in Figure 4.24. highlighted the significant factors within each response. The significant factors for tensile strength response included: temperature, crosslinking of polymer and the wt.% of filler. The higher the ambient temperature, the lower the tensile strength (Figure 4.24 (a)). CLCS has lower tensile strength than NCLCS as illustrated in Figure 4.24(b). The increase in the wt.% of the nanofiller led to an increase in the tensile strength as shown in Figure 4.24(b). The analysis of variance outcomes corresponded to the experimental results in section 4.3.8.1 where CLCS had a lower tensile strength than NCLCS. In section 4.3.8.2 and 4.3.8.3 the addition of nanofiller increased the tensile strength of both NCLCS and CLCS membranes. The results shown in

section 4.3.8.4 established the same effect of temperature on lowering tensile strength of the membranes as the software output.

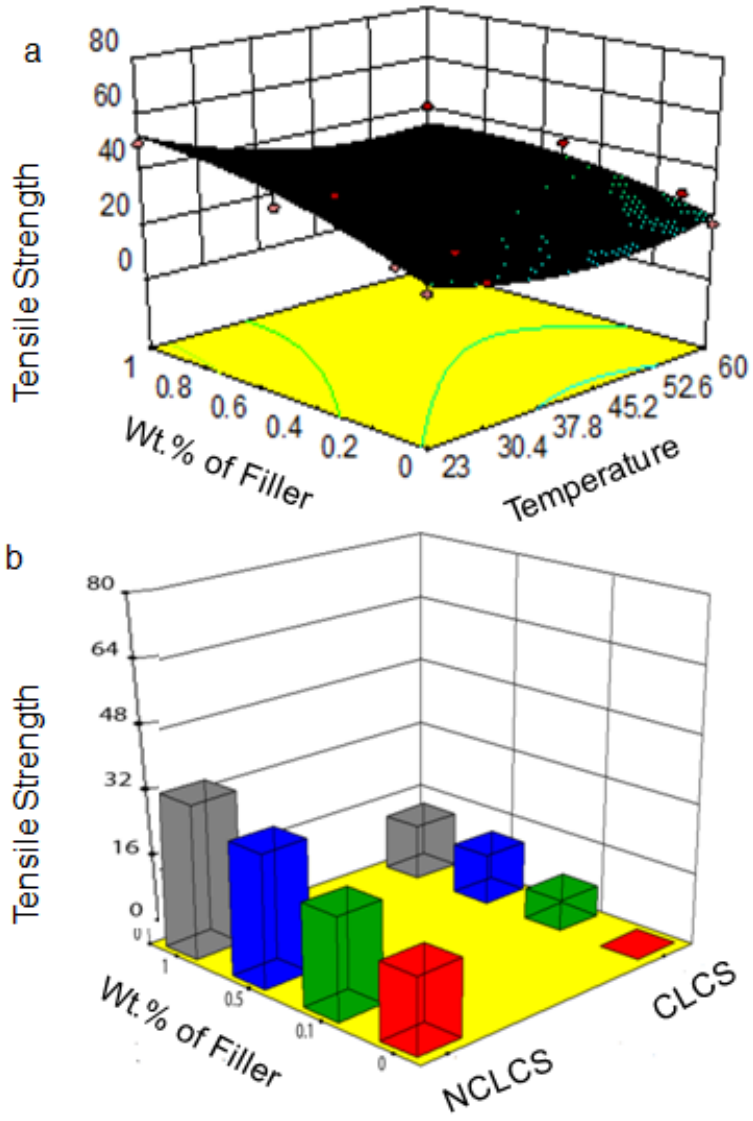

Figure 4.24 Output charts showing effect of temperature, cross-linking of the polymer and the wt.% of the nanofiller on the tensile strength response.

For the pore size response, there are several factors which were significant including significant factors: temperature, cross-linking of polymer, nanofiller type, the wt.% of filler and the interaction between the nanofiller type and the wt.% of the filler. As the temperature increase pore size increased as in Figure 4.25(a), the effect of increase of

wt.% of filler was quite clear in Figure 4.25(b). As wt.% of filler increase, the pore size decreased, thus increasing the barrier effect of the fabricated membranes. The experimental results were similar in sections 4.3.2. where the pore size decreased in Table 4.6 due to effect of nanofillers.

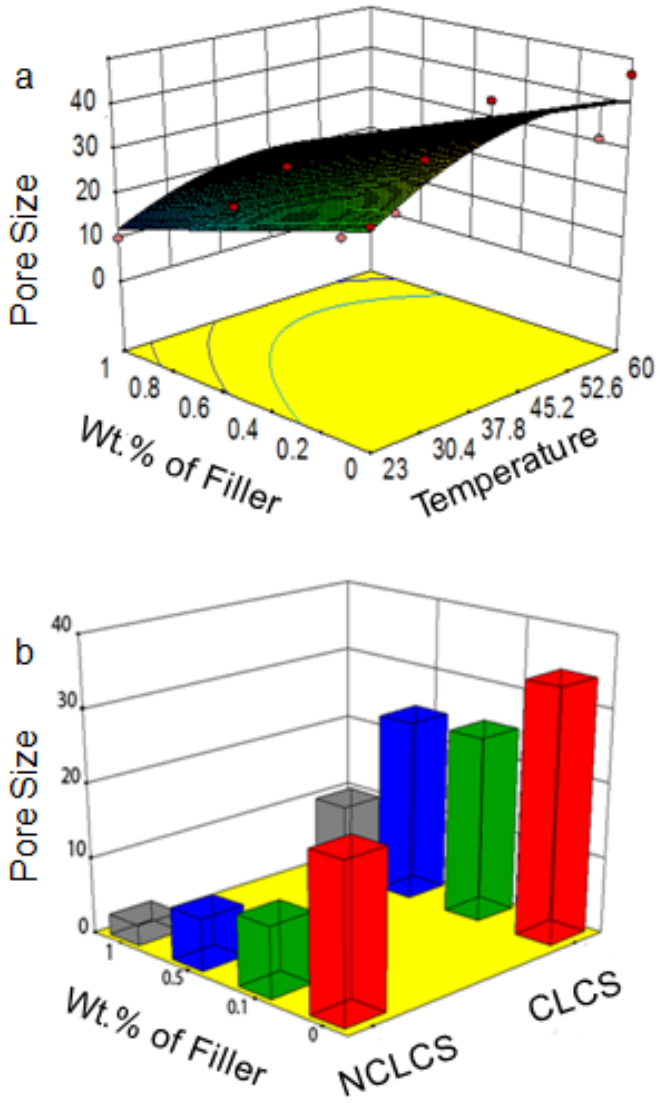

Figure 4.25 Output charts showing effect of temperature and the wt.% of the nanofiller on the pore size response

The significant factors for the third response, the diffusion time, were the temperature, cross-linking of polymer, nanofiller type, the wt.% of filler. The increase in

temperature decreased the diffusion time due to enlargement of the pore size because of the heating effect as revealed in Figure 4.26(a). The increase in the wt.% of the nanofiller shows a prolonged diffusion time due to blocking of the pores as illustrated in Figure 4.26(b).

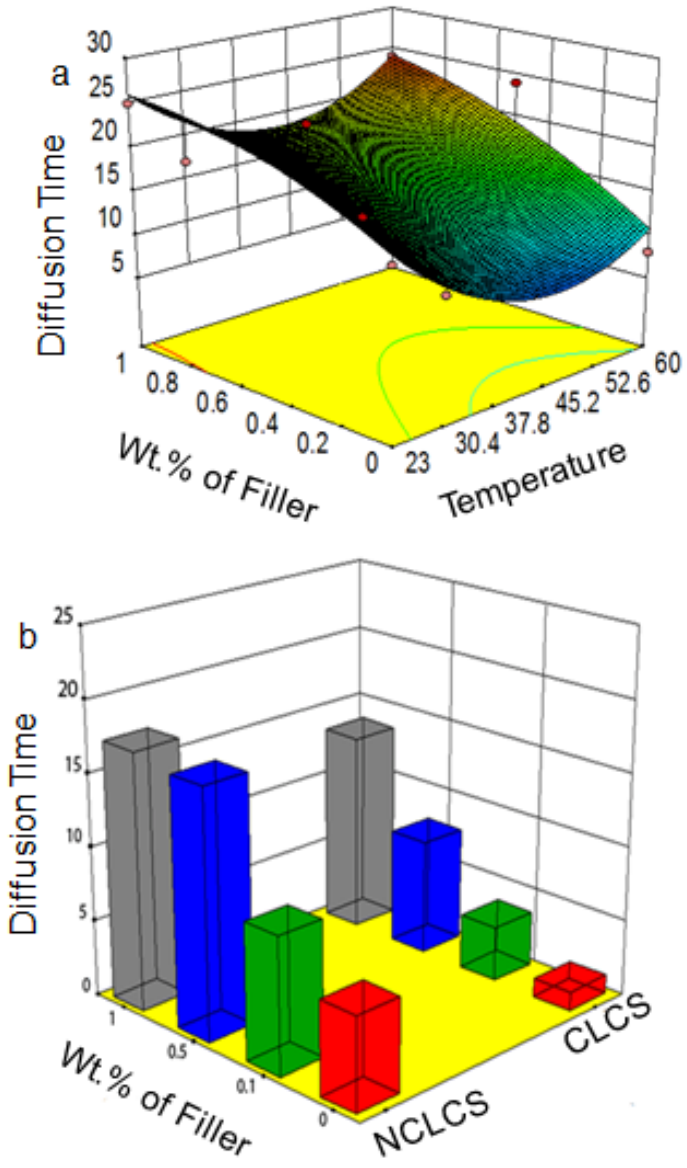

Figure 4.26 Output charts showing effect of temperature and wt.% of filler on diffusion time response

4.4.3. Desirability

The desirability function approach is one of the most widely used methods in industry for the optimization of multiple response processes. It was based on the idea that the "quality" of a product or process that has multiple quality characteristics, with one of them outside of some "desired" limits, is completely unacceptable. The method finds operating conditions that provide the "most desirable" response values. Table 4.12 illustrated each pore size with the corresponding type of polymer, type and wt.% of filler and the desirability of the membrane [91].

Table 4.12 Different pore size with (temp, polymer type, filler type, filler wt.%,) factors and desirability of membranes.

P.S.* nm	Temp °C	Polymer	Filler	Wt.% of filler	T.S.* MPa	D. T.* hrs	Desirability
0.21	32.61	NCLCS	G	1.00	42.30	19.43	0.58
0.67	42.87	NCLCS	G	1.00	35.31	17.55	0.59
0.10	25.72	CLCS	G	1.00	24.97	18.97	0.54
3.27	25.95	CLCS	G	1.00	24.72	18.83	0.54
3.48	60.00	NCLCS	G	0.83	35.08	22.97	0.81
3.61	60.00	NCLCS	G	0.84	35.05	23.04	0.81
3.89	60.00	NCLCS	G	0.86	34.98	23.23	0.81
4.05	25.24	NCLCS	F	0.10	34.60	15.44	0.66
4.13	60.00	NCLCS	G	0.88	34.91	23.37	0.81
4.26	60.00	NCLCS	G	0.89	34.87	23.45	0.81
4.38	26.40	NCLCS	G	0.10	32.71	15.93	0.63
4.95	60.00	NCLCS	G	0.95	34.53	23.87	0.81
5.02	60.00	NCLCS	G	0.95	34.49	23.91	0.81
5.22	60.00	NCLCS	G	0.97	34.36	24.02	0.81
5.28	60.00	NCLCS	G	0.98	34.31	24.06	0.81
5.40	27.69	NCLCS	F	0.50	38.08	16.23	0.64
5.44	60.00	NCLCS	G	0.99	34.20	24.14	0.81
5.51	60.00	NCLCS	G	1.00	34.14	24.18	0.81
5.55	60.00	NCLCS	G	1.00	34.10	24.21	0.81
5.56	27.92	NCLCS	F	0.50	37.82	16.06	0.64
5.66	33.92	NCLCS	G	0.50	34.46	18.99	0.54
6.61	47.22	NCLCS	G	0.50	30.00	16.87	0.37
7.21	23.16	NCLCS	F	0.00	28.10	15.92	0.61
7.86	60.00	NCLCS	F	0.83	29.74	12.84	0.59
7.86	60.00	NCLCS	F	0.83	29.73	12.84	0.59
7.86	60.00	NCLCS	F	0.82	29.74	12.83	0.59

7.86	60.00	NCLCS	F	0.82	29.75	12.83	0.59
7.87	60.00	NCLCS	F	0.79	29.74	12.81	0.59
7.88	60.00	NCLCS	F	0.89	29.62	12.83	0.59
7.93	60.00	CLCS	G	1.00	14.66	19.18	0.56
7.99	60.00	CLCS	G	1.00	14.70	19.15	0.56
8.12	60.00	CLCS	G	0.99	14.78	19.10	0.56
8.46	60.00	CLCS	G	0.97	15.00	18.96	0.56
8.46	24.50	NCLCS	F	1.00	53.68	15.69	0.71
8.55	60.00	CLCS	G	0.96	15.05	18.92	0.56
8.62	49.90	NCLCS	G	0.10	23.01	9.29	0.45
8.64	60.00	CLCS	G	0.96	15.11	18.88	0.56
8.92	60.00	CLCS	G	0.94	15.26	18.76	0.56
9.40	32.96	CLCS	G	1.00	18.73	14.98	0.39
9.47	33.11	CLCS	G	1.00	18.61	14.92	0.39
9.54	33.28	CLCS	G	1.00	18.49	14.86	0.39
9.91	34.10	CLCS	G	1.00	17.88	14.59	0.39
10.07	31.73	NCLCS	F	0.73	40.87	12.63	0.44
10.10	31.78	NCLCS	F	0.73	40.88	12.60	0.44
10.43	51.05	NCLCS	F	0.50	24.50	9.54	0.48
10.44	47.92	CLCS	G	1.00	11.68	14.45	0.35
10.48	50.82	NCLCS	F	0.50	24.51	9.50	0.48
10.74	52.89	NCLCS	F	0.10	19.04	6.34	0.48
10.81	52.66	NCLCS	F	0.10	19.02	6.30	0.48
10.88	52.43	NCLCS	F	0.10	19.01	6.25	0.48
11.27	31.22	NCLCS	F	1.00	43.59	11.90	0.55
11.30	23.00	NCLCS	G	0.00	27.33	15.84	0.58
11.80	32.44	NCLCS	F	1.00	42.20	11.29	0.55
11.94	32.79	NCLCS	F	1.00	41.82	11.13	0.55
12.02	33.00	NCLCS	F	1.00	41.59	11.03	0.55
12.12	33.26	NCLCS	F	1.00	41.31	10.91	0.55
12.20	33.49	NCLCS	F	1.00	41.08	10.82	0.55
12.28	33.70	NCLCS	F	1.00	40.85	10.72	0.55
12.87	35.56	NCLCS	F	1.00	38.98	10.00	0.55
13.01	36.07	NCLCS	F	1.00	38.49	9.82	0.55
13.18	36.74	NCLCS	F	1.00	37.88	9.61	0.55
13.83	32.49	NCLCS	G	0.00	21.81	10.48	0.49
14.09	23.00	CLCS	G	0.50	22.78	16.50	0.53
14.15	33.18	NCLCS	G	0.00	21.43	10.14	0.49
14.17	23.00	CLCS	G	0.10	17.46	12.87	0.53
14.28	49.44	NCLCS	F	1.00	31.05	8.37	0.56
14.31	33.54	NCLCS	G	0.00	21.25	9.96	0.49
14.37	33.70	NCLCS	G	0.00	21.17	9.89	0.49
14.40	48.98	NCLCS	F	1.00	31.21	8.29	0.56
14.45	48.74	NCLCS	F	1.00	31.30	8.25	0.56

16.88	60.00	NCLCS	F	0.00	17.64	7.10	0.55
17.01	23.00	CLCS	F	1.00	34.63	14.79	0.60
17.63	27.86	CLCS	G	0.31	14.05	11.68	0.47
18.08	58.99	NCLCS	G	0.00	23.05	9.34	0.58
18.55	58.05	NCLCS	G	0.00	22.41	8.88	0.58
20.05	23.00	CLCS	F	0.10	22.38	13.60	0.52
21.07	23.00	CLCS	G	0.00	2.53	10.50	0.24
21.58	23.47	CLCS	G	0.00	2.15	10.11	0.07
21.84	23.00	CLCS	F	0.50	26.18	12.73	0.54
22.34	60.00	CLCS	G	0.50	16.56	12.44	0.53
22.42	27.63	CLCS	F	1.00	28.30	10.42	0.62
22.43	27.75	CLCS	F	0.81	27.20	11.08	0.27
22.47	23.00	CLCS	F	0.00	7.21	12.65	0.37
22.65	27.93	CLCS	F	1.00	27.94	10.23	0.62
22.78	28.10	CLCS	F	1.00	27.74	10.12	0.62
22.95	28.32	CLCS	F	1.00	27.48	9.98	0.62
22.98	60.00	CLCS	G	0.10	12.44	7.66	0.53
23.47	29.02	CLCS	F	1.00	26.68	9.56	0.62
23.57	29.16	CLCS	F	1.00	26.52	9.48	0.62
24.22	30.09	CLCS	F	1.00	25.49	8.95	0.62
26.30	26.44	CLCS	F	0.00	4.02	9.67	0.20
27.47	60.00	CLCS	F	0.93	13.89	9.61	0.31
27.54	60.00	CLCS	F	0.92	14.01	9.61	0.31
27.59	60.00	CLCS	F	0.91	14.07	9.62	0.31
27.62	60.00	CLCS	F	0.90	14.12	9.62	0.31
27.65	60.00	CLCS	F	0.89	14.16	9.62	0.31
27.86	55.35	CLCS	F	1.00	12.53	8.48	0.54
27.93	55.12	CLCS	F	1.00	12.52	8.39	0.54
27.97	54.99	CLCS	F	1.00	12.52	8.33	0.54
27.98	60.00	CLCS	F	0.83	14.45	9.58	0.31
32.44	60.00	CLCS	F	0.10	10.26	5.40	0.57
33.68	60.00	CLCS	F	0.50	12.86	5.67	0.61
34.28	60.00	CLCS	G	0.00	3.59	5.07	0.39
34.62	59.03	CLCS	G	0.00	2.77	4.55	0.07

*P.S. Pore size,*T.S. Tensile Strength, * D.T. Diffusion Time

The results found in Table 4.12. are theoretical results that covered the whole range of pore sizes. The huge benefit behind this generated data was the selection of the pore size needed from Table 4.12. depending on the application of the membrane. All the factors corresponding to the pore size were specified. The membrane would be easily fabricated and the desirability of the membrane was also specified. This approach was utilized by lowa *et., al.* to find the appropriate stretching operating region for cellulose sheets based on the required levels of desirability [135].

4.4.9. Maximizing and minimizing Factors

Temperature played an important role in lowering the tensile strength. In order to avoid the weakness of tensile strength, the optimum filler type and wt.% were generated at minimum and maximum temperatures.

Table 4.13 Maximized and minimized factors with most desirable combinations

A:Temp	B:Polymer	C:Filler	D:% of filler	Tensile Strength	Pore size	Diffusion Time
Maximize	**is in range**	**is in range**	**is in range**	**Maximize**	**Maximize**	**Minimize**
60	CLCS	Fullerene	0.5	12.86	33.68	5.67
Minimize	**is in range**	**is in range**	**is in range**	**Maximize**	**Maximize**	**Minimize**
27.93	CLCS	Fullerene	1	27.94	22.65	10.23
Minimize	**is in range**	**is in range**	**is in range**	**Maximize**	**Minimize**	**Minimize**
24.53	NCLCS	Fullerene	1	53.68	8.46	15.67
Maximize	**is in range**	**is in range**	**is in range**	**Maximize**	**Minimize**	**Maximize**
60	NCLCS	Graphene	1	34.10	5.554	24.23

The corresponding three responses to maximum and minimum temperatures were also generated as shown in Table 4.13. This analysis made it easy to select membranes according to the temperature of the surrounding atmosphere. The same procedure was utilized by Mohruni *et. al.,* He used RSM to optimize in preparing the best composition of polyvinylidene fluoride (PVDF) composite membranes [136].

Chapter 5

SUMMARY AND CONCLUSIONS

5.1. Summary

In summary, the results produced from the current study showed that thw fabricated LDPE membranes are microporous, while the fabricated CS membranes are mesoporous. The pore size of LDPE ranges between 0.1 to 0.2µm. on the other hand, NCLCS membranes shows the formation of pore size of 10 nm, while CLCS membranes displayed 200% coarser pore sizes and 70% higher permeability. Moreover, the crosslinking of CS membranes increased the % elongation for CLCS by more than 75%.

The addition of F and G resulted in the enhancement of the tensile properties of LDPE and CS membranes. The yield tensile strength of LDPE membranes increased by 125% upon the addition of F-nanofiller and 160 % upon G-nanofiller addition. The yield tensile strength of NCLCS membranes increased by 46% for F and 40% for G. There was an increase in the tensile strength of CLCS membranes by 90 and 80% for F and G-nanofiller, respectively.

Moreover, the addition of nanofillers improved the membranes' gas barrier properties by decreasing the pore size in the LDPE, NCLCS, CLCS membranes by an average of 50, 80 and 50 % respectively. The preferred temperature range from 23 to 30º C offered the most suitable environment at which the tensile strength and pore size were most suitable to packaging applications. Increasing the temperature to 60 ºC resulted in a pore size increase in LDPE, NCLCS and CLCS membranes. This decreased tensile strength with an average of 20 %

Table 4.14 Permeant size and optimum membrane conditions from statistical analysis

Permeant	Permeant Size (nm)	pore size (nm)	Temp °C	Polymer	Filler	Wt.% of filler	T.S. (MPa)	Desirabili-ty
Gases(co_2-C_2H_4- Ch_4)	0.23-0.25	0.21	32.61	NCLCS	G	1	42.29	0.58
Pesticides Dust	1	0.67	42.87	NCLCS	G	1.00	35.31	0.59
Viruses	5	4.26	60	NCLCS	G	0.89	34.87	0.81
Combustion smoke	10	8.46	24.51	NCLCS	F	1	53.68	0.71
Flaming of Cooking Oil	30	27.93	55.12	CLCS	F	1	12.52	0.54
Sea Salt	35	32.44	60	CLCS	F	0.1	10.26	0.567
Bromine-lead-clay	103	100	23	LDPE	G	1	52	

The optimum membrane pore size, tensile strength, and operating temperature were calculated by RSM. Table 4.14 highlights a number of the filtration applications for the fabricated PNC membranes. The optimum membranes were selected according to the size of the permeant that needs to be filtered out.

5.2. Conclusions

1. The Challenge of fabricating PNC membranes lies in controlling their porosity while maintaining the tensile strength of membranes. LDPE (synthetic polymer) and CS (natural polymer) are selected according to their high performance index among other polymers.
2. The chemical nature of CS allows crosslinking, which is an additional factor in controlling the pore size of the membranes. On the other hand, this factor is not found in LDPE membranes.
3. The crosslinking of CS causes a decrease in tensile strength and an increase in % elongation of CLCS membranes, while the NCLCS membranes have a higher tensile strength with less ductility.
4. The addition of F and G- nanofillers enhance the tensile strength of LDPE, NCLCS and CLCS membranes associated with lower ductility.
5. The addition of nanofillers improves the barrier properties by blocking the membranes' pores. However, the blocking effect of nanofillers is not effective due to large pore size of LDPE membranes. Accordingly the LDPE / F, G are most suitable for filtering particles ≥100nm. The addition of nanofillers produces an average CS membrane pore size between 1 and 30nm, depending on the nanofiller type (F or G). The fine pore size of NCLCS membranes compared with LDPE membranes makes them suitable for various filtration of particles ranging from 2-10nm. The pore size of CLCS membranes allows for filtration of particles ranging from 10-30nm
6. The increase in temperature up to 30 ºC caused a slight decrease in the tensile strength due to coarsening of pores but the PNC membrane still retains its permeability and tensile strength at temperature up to 60 ºC (NCLCS/1% G).
7. In mass diffusion analysis, there is a decrease in normalized mass concentration with the increase in the wt.% of the nanofiller. In addition the diffusion rate through NCLCS,CLCS/G membranes is lower than that of NCLCS,CLCS/F.
8. The optimum type of membrane (determined by temperature, CLCS or NCLCS, F and G and wt.% of the nanofiller) is carefully selected by statistical analysis according to the application needed and the size of particles that will be filtered out.

9. The processing of CS membranes toke a shorter time compared to processing of LDPE membranes due to higher MFI of CS membranes. The MFI of CLCS membranes is increased via crosslinking of CS membranes.
10. After comparing the overall properties of CS and LDPE membranes (tensile strength, permeability, barrier effect, MFI), It is revealed that the LDPE membranes have similar tensile strength (at constant load and strain) to chitosan membranes but low barrier properties and MFI. The CS membranes have lower permeability accordingly this increases the barrier properties thus controlling the porosity of the membranes.
11. The NCLCS membranes retain their tensile strength and permeability at elevated temperatures. This widens the range of countries (ambient temperature to 60 ºC) that could utilize the NCLCS membranes.
12. The CLCS has higher ductility than NCLCS membranes. CLCS/1 wt.% F has a higher ductility and reasonable tensile strength. It can be stretched up to 20 % under constant load with time.

5.3. Future Perspectives

1. Further characterization on fabricated PNC membranes is required. Nanoindentation provide the capability to measure mechanical response at localized preselected regions, in very small volumes and at shallow depths, while monitoring time, depth and force response [137].
2. Structural analysis on the fabricated PNC membranes is required. The structural analysis is done using TEM.
    - Investigate the volume fraction of crosslinking as a function of the processing parameters of chitosan
    - Investigate the nature of the nanofiller (F,G)
    - Investigate the nanofiller- matrix interface
    - In depth study of the nanofiller morphology within the various matrices
    - Investigate the influence of the initial nanofiller cluster size, especially G if it is initially at the nanoscale.
3. Fabrication of membranes with electrospinning technique is required. Membranes fabricated using electrospun nanofibers can be used in variety of applications like filtration, tissue engineering, drug delivery. The membrane properties are governed by their surface properties and pore distribution, as well as their morphology. A comparison between the fabricated PNC membranes and electrospun membranes can be useful to evaluate the performance of the fabricated PNC membranes.
4. Reinforcement of membranes with nanofibers (as a replacement for nanofillers) and comparing the nanofibers mats versus the fabricated PNC membranes can be performed. Nanofibers insure uniformity of size and distribution, hence enhance the membrane filtration properties [138]. The new nanofibers technology provides excellent adhesion to the substrate as well as durable structural stability of the nanofibers [139-140].

References

[1] Pollutants and Sources. (2013). Retrieved April 24, 2015, from

http://www.epa.gov/airtoxics/pollsour.html

[2] Abel, P. (1996). *Water pollution biology* (2nd ed.). London: Taylor and Francis.

[3] Seinfeld, J., and Pandis, S. (1998). *Atmospheric chemistry and physics from air pollution to climate change*. New York: Wiley.

[4] Plain English guide to the Clean Air Act. (2014, October 28). Retrieved April 22, 2015, from http://www.epa.gov/airquality/peg_caa/index.html

[5] World resources institute: Monthly update: air pollution's causes, consequences and solutions. (2008). Retrieved on April 17, 2015 from http://thecityfix.com/blog/air-pollutions-causes-consequences-and-solutions.

[6] Allhands, M., and Prochaska, J. (2002). *Disc filtration: Something old, something new*. Retrieved April 2, 2015, from
http://www.ksre.ksu.edu/sdi/Abstracts/discfiltration.htm

[7] Strathmann, H. (2011). *Introduction to membrane science and technology*. Weinheim, Germany: Wiley-VCH Verlag and Co.

[8] Li, N., Fane, A., Ho, W., and Matsuura, T. (Eds.). (2008). *Advanced membrane technology and applications*. Hoboken, N.J.: Wiley.

[9] Amjad, Z. (1993). *Reverse osmosis: Membrane technology, water chemistry and industrial applications*. New York: Van Nostrand Reinhold.

[10] Desalination. (n.d.). Retrieved December 23, 2014, from http://www.trusselltech.com/technologies/desalination

[11] Ravanchi, M., Kaghazchi, T., and Kargari, A. (n.d.). Application of membrane separation processes in petrochemical industry: A review. *Desalination,* 199-244.

[12] Alberti, G., Narducci, R., and Sganappa, M. (2008). Effects of hydrothermal/thermal treatments on the water-uptake of Nafion membranes and relations with changes of conformation, counter-elastic force and tensile modulus of the matrix. *Journal of Power Sources, 178*, 575-583.

[13] Satterfield, M., and Benziger, J. (2009). Viscoelastic properties of Nafion at elevated temperature and humidity. *Journal of Polymer Science Part B: Polymer Physics, 47*, 11-24.

[14] Majsztrik, P., Bocarsly, A., and Benziger, J. (2008). Viscoelastic Response of Nafion. Effects of Temperature and Hydration on Tensile Creep. *Macromolecules, 41*, 9849-9862.

[15] GCSE CHEMISTRY - What are the Properties of Polymers? - Chain Length - Cross Links - Crystallinity - What is a Plasticizer? - GCSE SCIENCE. (n.d.). Retrieved April 2, 2015, from http://www.gcsescience.com/o59.htm

[16] Costamagna, P., Yang, C., Bocarsly, A. and Srinivasan, S. (2002). Nafion® 115/zirconium phosphate composite membranes for operation of PEMFCs above 100°C. *Electrochimica Acta, 47*, 1023-1033.

[17] Young, S., and Mauritz, K. (2001). Dynamic mechanical analyses of Nafion/organically modified silicate nanocomposites. *Journal of Polymer Science Part B: Polymer Physics, 39*, 1282-1295.

[18] Nano-enabled Packaging for the Food and Beverage Industry – A Global Technology, Industry and Market Analysis." (2009). Innovative Research and Products Inc. 107. Retrieved April 2, 2015, from http://www.plastemart.com/upload/Literature/Nano-enabled-packaging-food-beverage-estimated-US$7.3%20bln-by-2014.asp

[19] Webb, S., and Pruess, K. (2003). The Use of Fick's Law for Modeling Trace Gas Diffusion in Porous Media. *Transport in Porous Media, 51*, 327-341.

[20] Crank, J., and Park, G. (1968). *Diffusion in polymers.* London: Academic Press.

[21] Yu, B., and Jiang, X. (2014). A Fractional Anomalous Diffusion Model and Numerical Simulation for Sodium Ion Transport in the Intestinal Wall. *Advances in Mathematical Physics, 2015*, 1-8.

[22] Gorrasi, G., Tortora, M., Vittoria, V., Pollet, E., Lepoittevin, B., Alexandre, M., and Dubois, P. (2003). Vapor barrier properties of polycaprolactone montmorillonite nanocomposites: Effect of clay dispersion. *Polymer, 44*, 2271-2279.

[23] Auras, R., Harte, B., and Selke, S. (2004). Effect of water on the oxygen barrier properties of poly(ethylene terephthalate) and polylactide films. *Journal of Applied Polymer Science, 92*, 1790-1803.

[24] DoITPoMS. (n.d.). Retrieved March 24, 2015, from http://www.doitpoms.ac.uk/tlplib/polymerbasics/crystallinity.php

[25] Baker, R. (2004). *Membrane technology and applications* (2nd ed.). Chichester: J. Wiley.

[26] Nunes, S., and Peinemann, K. (2001). *Membrane technology in the chemical industry*. Weinheim: Wiley-VCH.

[27] CIEC Promoting Science at the University of York, York, UK. (n.d.). Retrieved Feruary 22, 2015, from http://www.essentialchemicalindustry.org/index.php.

[28] Haynie, D. (2008). *Biological thermodynamics*. Cambridge: Cambridge University Press.

[29] Mason, E. (1991). From pig bladders and cracked jars to polysulfones: An historical perspective on membrane transport. *Journal of Membrane Science, 60*, 125-145.

[30] Groth, E. (1998). Endocrine Disrupting Chemicals in Plastic Wraps Letter From Consumers Union to FDA 5jun98. Retrieved April 5, 2015, from http://www.mindfully.org/Plastic/EDs-Plastic-Wraps-CU5jun98.htm

[31] Compañ, V., Castillo, L., Hernández, S., López-González, M., and Riande, E. (2010). Crystallinity effect on the gas transport in semicrystalline coextruded films based on linear low density polyethylene. *Journal of Polymer Science Part B: Polymer Physics, 48*(6), 634-642.

[32] Shah, D., Maiti, P., Gunn, E., Schmidt, D., Jiang, D., Batt, C., and Giannelis, E. (2004). Dramatic Enhancements in Toughness of Polyvinylidene Fluoride Nanocomposites via Nanoclay-Directed Crystal Structure and Morphology. *Advanced Materials, 16*, 1173-1177.

[33] Bassett, D. C. (1982). *Development in Crystalline Polymers*. London: Applied Science Publishers.

[34] Gijsbertsen-Abrahamse, A., Cornelissen, E., and Hofman, J. (2006). Fiber failure frequency and causes of hollow fiber integrity loss. *Desalination, 194*, 251-258.

[35] Wu, K., Qiu, P., Wang, Z., and Wang, J. (2000). Large pore size polyacrylonitrile membrane for ultrafiltration. *Journal of Environmental Sciences, 12*.

[36] Gerald, S.(2002). *Degradable Polymers: Principles and Applications*. Netherlands: Springer.

[37] Municipal Solid Waste in the United States: 2000 Facts and Figures. (2002, June 1). Retrieved May 2, 2015, from http://www.epa.gov/epaoswer/non-hw/muncpl/pubs/report00.pdf

[38] Tharanathan, R. (2003). Biodegradable Films And Composite Coatings: Past, Present And Future. *Trends in Food Science and Technology, 14*, 71-78.

[39] Companies / Manufacturers-Plastics Industry. (n.d.). Retrieved April 24, 2015, from http://www.plastemart.com/Plastic-Manufacturer.asp

[40] Srinivasa, P., and Tharanathan, R. (2007). Chitin/Chitosan — Safe, Ecofriendly Packaging Materials with Multiple Potential Uses. *Food Reviews International, 23*(1), 53-72.

[41] Loeb, S., and Sourirajan, S. (2009). Sea Water Demineralization by Means of an Osmotic Membrane. In *Advances in Chemistry* (Vol. 38). American Chemical Society.

[42] Mchugh, T., and Krochta, J. (1994). Sorbitol- vs Glycerol-Plasticized Whey Protein Edible Films: Integrated Oxygen Permeability and Tensile Property Evaluation. *Journal of Agricultural and Food Chemistry, 42*(4), 841-845.

[43] Ravi Kumar, M. (2000). A Review Of Chitin And Chitosan Applications. *Reactive and Functional Polymers, 46*, 1-27.

[44] Product Information: GE Osmonics AG and CE Desal Membranes. (n.d.). Retrieved April 2, 2015, from http://www.gewater.com/

[45] Kesting, R. E.(1977). In Reverse Osmosis and Synthetic Membranes: Theory-Technology- Engineering. National Research Council Canada, Ottawa, 89-110.

[46] Kaplan, D. (1998). Introduction. In *Biopolymers from renewable resources*. Berlin: Springer.

[47] lawter, M., and Fisher, G.(2000). Potential of starch based packaging for the food industry, The food biopack conference. Copenhagen.

[48] Srinivasa, P., Ramesh, M., Kumar, K., and Tharanathan, R. (2004). Properties of chitosan films prepared under different drying conditions. *Journal of Food Engineering, 63*(1), 79-85.

[49] Sebti, I., Chollet, E., Degraeve, P., Noel, C., and Peyrol, E. (2007). Water Sensitivity, Antimicrobial, and Physicochemical Analyses of Edible Films Based on HPMC and/or Chitosan. *Journal of Agricultural and Food Chemistry, 55*(3), 693-699.

[50] Winterowd, J., and Sanford, P. (1995). Chitin and Chitosan. In *Food Polysaccharides and Their Applications*. New York: Marcel Dekker.

[51] Caner, C., and Cansiz, O. (2007). Effectiveness of chitosan-based coating in improving shelf-life of eggs. *Journal of the Science of Food and Agriculture, 87*, 227-232.

[52] Gällstedt, M., Törnqvist, J., and Hedenqvist, M. (2001). Properties of nitrocellulose-coated and polyethylene-laminated chitosan and whey films. *Journal of Polymer Science Part B: Polymer Physics, 39*, 985-992.

[53] Marzouqi, M., Abdulkarim, M., Marzouk, S., El-Naas, M., and Hasanain, H. (2009). Facilitated Transport of CO2 through Immobilized Liquid Membrane. *Industrial and Engineering Chemistry Research, 48*.

[54] Yu, X., Wang, Z., Zhao, J., Yuan, F., Li, S., Wang, J., and Wang, S. (n.d.). An Effective Method to Improve the Performance of Fixed Carrier Membrane via Incorporation of CO2-selective Adsorptive Silica Nanoparticles. *Chinese Journal of Chemical Engineering,* 821-832.

[55] Gontard, N., Thibault, R., Cuq, B., and Guilbert, S. (1996). Influence of Relative Humidity and Film Composition on Oxygen and Carbon Dioxide Permeabilities of Edible Films. *Journal of Agricultural and Food Chemistry, 44*, 1064-1069.

[56] D. Xu, S. Hein, and K. Wang, *Chitosan membrane in separation applications*. CRC Press, Boca Raton, 2006.

[57] Pabby, A. (2009). *Handbook of membrane separations: Chemical, pharmaceutical, food, and biotechnological applications*. Boca Raton: CRC Press.

[58] I. Pinnau, and B. D. Freeman," In Formation and Modification of Polymeric Membranes," American Chemical Society , Washington, 2009.

[59] Daubresse, C., Sergent-Engelen, T., Ferain, E., Schneider, Y., and Legras, R. (1995). Characterization of energetic heavy ion track in PVDF: Production of PVDF track-etched membrane and application. *Nuclear Instruments and Methods in Physics Research Section B: Beam Interactions with Materials and Atoms, 105*, 126-129.

[60] Gowin, P., Faibish, R., El-Dessouky, H., and Ettouney, H. (2002). Evaluating the Economics of Desalination. *Chemical Engineering Progress*.

[61] Jollès, P. and Muzzarelli, R.(1999). *Chitin and Chitinases*. Switzerland: Springer.

[62] Kouchak, M., Ameri, A., Naseri, B., Kargar Boldaji, S. (2014). Chitosan and polyvinyl alcohol composite films containing nitrofurazone: preparation and evaluation. *Iranian Journal of Basic Medical Sciences, 17*, 14-20.

[63] Zeng, X., and Ruckenstein, E. (1996). Control of Pore Sizes in Macroporous Chitosan and Chitin Membranes. *Industrial and Engineering Chemistry Research, 35*, 4169-4175.

[64] He, W., Guo, X., Xiao, L., and Feng, M. (2009). Study on the mechanisms of chitosan and its derivatives used as transdermal penetration enhancers. *International Journal of Pharmaceutics, 382*, 234-243.

[65] Muzzarelli, R. (2009). Genipin-crosslinked chitosan hydrogels as biomedical and pharmaceutical aids. *Carbohydrate Polymers, 77*, 1-9.

[66] Tiwary, A., and Rana, V. (2010). Cross-linked chitosan films: Effect of cross-linking density on swelling parameters. *Pakistan Journal of Pharmaceutical Sciences, 23*.

[67] Kawashima, Y., Handa, T., Kasai, A., Takenaka, H., Lin, S., and Ando, Y. (1985). Novel method for the preparation of controlled-release theophylline granules coated with a polyelectrolyte complex of sodium polyphosphate–chitosan. *Journal Of Pharmaceutical Sciences, 74*, 264-268.

[68] Calvo, P., Remunan-Lopez, C., Vila-Jato, J., and Alonso, M. (1997). Novel hydrophilic chitosan-polyethylene oxide nanoparticles as protein carriers. *Journal of Applied Polymer Science, 63*, 125-132.

[69] Ross-Murphy, S. (1994). Rheological characterization of polymer gels and networks. *Polymer Gels and Networks, 2*, 229-237.

[70] Knaul, J. Z. Hudson, S. M. and Creber, K. A. M. (1999). Mechanical properties of chitosan fibers. *Journal of Applied Polymer Science,* 72, 1721-1732.

[71] Basan, H., Gümüşderelíoğlu, M., and Orbey, T. (2002). Diclofenac sodium releasing pH-sensitive monolithic devices. *International Journal of Pharmaceutics, 245*, 191-198.

[72] Hamdi, G., Ponchel, G., Duchêne, D. (2001). Formulation of epichlorohydrin cross-linked starch microspheres. *Journal of Microencapsulation, 18*, 373-383.

[73] Knaul, J. K. and Creber, K. A. M. (1997). Coagulation rate studies of spinnable chitosan solutions. *Journal of Applied Polymer Science*, 72, 1721-1732.

[74] Rao, C., Sood, A., Voggu, R., and Subrahmanyam, K. (2010). Some Novel Attributes of Graphene. *The Journal of Physical Chemistry Letters, 1*, 572-580.

[75] Carey, K., Jerome, T. and Karna, S.Army Research Laboratory. (2010). Carbon Nanotube Aluminum Matrix Nanocomposites. (ARL-TR-5252). *Weapons and Materials Research Directorate*.

[76] Okada, A., et al. Composite material and process for manufacturing same. Kabushiki Kaisha Toyota Chou Kenkyusho., US Patent 4739007, 1998.

[77] Kawasumi, M., et al. Process for producing composite material. Kabushiki Kaisha Toyota Chuo Kenkyusho. US Patent 4810734, 1989.

[78] Pavlidou, S., and Papaspyrides, C. (2008). A review on polymer–layered silicate nanocomposites. *Progress in Polymer Science, 33*(12).

[79] Nguyen, Q., and Baird, D. (2006). Preparation of polymer–clay nanocomposites and their properties. *Advances in Polymer Technology, 25*, 270-285.

[80] Lin, K., Chang, J., Liu, X., Chen, L., and Zhou, Y. (2011). Synthesis of element-substituted hydroxyapatite with controllable morphology and chemical composition using calcium silicate as precursor. *Cryst.Eng. Comm, 13*, 4850-4850.

[81] Wujcik, E., and Monty, C. (2013). Nanotechnology for implantable sensors: Carbon nanotubes and graphene in medicine. *Wiley Interdisciplinary Reviews: Nanomedicine and Nanobiotechnology,* 233-249.

[82] Gorrasi, G., Tortora, M., Vittoria, V.,Pollet, E., Lepoittevin, B., Alexandre , M., and Dubois, P. (2003). Improving Barrier Properties of HDPE using Pva as Clay Modifier. *Polymer*, 44, 2279-2604.

[83] Hosokawa, J., Nishiyama, M., Yoshihara, K., and Kubo, T. (1990). Biodegradable film derived from chitosan and homogenized cellulose. *Industrial and Engineering Chemistry Research, 29*, 800-805.

[84] Choudalakis, G., and Gotsis, A. (2009). Permeability of polymer/clay nanocomposites: A review. *European Polymer Journal, 45*, 967-984.

[85] Tjong, S. (2006). Structural and mechanical properties of polymer nanocomposites. *Materials Science and Engineering: R: Reports, 53*, 73-197.

[86] Patro, T., Mhalgi, M., Khakhar, D., and Misra, A. (2008). Studies on poly(vinylidene fluoride)–clay nanocomposites: Effect of different clay modifiers. *Polymer, 49*, 3486-3499.

[87] Montgomery, D., and Runger, G. (2003). *Applied statistics and probability for engineers*. New York: John Wiley and Sons.

[88] USC: Department of Statistics. (n.d.). Retrieved February 3, 2015, from http://www.stat.sc.edu

[89] Macal, C. (2005). Model Verification and Validation. In *Threat Anticipation: Social Science Methods and Models*. Chicago: The University of Chicago and Argonne National Laboratory.

[90] Silva, M. (2013). *Design of Experiments - Applications*. InTech.

[91] Bettinger, D., and Chinnici, J. (1991). Utiliization of response surface modeling to evaluate the interaction between aflatoxin B1 and caffeine on egg adult viability in drosophila meganogaster. *Virginia Journal of Science, 42*.

[92] Duncan, B., Urquhart, J. and Roberts, S. (2005). Review of Measurement and Modeling of Permeation and Diffusion in Polymers. NPL REPORT.

[93] Choi, M., Kwon, K., Park, C., Kim, S., and Hahn, S. (1999). Estimate of the Thermal Diffusivity of Films with a Sandwich Structure by Using Pulsed Transient Analysis and AC Calorimetry. *Journal of the Korean Physical Society, 34*.

[94] Amooghin, A., Sanaeepur, H., Kargari, A., and Moghadassi, A. (2011). Direct determination of concentration-dependent diffusion coefficient in polymeric membranes based on the Frisch method. *Separation and Purification Technology, 82*, 102-113.

[95] Bhunia, K., Dhawan, S., and Sablani, S. (2012). Modeling the Oxygen Diffusion of Nanocomposite-based Food Packaging Films. *Journal of Food Science, 77*, N29-N38.

[96] Morehouse, J., Lloyd, D., Freeman, B., Lawler, D., Liechti, K., and Becker, E. (2006). Modeling the stretching of microporous membranes. *Journal of Membrane Science, 283*, 430-439.

[97] Fahim, I., Marei, N., Salem H., G., and Mamdouh, W. (2015). Effect of Graphene and Fullerene Nanofillers on Controlling the Pore Size and Physicochemical Properties of Chitosan Nanocomposite Mesoporous Membranes. *Journal of nanomaterials*, 10.

[98] Perry T., Shreyas S., Manish C., and Ki-Bum L. (2013). Design, Synthesis, and Characterization of Graphene−Nanoparticle Hybrid Materials for Bioapplications. *Chemical Reviews*.

[99] Farag, M. (1979). *Materials and Process Selection for Engineering Design.* LondonApplied Science Publisher.

[100] Goldstein, J. (2003). *Scanning Electron Microscopy and X-ray Microanalysis*. S.l.: Kluwer Academic/Plenum.

[101] Pascau, J. and Pérez, J. (2013). I*mage Processing with ImageJ*. United Kingdom: Packt Publishing.

[102] ASAP2020-Physisorption Analyzer. (n.d.). Retrieved from http://www.micromeritics.com/Product-Showcase/ASAP-2020-Physisorption.aspx

[103] D1238 - 13 Standard Test Method for Melt Flow Rates of Thermoplastics by Extrusion Plastometer, melt flow rate, melt index, volume flow rate. (n.d.). Retrieved April 1, 2015, from http://www.astm.org/Standards/D1238.htm.

[104] D882-91 Standard Test Method for Tensile Testing of Thin Plastic Sheeting (Film). (n.d.). Retrieved April 1, 2015, from http://www.astm.org/Standards/D882.htm.

[105] Myers, R. H., and Montgomery, D. C. (1995). *Response surface methodology: Process and product optimization using designed experiments*. New York: Wiley.

[106] LDPE products and applications. (2015, January 1). Retrieved April 10, 2015, from http://www.exxonmobilchemical.com/Chem-English/productsservices/polymers-ldpe-products-applications.aspx

[107] He, W., Guo, X., Xiao, L., and Feng, M. (2009). Study on the mechanisms of chitosan and its derivatives used as transdermal penetration enhancers. *International Journal of Pharmaceutics,382, 234-243.*

[108] Checchetto, R., Miotello, A., Nicolais, L., and Carotenuto, G. (2014). Gas transport through nanocomposite membrane composed by polyethylene with dispersed graphite nanoplatelets. *Journal of Membrane Science, 463*.

[109] Hosseinkhanli, H., Sharif, A., Aalaie, J., Khalkhali, T., and Akhlaghi, S. (2013). Oxygen permeability and the mechanical and thermal properties of (low-density polyethylene)/poly (ethylene-co-vinyl acetate)/organoclay blown film nanocomposites. *Journal of Vinyl and Additive Technology, 19*(2), 132-139.

[110]American Membrane Corporation. (n.d.). Retrieved April 10, 2015, from http://www.americanmembrane.com.

[111] Popli, R., Glotin, M., Mandelkern, L., and Benson, R. (1984). Dynamic mechanical studies of α and β relaxations of polyethylenes. *Journal of Polymer Science: Polymer Physics Edition, 22*, 407-448.

[112] Carotenuto, G., Nicola, S., Palomba, M., Pullini, D., Horsewell, A., Hansen, T.,and Nicolai, L.(2012). Mechanical properties of low-density polyethylene filled by graphite nanoplatelets. *Nanotechnology*, 23,48.

[113] Godovsky, D.Y. (2000).Device applications of polymer-nanocomposites. *Adv. Polym. Sci.* 153, 163–205.

[114] She, Y, H., Chen, G.H., and Wu, D,W. (2007). Fabrication of polyethylene /graphite nanocomposite from modified expanded graphite. *Polymer International*, 56 679-685.

[115] Akinci, A. (2009). Mechanical and structural properties of polypropylene composites filled with graphite flakes. *Archives of Materials Science and ,* 35, 91-94.

[116] Giuliana, G., Roberta, D., Lieto, and G. (2011). Structure-property relationships on uniaxially oriented carbon nanotube/polyethylene composites. *Journal of Polymer*, 52 1124-1132

[117] Li, Q., Dunn, E., Grandmaison, E., and Goosen, M. (1992). Applications and Properties of Chitosan. *Journal of Bioactive and Compatible Polymers, 7*(4), 370-397.

[118] Kenawy, E., Kamoun, E., Eldin, M., and El-Meligy, M. (2014). Physically crosslinked poly(vinyl alcohol)-hydroxyethyl starch blend hydrogel membranes: Synthesis and characterization for biomedical applications. *Arabian Journal of Chemistry, 7*(3).

[119] Bharadwaj, R. (2001). Modeling the Barrier Properties of Polymer-Layered Silicate Nanocomposites. *Macromolecules, 34*(26), 9189-9192.

[120] Crank, J. (1975) *The Mathematics of Diffusion*, Oxford:Clarendon Press.

[121] Hedenqvist, M.S., Yousefi, H., Malomstrom, E., and Hedrick, J.L. (2000). Transport properties of hyperbranched and dendrimer-like star polymers. *Polymer.* 41 , 1827-1840.

[122] Rzayev, Z.(2011). "Graft Copolymers of Maleic Anhydride and Its Isostructural Analogues: High Performance Engineering Materials." *International Review of Chemical Engineering,* 3(2).

[123] Gebben, B., Berg, H., Bargeman, D., and Smolders, C. (1985). Intramolecular crosslinking of poly(vinyl alcohol). *Polymer,* 1737-1740.

[124] Muzzarelli, R. (2011). Chitin nanostructures in living organisms. In *Chitin Formation and Diagenesis* (Vol. 34). Springer.

[125] Fahim, I., Marei, N., Salem, N. and Mamdouh, W. (2015). "Effect of graphene and fullerene nanofillers on controlling the pore size and physicochemical properties of chitosan nanocomposite mesoporous membranes. *Journal of Nanomaterials*, 10.

[126] Muzzarelli, R. (1986). *Chitin in nature and technology*. New York: Plenum Press.

[127] Sannan, T., Kurita, K., and Iwakura, Y. (2003). Studies on chitin, 1. Solubility change by alkaline treatment and film casting. *Macromolecular Chemistry and Physics, 176*(4).

[128] Daniels, C. (1989). *Polymers: Structure and Properties*, Lancaster: CRC Press.

[129] Wang, W., Roberts, G., Domard, A., Roberts, G., and Varum, K. (1998). *Advances in Chitin Science*, Lyon: Jacques Andre Publisher Press.

[130] Zuev, V., Kostromin, S., and Shlykov, A. (2010). Mechanics of polymer nanocomposites modified with fulleroid nanofillers. *Polymer Science Series A, 52*(5), 532-536.

[131] Sung, H., Liang, I., Chen, C., Huang, R., and Liang, H. (2001). Stability of a biological tissue fixed with a naturally occurring crosslinking agent (genipin). *Journal of Biomedical Materials Research, 55*, 538-546.

[132] Chaharmahali, M., Hamzeh, Y., Ebrahimi, G., Ashori, A., and Ghasemi, I. (2014). Effects of nano-graphene on the physico-mechanical properties of bagasse/polypropylene composites. *Polymer Bulletin, 71*, 337-349.

[133] Alexeev, V., Keberg, E., and Evmenenko, G. (n.d.). Development and characterization of chitosan film. *International Journal of Engineering Research and Applications*, 1(2), 292-299.

[134] Siracusa, V., Rocculi, P., Romani, S., and Rosa, M. (2008). Biodegradable Polymers For Food Packaging: A Review. *Trends in Food Science and Technology, 19*, 634-643.

[135] Lowa, S. C., Ahmada, A. L., Abd Shukora, S. R., and Ismail, A. (2009). Optimization of membrane performance by thermal-mechanical stretching process using responses surface methodology (RSM). *Separation and Purification Technology*, 66 , 177–186.

[136] Mohrunia, A. S., Yuliwatib, E., and Ismailc, A.F. (2013). Application of response surface methodology on optimizing for PVDF composite membrane ultrafiltration. International Conference on Recent Advances of Material Science and Technology, Karnataka, India.

[137] Saha, R., and William, D. (2002). Effects of the substrate on the determination of thin film mechanical properties by nanoindentation. *Acta Materialia* 50, 23–38.

[138] Gibson, P., Schreuder-Gibson, H., and Rivin, D. (2001). Transport properties of porous membranes based on electrospun nanofibers. *Colloids and Surfaces A: Physicochemical and Engineering Aspects,* 187,188, 469–481

[139] Setayesh, S., Marsitzky, D., and Müllen, K. (2000). Bridging the Gap between Polyfluorene and Ladder-Poly-p-phenylene: Synthesis and Characterization of Poly-2,8-indenofluorene. *Macromolecules*, 33, 2016.

[140] Advantages Of A New And Advanced Nanofiber Coating Technology For Filtration Media Compared to The Electrospinning Process. (n.d.). Retrieved April 21, 2015 from http://www.hollingsworth-vose.com.

Appendix 1.

1. The normality assumption

A check of normality assumption was made by plotting a normal probability plot as shown in Figure 1. The underlying error distribution was normal, thus it resembled a straight line. In visualizing the straight line, more emphasis was done on the central values of the plot than on the extremes. The normal probability plot indicates whether the residuals follow a normal distribution [89].

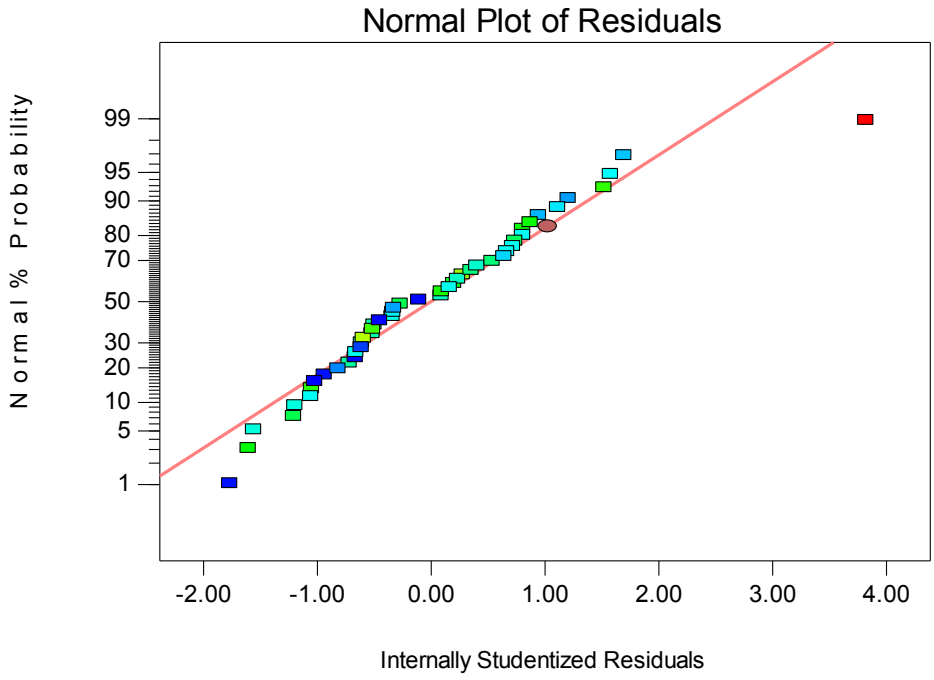

Figure 1. Normal Plot of Residuals

2. Constant variance assumption

A check on the assumption of constant variance was also performed. The plot for residuals vs. ascending predicted response values illustrated in Figure 4.28., tested the

assumption of constant variance. The plot was a random scatter. This confirmed the constant range of residuals across the graph [90].

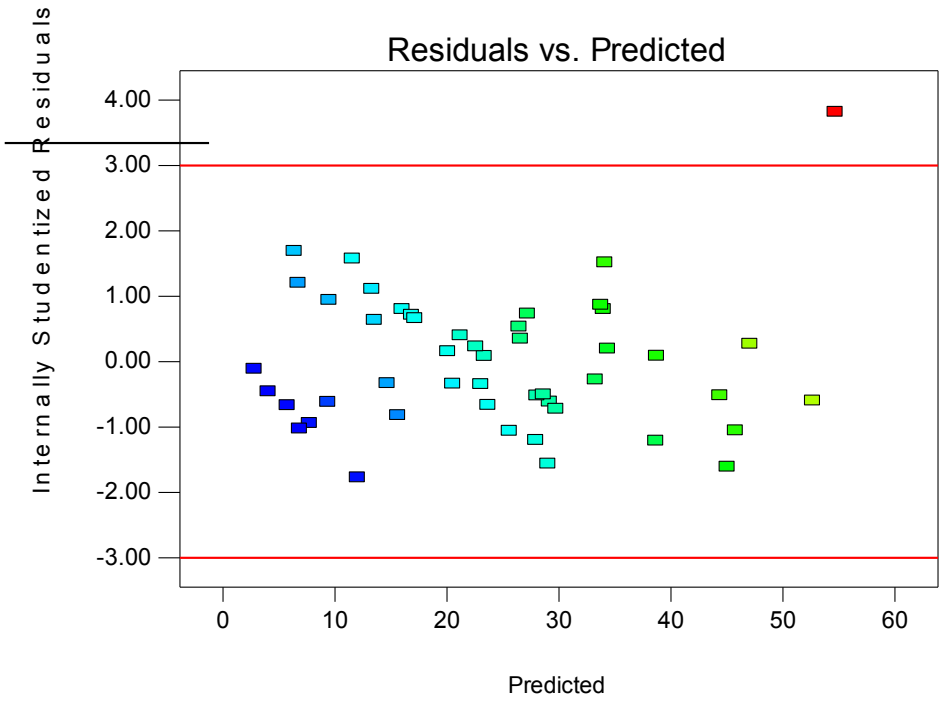

Figure 2. Residuals Vs. Predicated plot

3. Residuals versus Run assumption

This plot of the residuals versus the experimental run order shown in Figure 3., checked for lurking variables that may have influenced the response during the experiment. The plot shows a random scatter. This behaviour confirmed that there were no trends indicated. Randomization provided insurance against trends ruining the analysis [89].

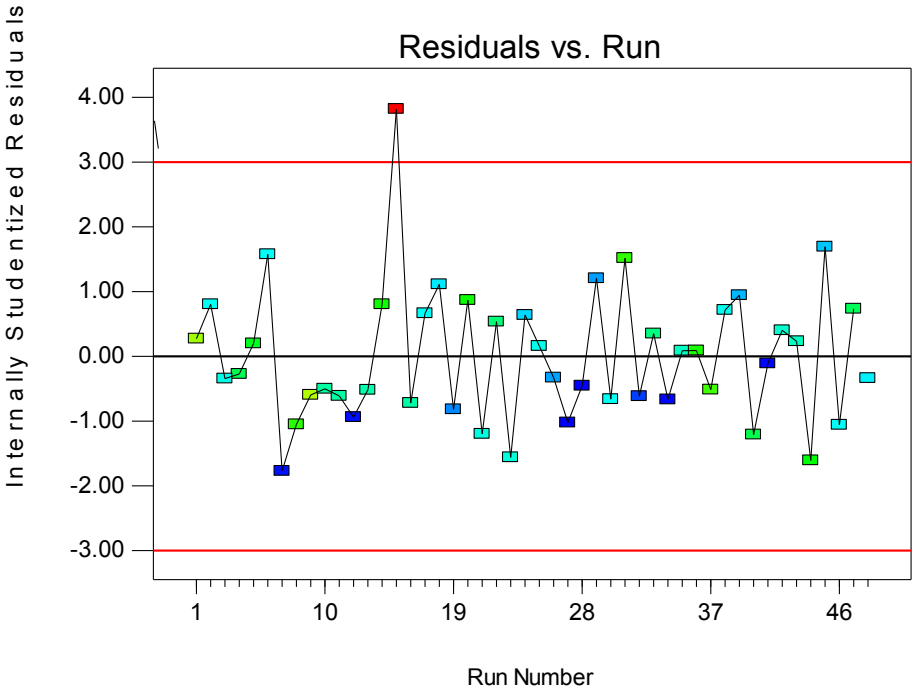

Figure 3. Residuals Vs. Run plot

4. Predicted vs. Actual assumption

A graph of the predicted response values versus the actual response values was illustrated in Figure 4. It helped to detect a value, or group of values, that were not easily predicted by the model. It shows should a straight line according to normality assumption confirming that all data are predicted by the model [87].

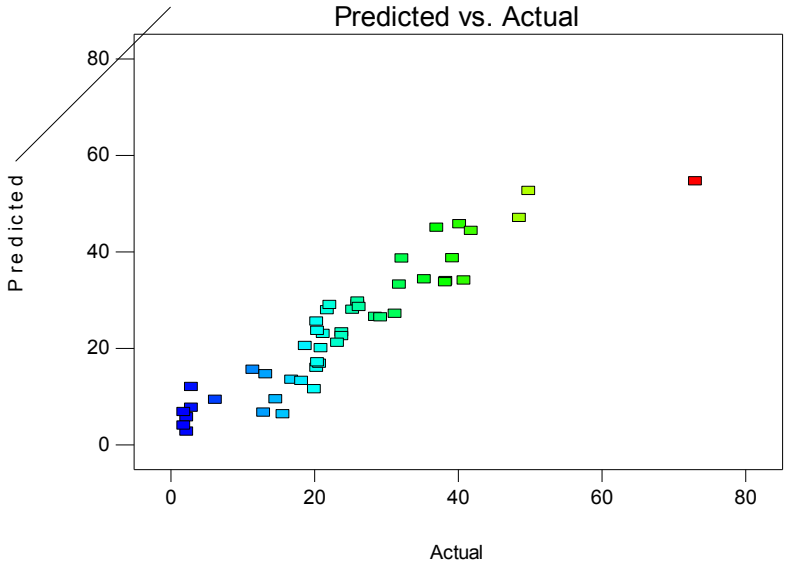

Figure 4. Predicted Vs. Actual plot

5. Residuals versus factor assumption

Residuals versus every factor plot shown in Figure 5., checked whether the variance not accounted for by the model is different for different levels of a factor. The plot exhibited a random scatter with no curvature. This assumption indicated that all factors were accounted for in the model [87].

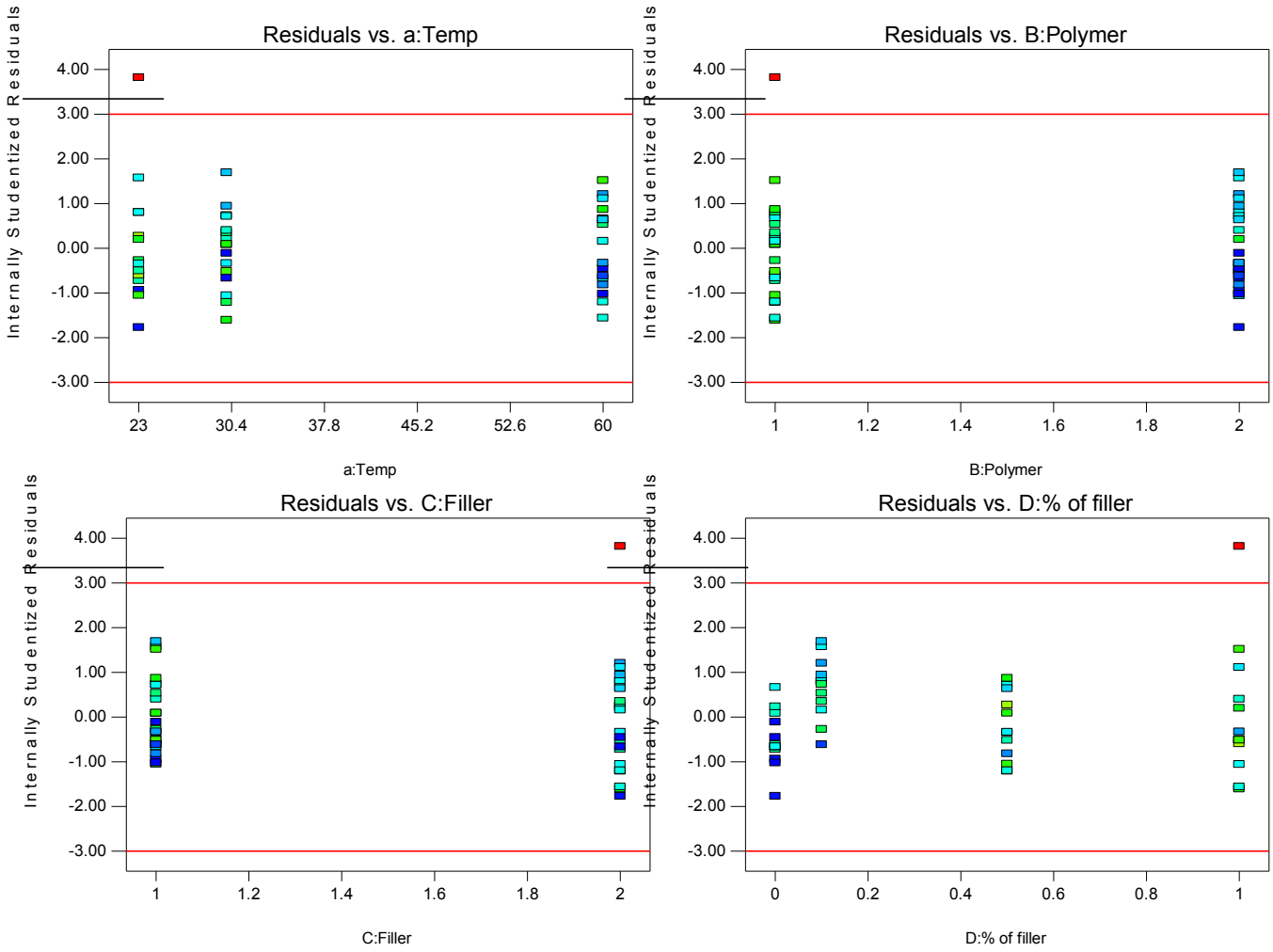

Figure 5. Residuals Vs Factor plots